Pharmacokinetic / Pharmacodynamic Modeling and Simulation of Biomarker Response to Venlafaxine and Sunitinib Administration

Dissertation
zur Erlangung des Doktorgrades (Dr. rer. nat.)
der Mathematisch-Naturwissenschaftlichen Fakultät
der Rheinischen Friedrich-Wilhelms-Universität Bonn

vorgelegt von
Andreas Lindauer
aus
Tettnang

Bonn 2010

Für meine Familie

*"Although it may seem a paradox,
all exact science is dominated
by the idea of approximation."*

Bertrand Russell (1872-1970)

Danksagungen

Table of Contents

Abbreviations

5-HT	serotonin
AUC	area under the curve
BP	blood pressure
CI	confidence interval
CL	clearance
CV	coefficient of variation
CWRES	conditional weighted residuals
df	degrees of freedom
FDA	United States Food and Drug Administration
FIM	Fisher information matrix
GIST	gastrointestinal stromal tumor
IPRED	individual predictions
IWRES	individual weighted residuals
MAT	mean absorption time
mRCC	metastatic renal cell carcinoma
NE	norepinephrine
NLME	nonlinear mixed-effects (modeling)
ODV	O-desmethylvenlafaxine
OFV	objective function value
PD	pharmacodynamic(s)
PK	pharmacokinetic(s)
PRED	population predictions
SD	standard deviation
V	volume of distribution

VEGF   vascular endothelial growth factor

VEGFR   vascular endothelial growth factor receptor

VEN   venlafaxine

VPC   visual predictive check

WRES   weighted residuals

1   Introduction

1.1   Pharmacokinetic/Pharmacodynamic Modeling and Simulation

1.1.1   History and Overview

With the introduction of the concepts of pharmacokinetics by Dost in his 1953's book *"Der Blutspiegel - Kinetik der Konzentrationsabläufe in der Kreislaufflüssigkeit"* [1] and the first review of the four kinetic elements, absorption, distribution, metabolism, and excretion in an international scientific journal by Nelson in 1961 [2], the importance of pharmacokinetics was recognized in the area of (clinical) pharmacology. Nelson made extensive reference to the pioneering work of Toerell who in 1937 first described the behavior of xenobiotics in the human body with mathematical equations [3,4]. These concepts are the basis of modern model-based pharmacokinetic (PK) data analysis.

The by far most widely used mathematical models to describe the time course of drug concentration in body fluids (e.g., blood or plasma) are the mamillary compartmental models, where the human body is simplified to a system of connected tanks (i.e., compartments) with drug input and output to and from a central compartment. These models can be described as systems of differential equations or, after integration, as polyexponential terms. Many modifications to this basic model structure, such as delayed absorption or saturable elimination, have been described, demonstrating its flexibility [5]. Figure 1-1 shows a two-compartment model with absorption and elimination according to first-order processes together with the model equations.

Pharmacodynamic (PD) models are often grounded on the law of mass action or Langmuir's law of adsorption-desorption and were later reformulated by Ariens [6] and Stephenson [7] for the case of drug-receptor binding and agonist action. Fundamental models of pharmacological response in relation to drug concentrations were reviewed by Holford and Sheiner emphasizing the importance of quantitative prediction of drug effects in man [8]. One of those basic PD models is the E_{max} model, where a hyperbolic function relates a measure of drug exposure (e.g., blood concentration, area under the curve [AUC], dose) to some measure of pharmacological response (Figure 1-2).

$$\frac{dA_d}{dt} = -k_a \cdot A_d$$

$$\frac{dA_1}{dt} = k_a \cdot A_d - k_{12} \cdot A_1 + k_{21} \cdot A_2 - k_{10} \cdot A_1$$

$$\frac{dA_2}{dt} = k_{12} \cdot A_1 - k_{21} \cdot A_1$$
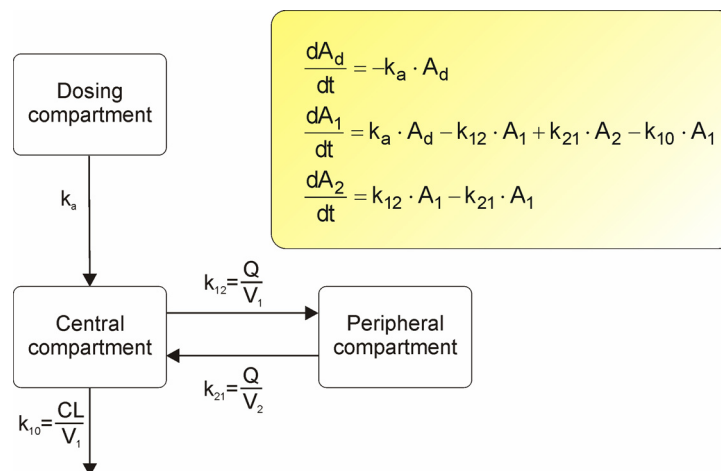
Figure 1-1   Mamillary two-compartment model. The amount of drug in the dosing compartment (A_d) enters the central compartment by a first-order process with a rate constant k_a. Distribution of the drug to and from the peripheral compartment is described by k_{21} and k_{12}. The drug's elimination from the central compartment is quantified by the first-order rate constant k_{10}. Rate constants can be easily transformed to the pharmacokinetic parameters clearance (CL), volumes of distribution of the central (V_1) and peripheral (V_2) compartment, and intercompartmental clearance (Q). The yellow box shows the system of differential equations describing the processes of absorption, distribution, and elimination.

A_1: amount in the central compartment; A_2: amount in the peripheral compartment.

The variety of useful pharmacodynamic models is tremendous, ranging from simple linear models to complex mechanistic models describing, for example, the receptor/gene-mediated effects of corticosteroids [9,10].

$$\text{Effect} = E_0 + \frac{E_{max} \cdot C}{EC_{50} + C}$$
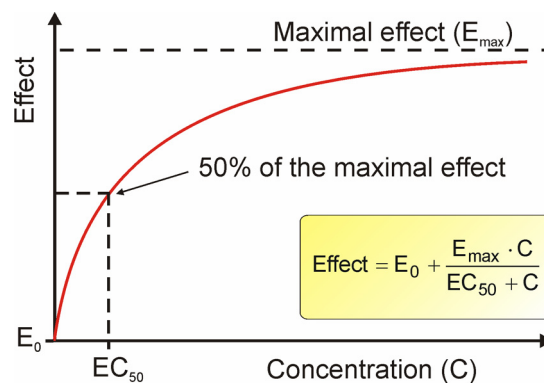
Figure 1-2   Maximal effect (E_{max}) model.

E_0: baseline effect; EC_{50}: concentration eliciting half the maximal effect.

A key part of model-based data analysis is the estimation of model parameters by nonlinear regression. Many different algorithms and estimation procedures have been developed for the purpose to "fit" some mathematical function to a given set of observations [5]. The most widely used method is the maximum likelihood estimation, developed by Fisher between 1912 and 1922 [11]. Sophisticated optimization algorithms (e.g., Gauss-Newton, Levenberg-Marquardt) are then applied trying to find the maximum of the likelihood function by iteratively changing the value of the model parameters. Specialized software has to be used for this purpose and the introduction of the NONMEM software by Sheiner and Beal in the early 1980's was one of the groundbreaking developments in the field of modeling and simulation [12-14]. For the first time the method of nonlinear mixed effects modeling (described in section 3.1.1) was incorporated into a piece of software, permitting the estimation of parameters from spares data and, importantly, providing estimates of the variability in model parameters between patients in a population [15]. Over the years NONMEM has become the by far most widely used software for the purpose of (population) pharmacokinetic/pharmacodynamic (PK/PD) modeling.

While models used for the mere description of data can provide additional insight into the behavior of a drug in an individual or in a population, compared to non-model-based techniques, their strength lie in their ability to make predictions, that means to simulate unstudied situations and "what-if"-scenarios. Important questions like: "How would a patient's response to a drug treatment change if his renal function declines?" or "Could additional benefit be gained giving a certain drug in a twice-daily schedule instead of only once a day?", may be addressed with simulations.

Over the past three decades the modeling and simulation approach has been increasingly recognized in preclinical and clinical research and drug therapy, and has eventually developed to an own discipline: Pharmacometrics - the science of quantitative pharmacology [16]. The following sections try to highlight some of the implications this approach had - and continues to have - on the development of new medicines and pharmacotherapy in clinical practice, and elucidate the key role that biomarkers play in this context.

1.1.2   Applications in Drug Development

The ever increasing costs for the development of new drugs (over 1 billion US Dollars per approved drug in 2008) and stagnation of approval rates rises concern on the efficiency of the drug development process [17]. In 2004, the United States Food and Drug Administration (FDA) issued a key document entitled "Innovation or Stagnation? Challenge and opportunity on the critical path to new medical products" [18], where they recommended the use of new tools to improve the drug development process. One such tool they mentioned, is model-based drug development as a framework for the "mathematical and statistical characterizations of the time course of the disease and drug using available clinical data to design and validate the model" [18]. In fact, much of the inefficiency in the drug development process is attributable to a lack of understanding of the exposure-response relationship of a new substance, leading to the selection of inappropriate doses for phase III trials or even for labeling [19]. In a seminal publication, Sheiner argued for an increasing use of exploratory studies, with study designs appropriate to learn as much as possible about the behavior (i.e., the exposure-response relationship) of a drug across a wide range of doses and different patient populations [20]. What has been learned from these exploratory studies can then be used to design larger confirmatory trials (e.g., phase III trials) where the objective is to demonstrate efficacy and safety in a representative patient population.

Modeling and simulation are essential tools in this learning and confirming concept and have a multitude of possible applications. PK/PD models developed on data from exploratory studies permit the examination of most beneficial dosing regimens. Data from larger studies can be used to identify patient characteristics (i.e., covariates) influencing the dose-concentration-response relationship. The models are then used to plan future clinical trials by simulating different trial designs in order to identify the one with the highest probability of success [21]. Defining optimal sampling times for concentration and response measurements within such trials complements this strategy [22]. In essence, the information gained with modeling and simulation supports the decision making on "whether" and "how" to continue the development of a new drug, with less room for subjective empiricism and wishful thinking.

Modeling techniques are helpful at any stage of the development process [23]. Expected concentration-time profiles in humans can be predicted with, for example,

physiologically-based PK models, incorporating information obtained from *in vitro* and preclinical animal studies. A guideline on the strategy to identify risks of first-in-human studies, issued by the European Medicines Agency, explicitly recommends the use of PK/PD models for the estimation of the first dose in humans of high-risk drugs (e.g., monoclonal antibodies) [24]. Measurements of response (i.e., biomarkers, see section 1.2) in phase I studies in healthy volunteers provide the first insight into the concentrations-response relationship of a drug in humans and are subsequently refined with data from studies in patients. In fact, the ability of models to be up-dated with newly arriving data, in other words, the propagation of knowledge from one step to the next, is an attractive characteristic of this approach. It is worth noting, that knowledge has not even to be created by oneself (i.e., the investigating company), but can be "borrowed" from the literature. An interesting example is given by Mandema et al., who evaluated the potential benefits of a new lipid lowering agent (gemcabene) over the competitor ezetimibe, using simulations from a PK/PD model developed with available information from the literature [25]. More examples how modeling and simulation have influenced drug development in recent years have been reviewed both from the pharmaceutical industry perspective [26-30] and from the regulatory point of view [31]. Initial skepticism about the model-based approach has continuously diminished and recent publications like the FDA's guidance on "End-of-Phase 2A Meetings" [32], strongly recommend the use of this method. A major management consulting company issued a business outlook on PK/PD modeling and simulation entitled "Pharma 2020: Virtual R&D" [33], underpinning the importance of the this approach for the efficient development of innovative medicines in the future.

1.1.3   Applications in Treatment Individualization

Many drugs are on the market with their package insert pretending that the same dose should be equally effective (safe) for every individual, from the young, maybe obese patient, to the 50-kg-weighing retiree. Alternatively, the use in such "non-normal" patient populations is simply not recommended due to lack of knowledge, preventing these patients to benefit from the drug or leaving the decision on the appropriate dose to the physician, without guidance. A retrospective evaluation of drugs approved by the FDA between 1980 and 1999 revealed that in 1 out of 5 drugs the initially claimed standard dose had to be changed after approval – in most cases (80%) it had to be

reduced [34]. This is because of insufficient knowledge of the dose-response relationship, as explained in the previous section, but more importantly because traditional drug development programs have been focused too much on finding a dosing regimen that is simple and easy to use for physicians and patients [19].

Fortunately, the paradigm of one-size-fits-all does not apply to the majority of newly approved drugs. For about 50% of new drugs registered in Germany in 2008 and 2009 *a priori* dose individualization based on patient characteristics like body weight, age, or organ function (e.g., creatinine clearance) is recommended [35]. Population PK/PD modeling can be used to identify such characteristics. However, for drugs with a narrow therapeutic window *a priori* individualization of the dose may not be sufficient. Dose adjustments based on the occurrence of side effects, the absence of effect, a biomarker measurement (e.g., blood pressure, blood glucose), or drug concentrations is frequently done in clinical practice, although it may not be stated explicitly in the drug's label. These *a posteriori* dose individualization strategies could greatly benefit from PK (or PK/PD) models, guiding dose adjustment instead of leaving it to trial-and-error. With a PK model at hand, individual PK parameters (e.g., clearance) of a patient can be derived using Bayesian estimation. The Bayesian method combines previous knowledge of the PK characteristics of a drug in a population (i.e., average parameter values and associated between-patient variability) and individual patient information (e.g., body weight, plasma concentrations etc.) in order to estimate individual PK parameters. Knowing the individual clearance (CL_{ind}) of a patient, for example, permits the calculation of the maintenance dose (MD) necessary to obtain a predefined target concentration:

$$\frac{MD}{\tau} = C_{target}^{ss} \cdot CL_{ind}$$

equation 1-1

where τ is the dosing interval and C_{target}^{ss} the desired steady-state target concentration. This method has the advantage that only a few concentration measurements per patient are necessary to obtain valid PK parameter estimates.

With a PK/PD model the above example could be extended to calculate the dose that most likely achieves a desired biomarker response in a patient, thus not only accounting for PK variability between patients, but also for variation in the pharmacological response. Whereas many examples exist for PK-guided dose individualizations (e.g.,

aminoglycosides, vancomycin, theophylline) [36-39], PK/PD models for this purpose are rare. One fit-for-purpose example has recently been proposed for the dose adaptation of etoposide based on the number of neutrophil granulocytes as a biomarker of myelosuppression [40].

In the light of increasing public interest in terms like "personalized medicine" and "tailored therapy" PK/PD-guided dose individualization may also receive growing attention and more examples like these will be seen in the future [41].

1.2   Biomarkers

1.2.1   Definitions and Overview

In 2001 the Biomarker Definitions Working Group published the following comprehensive definition of a biological marker (biomarker) [42]:

"...a characteristic that is objectively measured and evaluated as an indicator of normal biological processes, pathogenic processes, or pharmacological responses to a therapeutic intervention."

Biomarkers can be further divided into two groups [43]:

- biochemical biomarkers (e.g., blood glucose, cytokines)
- clinical biomarkers (e.g., blood pressure, tumor size)

In oncology it is often distinguished between prognostic and predictive biomarkers. Prognostic biomarkers provide information about the patients overall cancer outcome, independent of therapy (e.g., prostate-specific antigen [PSA]), while predictive biomarkers can be used to estimate the response of a particular patient to a specific treatment (e.g., expression of human epidermal growth factor receptor 2 [HER2/neu] as a predictor of response to treatment with trastuzumab).

Biomarkers should have a profound theoretical relation to the underlying disease mechanism and/or the mechanism of action of a pharmacological intervention. Moreover, biomarkers, particularly biochemical biomarkers, should be measured meeting acknowledged analytical standards in terms of stability, specificity, reproducibility, precision, and accuracy. However, it should be noted that assay development and validation for a biochemical biomarker is not as straightforward as it is for a drug assay and several issues may be challenging (e.g., lack of analyte-free matrices, availability of reference standards) [43].

Biomarkers that proved to predict precisely and accurately clinical benefit may substitute for a clinical endpoint (i.e., a characteristic reflecting how a patient feels, functions, or survives [42]) and are therefore called surrogate endpoints. According to the International Conference on Harmonization's guideline on "Statistical Principles for Clinical Trials" a surrogate endpoint must meet the following criteria [44]:

- biological plausibility
- prognostic value of the surrogate for the clinical outcome

- evidence from clinical trials that treatment effects on the surrogate correspond to effects on the clinical outcome

Popular examples of reliable surrogate endpoints, accepted by regulatory agencies, are the human immunodeficiency virus (HIV) plasma viral load in conjunction with CD4 cell counts for the evaluation of antiretroviral agents in patients with HIV infection, or blood pressure as a predictor for life-threatening cardiovascular events in hypertensive patients [45].

1.2.2   Applications of Biomarkers

Of course, clinical endpoints are generally the most reliable characteristics to assess the outcome of a therapeutic intervention and should be preferred over surrogate endpoints whenever possible. However, some clinical endpoints, such as survival, need long observation periods and a large number of patients in clinical trials to be robustly evaluated. This is impractical in many situations and renders clinical development of new drugs inefficient. The great demand for readily and timely measurable surrogate endpoints in order to accelerate approval of new drugs is obvious [18].

Although it is desirable that a biomarker eventually becomes a surrogate endpoint, a biomarker that cannot substitute for a clinical endpoint may still be of great value in drug development and patient care.

A measurable change of a biomarker in response to a pharmacological intervention may serve as proof-of-concept (POC) in early phases of development. This is valuable information when, for example, a selection has to be made between several candidate compounds. The POC is often possible even in preclinical animal testing if the biomarker exists (and behaves similarly) in species other than humans. Since the vast majority of drugs act on receptors or physiological structures that exist in humans irrespective of a disease, POC studies in healthy volunteers can provide important information. For example, a new antihypertensive drug that does not reduce blood pressure in healthy subjects will probably not be effective in hypertensive patients either. Integrating quantitative biomarker information into a PK/PD model (the biomarker represents the PD part then) facilitates rational decision making regarding dose selection and trial design (see section 1.1.2) or discontinuation of a project due to insufficient biomarker response.

In clinical practice physicians have been successfully using biomarkers to guide treatment individualization (e.g., international normalized ratio [INR] for the treatment with oral anticoagulants, blood glucose for insulin treatment) for years, although many of them do not have the status of a surrogate endpoint required for regulatory approval. The potential of biomarker-guided treatment individualization is tremendous both for drugs yet exiting and those that will be developed in the future.

1.3 Venlafaxine

1.3.1 Therapeutic Use and Clinical Pharmacology

Venlafaxine (Effexor[®], Trevilor[®], Wyeth Pharmaceuticals Inc.) is approved for the treatment of major depressive disorder, generalized anxiety disorder, panic disorder and social phobia [46]. It also showed to be effective for the relapse and recurrence prevention of major depressive episodes [47], and is currently the only antidepressant approved for this indication [46,48]. The recommended starting dose is 75 mg/day which can be increased up to 375 mg/day in severely depressed patients. The most common side effects during treatment with venlafaxine are gastrointestinal disorders, excessive sweating, and dry mouth [46].

Venlafaxine is rapidly absorbed after oral administration of an immediate release formulation reaching maximal plasma concentrations by approximately 3 hours [49]. It is metabolized to its major active metabolite O-desmethylvenlafaxine via the cytochrome P450 (CYP) 2D6 enzyme system in the liver and undergoes an extensive first-pass metabolism (Figure 1-3) [49]. In a mass balance study with radioactive labeled venlafaxine, over 90% of total radioactivity was recovered in urine: 5% as unchanged venlafaxine, 55% as conjugated and unconjugated O-desmethylvenlafaxine, and 15% as other, less active, N-desmethyl metabolites [50,51]. Binding to plasma proteins is relatively low with values of 27 and 30% for venlafaxine and O-desmethylvenlafaxine, respectively. The terminal half-lives of venlafaxine and O-desmethylvenlafaxine are 5 and 11 hours, respectively [46].

Venlafaxine (MW: 277 g/mol)   **O-desmethylvenlafaxine** (MW: 263 g/mol)
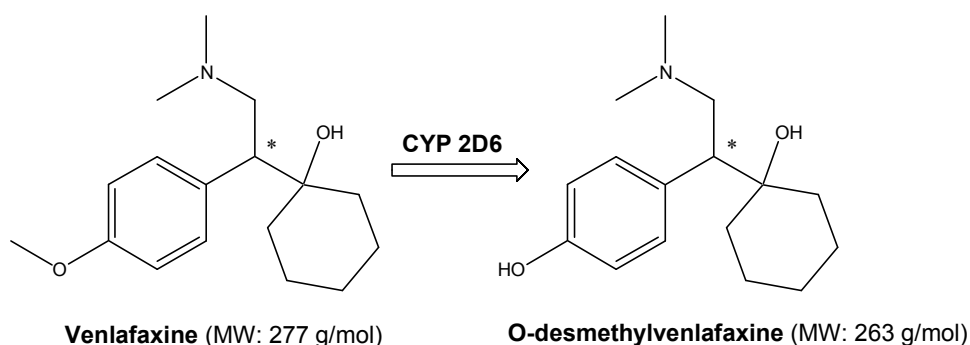
Figure 1-3   Chemical structure of venlafaxine and its major metabolite. The asymmetric center is marked with an asterix. Only the racemate is on the marked.

CYP: Cytochrome P450; MW: Molecular weight.

Venlafaxine and O-desmethylvenlafaxine achieve their pharmacological effect by inhibition of serotonin (5-HT) and norepinephrine (NE) reuptake from the synaptic gap. Preclinical findings showed that the affinity of venlafaxine and O-desmethylvenlafaxine for 5-HT transporters is about 3-fold higher as for NE transporters [52]. This property is of clinical relevance, as it has been demonstrated that with higher doses of venlafaxine, additional antidepressant effects can be achieved which could not be attributed to a single saturable dose-response relationship [53,54]. This means that at low doses, inhibition of 5-HT reuptake is the main mechanism of action, whereas at higher doses inhibition of NE reuptake exerts an additional effect [55].

1.3.2   Biomarkers of Interest

The pharmacological treatment of depression and the development of new antidepressants could potentially benefit from a reliable and readily measurable biomarker. There is a considerable latency of about two weeks between the start of the treatment and noticeable improvement of the patients' mood [56]. An early responding biomarker could be useful to adjust the dose without having to wait until the first signs (or lack of them) of clinical response are evident.

During clinical development of a new antidepressant, a biomarker could be of use in POC studies in healthy subjects and, at later stages, it could help to establish the dose-response relationship. A noninvasive test system to indirectly measure inhibition of NE reuptake (i.e., noradrenergic response) is pupillography. Constriction and subsequent dilatation of the pupil after a short light flash (i.e., the pupillary light reflex) is controlled by the parasympathetic and sympathetic nervous system and therefore is sensitive to inhibition of NE reuptake.

In detail, an incoming light signal is transmitted by the optic nerve to the protectal area from which it is further passed to the Edinger-Westphal nucleus. Its axons run along the oculomotor nerve and synapse in parasympathetic cilliary ganglion neurons innervating the pupillary constrictor muscle of the iris. Projections from the midbrain contact thoracic segments of the spinal cord from which the sympathetic innervation of the pupillary dilatator muscle originates. The Edinger-Westphal nucleus is under tonic inhibitory noradrenergic control from the locus coeruleus and the corticolimbic system. Venlafaxine increases this inhibitory control by blocking the NE uptake form the synaptic gap, leading to a reduction of parasympathetic signals going to the eye.

Inhibition of NE uptake at the pupillary dilatator muscle by venlafaxine directly affects the pupil size. Figure 1-4 illustrates this pathway of the pupillary light reflex and the supposed sites of action of venlafaxine.
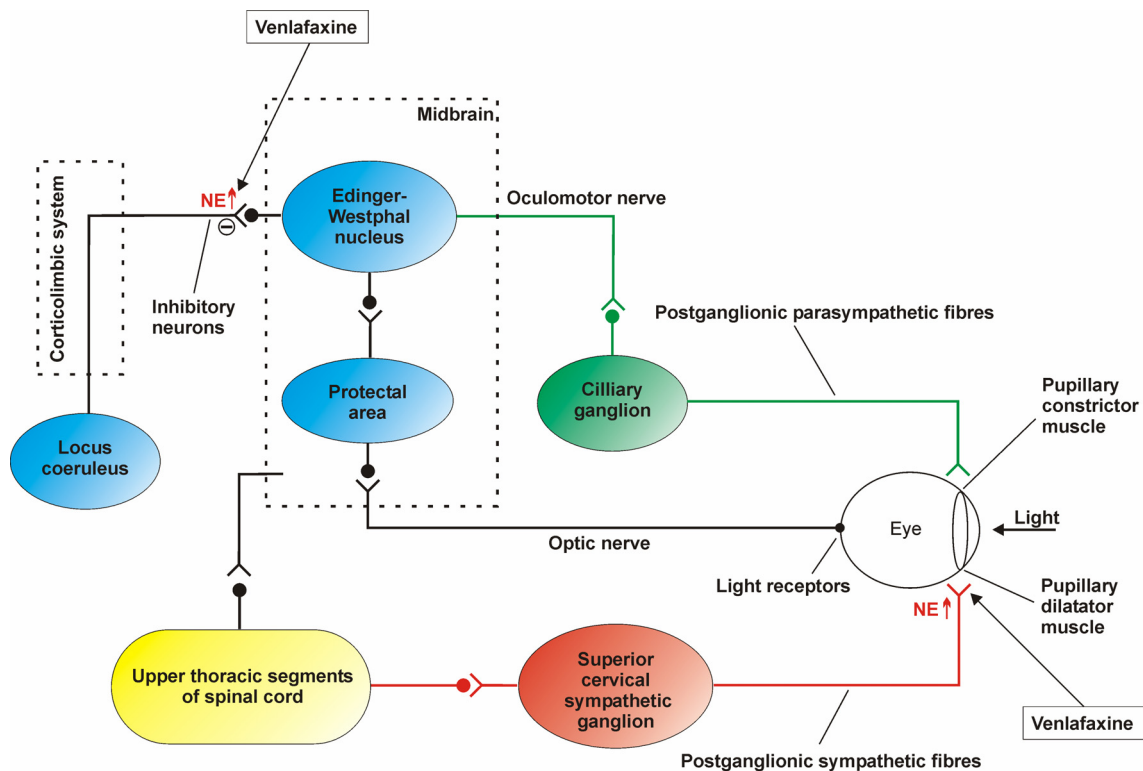
Figure 1-4 Schematic representation of the neuronal pathway of the pupillary light reflex. (Modified from White & Depue [57]; further explanations see text)

Changes of the pupil diameter after emission of a short light flash can be recorded with a pupillographic device shown in Figure 1-5. Four relevant parameters can be derived from such records:

- Resting pupil diameter (i.e., the diameter shortly before the light flash)
- Latency (i.e., the time difference between the end of the light flash and the onset of pupil constriction)
- Amplitude (i.e., the difference between the initial and the minimal diameters)
- Recovery time (i.e., the time it takes to redilatate to a predefined percentage of the initial diameter)

The time course of a typical light reflex response is shown in Figure 1-6.
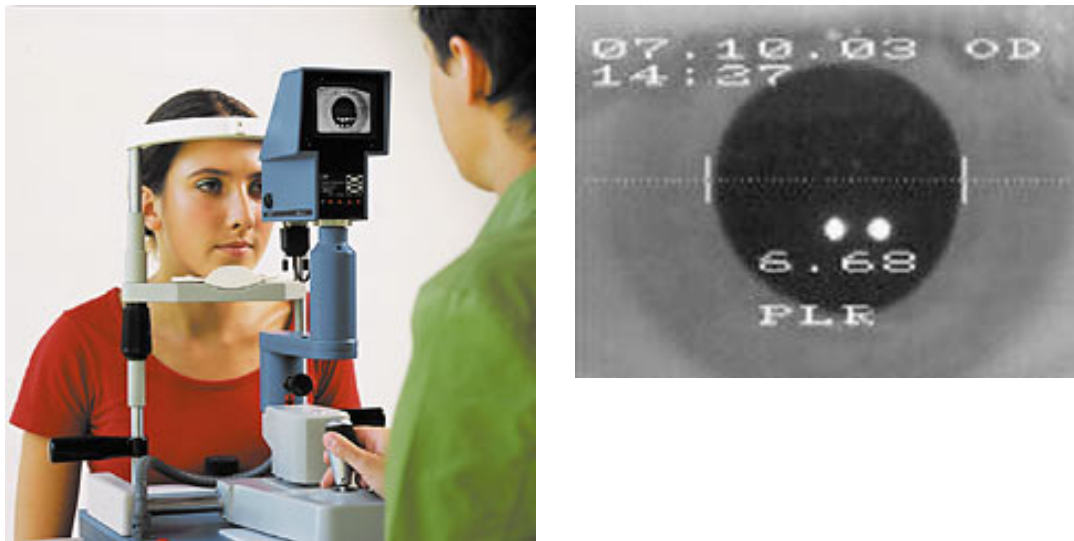
Figure 1-5   Subject during a pupillographic measurement (left photograph) and the operator's view on the pupil (right photograph). (From AMTech GmbH, Dossenheim with permission)
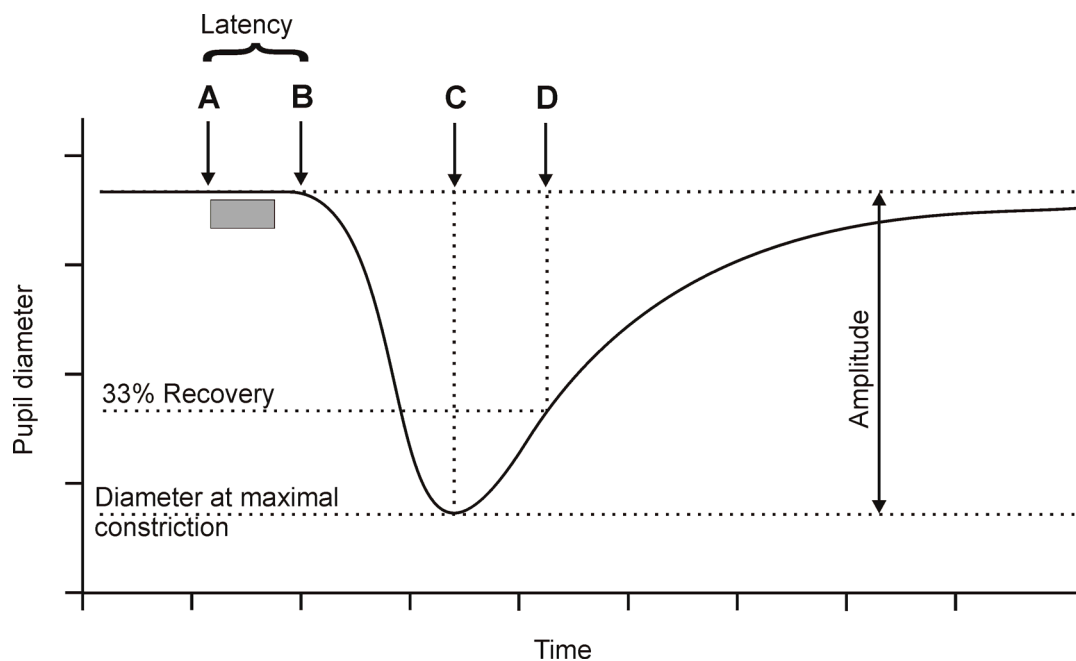
Figure 1-6   Example of a light reflex response. Grey bar: light stimulus; A: onset of light stimulus; B: onset of response; C: time at maximal constriction. D: time at which 33% recovery is attained. (Modified after Bitsios et al. [58])

The resting pupil diameter reflects the balance between the opposing effects of sympathetic and parasympathetic innervations of the iris. A parasympatholytic drug like atropine for example, shifts the balance towards sympathetic activity resulting in an

increased pupil diameter. The recovery time is thought to reflect sympathetic activity in the iris, whereas the amplitude and latency are generally attributed to parasympathetic effects [58]. Bitsios et al. reported significant changes of the pupillary light reflex parameters 100 min after administration of a single dose of venlafaxine (75 mg or 150 mg) to healthy subjects [58]. However, the time course of changes in pupillary light reflex parameters and its relation to plasma concentrations of venlafaxine and O-desmethylvenlafaxine have not been studied so far.

1.4   **Sunitinib**

1.4.1   **Therapeutic Use and Clinical Pharmacology**

Sunitinib malate (Sutent[®], Pfizer Inc.) is a multitargeted tyrosine kinase inhibitor that inhibits tumor cell proliferation and angiogenesis. It is approved for the treatment of renal cell carcinoma (RCC) and imatinib-resistant gastrointestinal stromal tumor (GIST) [59]. Its activity in other tumor types such as hepatocellular carcinoma or non-small cell lung cancer is currently investigated in numerous clinical trials (see www.clinicaltrials.gov). Sunitinib is given orally, once daily as a 50 mg capsule over 4 weeks, followed by a 2-weeks rest period in repeated 6-weeks treatment cycles. At this dose, the most frequently observed adverse effects are fatigue, hypertension, diarrhea, stomatitis and hand-foot syndrome [59].

Following oral administration sunitinib is slowly absorbed from the gastrointestinal tract reaching maximum plasma concentrations after about 6 to 12 hours. It is primarily metabolized by CYP 3A4 to its active N-desethyl metabolite (SU12662) and is subject to presystemic metabolism by this enzyme (Figure 1-7) [60]. In a mass balance study in humans with ^{14}C-labeled sunitinib, 61% of the radioactive dose was recovered in feces and 16% in urine. In plasma samples sunitinib and SU12662 accounted for 71 and 20.5% of the total radioactivity, respectively [61]. Approximately 95% (90%) of sunitinib (SU12662) is bound to plasma proteins. Because of the long terminal half-lives of sunitinib and SU12662 (40 to 60 h and 80 to 110 h, respectively), steady-state concentrations are not achieved until 2 weeks of continuously daily dosing.
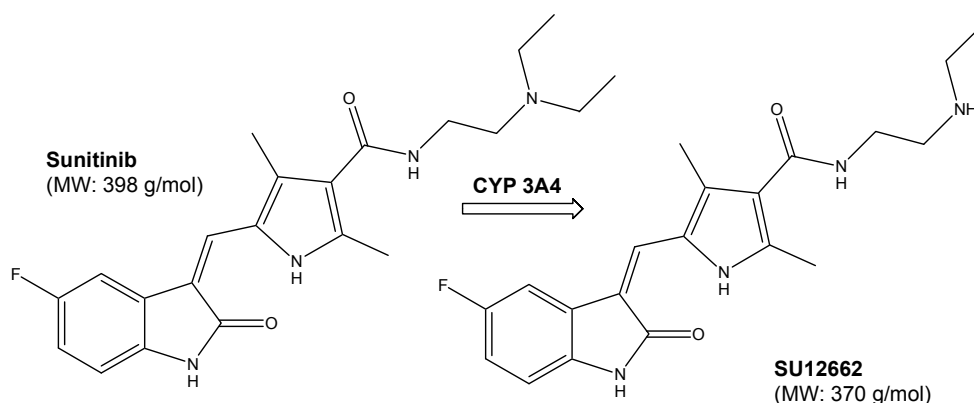
Figure 1-7   Chemical structure of sunitinib and its major metabolite SU12662.
CYP: Cytochrome P450; MW: Molecular weight.

Sunitinib and SU12662 inhibit a variety of receptor tyrosine kinases (RTK) by reversibly binding to intracellular adenosine triphosphate (ATP)-binding sites [62]:

- vascular endothelial growth factor receptor (VEGFR) -1, -2 and -3
- platelet-derived growth factor receptor (PDGFR) alpha and beta
- stem-cell growth factor receptor (KIT)
- fms-related tyrosine kinase-3 (FLT3)
- colony stimulating factor-1 receptor (CSF1R)

Inhibition of VEGFR-2 and PDGFR-β is predominantly responsible for the reduction of tumor-related blood vessel formation, which explains its activity against the highly vascular RCC [63]. By contrast, GIST is susceptible to sunitinib probably because of a high expression of KIT by this tumor [64].

VEGF-A is released by tumor cells, as well as fibroblasts and other stromal cells (Figure 1-8 **a**). A trigger for the production of VEGF-A is tissue hypoxia. The decreasing oxygen supply in a growing tumor stimulates the production of hypoxia inducible factor-1 (HIF-1) which in turn increases the transcription of VEGF-A. It has further been shown that an inactivated von Hippel-Lindau tumor suppressor gene - occurring in about 50% of RCC tumors - leads to a higher expression of HIF-1 [65].

Tumor-derived PDGF plays an important role in tumor-vessel stability by recruiting pericytes to newly formed vessels. Via its receptor alpha it regulates VEGF-A derived from fibroblasts [66].

After binding of VEGF-A to VEGFR-2 on the surface of endothelial cells, a signaling cascade is initiated leading to cell survival, proliferation, migration, and vascular permeability. Sunitinib inhibits the tyrosine kinase-mediated autophosphorylation of the receptor, thus blocking this signaling process (Figure 1-8 **b**).

At present only two other antiangiogenic agents are on the market: the monoclonal antibody bevacizumab (Avastin®) and the tyrosine- and raf-kinase inhibitor sorafenib (Nexavar®). Development of new angiogenesis inhibitors is, however, a major area in oncology research and many promising drugs targeting the VEGF-pathway, such as telatinib and axitinib, are in the pipelines of pharmaceutical companies [68-70].
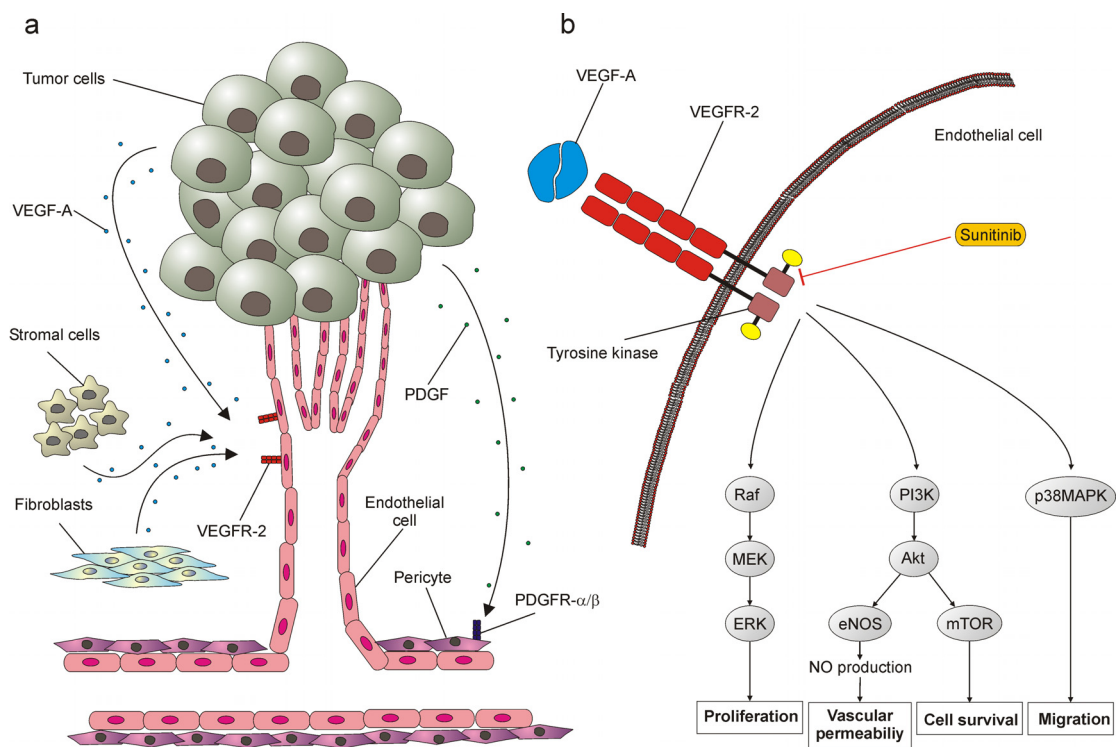
Figure 1-8   The role of VEGF-A in tumor angiogenesis. **a** release of growth factors in the tumor environment. **b** VEGF-A induced signaling process in the endothelial cell. (Adapted from Hicklin et al. [66], Takahashi et al. [67] and Faivre et al. [62])

VEGF: vascular endothelial growth factor; PDGF: platelet derived growth factor; Raf: rat fibrosarcoma (kinase); MEK: mouse embryonic kinase; ERK: extracellular signal-regulated kinase; PI3K: phosphatidylinositol 3-kinase; eNOS: endothelial nitric oxygen synthase; NO: nitric oxygen; mTOR: mammalian target of rapamycin; p38MAPK: protein 38 mitogen-activated protein kinase.

1.4.2   **Biomarkers of Interest**

For anti-VEGF drugs it is a major challenge to find the optimal biological dose associated with a low risk of toxicity and high efficacy [71,72]. The concept of using the maximum tolerated dose (MTD) as it is traditionally applied for cytotoxic agents may not always be appropriate for these substances. The mechanism of action of cytotoxic drugs often involves interaction with the tumor DNA, a virtually nonsaturable target structure, thus efficacy increases almost proportionally with the dose and the only limitation is toxicity.

However, targeted drugs act on receptors (or other functional proteins) and from classical receptor theory it is known that the maximum effect is achieved when all

binding sites are occupied [7]. Increasing the dose further would then have no additional benefit. Applying the MTD concept in dose-finding studies of these new drugs could therefore result in unnecessarily high doses, when in fact lower, less toxic doses would be equally effective. To determine the optimal biological dose level, objectively measurable markers of early response to treatment have to be found. Biomarkers associated with target modulation have the potential to meet this challenge. In numerous reports it was shown that several circulating proteins (e.g., VEGF-A and VEGF-C, soluble (s) VEGFR-2 and -3) as well as blood pressure (BP) consistently changed in response to antiangiogenic therapy [73-81].

Ebos et al. observed increasing VEGF-A and decreasing sVEGFR-2 concentrations after administration of sunitinib to nontumor bearing mice, to a similar extent as it was seen in xenograft models [73]. Tumor being the only (major) source of release of proangiogenic factors is therefore unlikely. In fact, these authors showed that the increase in VEGF-A is highest in heart and spleen tissue and the decrease in sVEGFR-2 is highest in liver, heart, and spleen. In extensive studies in mice, it could be demonstrated that high levels of VEGF-A (induced by adenoviral-mediated delivery of the human VEGF-A gene) lead to a subsequent decrease in sVEGFR-2 plasma concentrations. Further *in vitro* experiments indicated that VEGF-A mediates the down-regulation of VEGFR-2, which in turn leads to reduced levels of the soluble form of this receptor [82].

Despite these elaborate preclinical studies it is unclear whether VEGF <u>directly</u> mediates the decrease in sVEGFR-2 production. Since sunitinib blocks the activation of VEGFR-2 by VEGF-A, the signal for the downregulation of VEGFR-2 may not be trigged by this very same receptor in the presence of the drug. Given that a multitude of circulating proteins are involved in the regulation of angiogenesis, potentially interacting and influencing each other, it may be possible that the downregulation of VEGFR-2 is only <u>indirectly</u> mediated by VEGF [73].

Based on clinical and preclinical observations it appears plausible that some sort of feedback mechanism controls plasma concentrations of VEGF-A, leading to higher levels when its receptor is blocked [73,76]. Figure 1-9 illustrates a proposed mechanism of biomarker response to VEGF receptor inhibition.
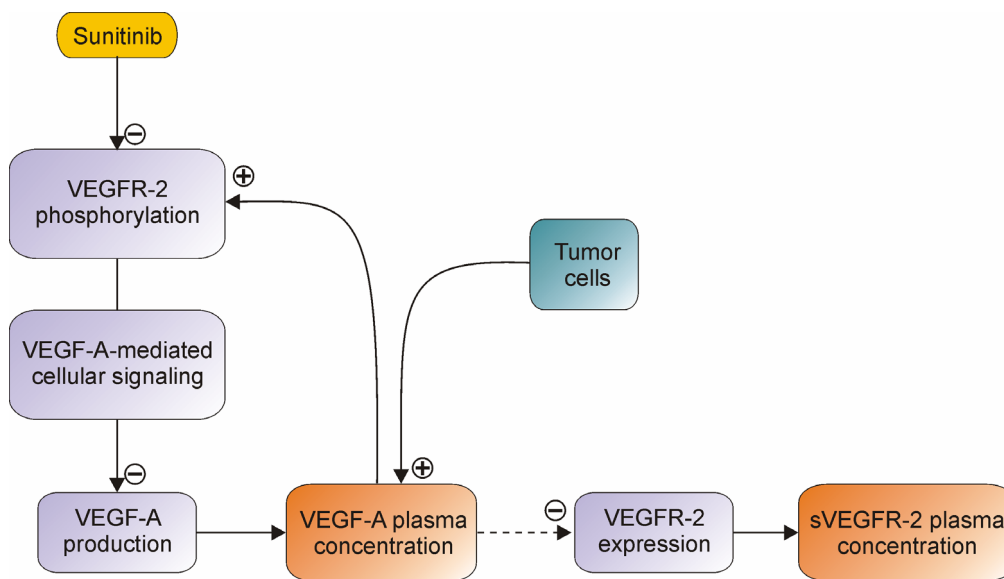
Figure 1-9   Proposed mechanism of biomarker response to VEGF receptor inhibition. The activation of VEGFR-2 by VEGF-A leads to a decreased cellular production of VEGF-A and thus controlling the plasma levels of VEGF-A. VEGF-A is involved in the downregulation of VEGFR-2 which in turn regulates plasma concentrations of sVEGFR-2. In the absence of tumor or VEGFR inhibitors the system is at equilibrium.

Considerable increase in blood pressure has been reported in many studies with different antiangiogenic drugs as a frequent side effect, so that it is now considered as a class effect [83-87]. Mainly two mechanisms of action are discussed, (i) reduction in endothelial nitric oxide synthase (eNOS) expression which is controlled by VEGF signaling (Figure 1-8 b), and (ii) vascular rarefaction, that is, a decrease in perfused microvessels and a reduction in capillary density both controlling peripheral vascular resistance. Moreover, VEGF inhibition may induce renal thrombotic microangiopathy leading to blood pressure disequilibrium and proteinuria, another common side effect of VEGFR inhibition [87,88]. In a recent publication Keizer et al. presented an interesting PK/PD model for hypertension and proteinuria following treatment with a new VEGF-inhibitor currently under clinical development [89].

Generally, hypertension caused by antiangiogenic drugs can be well controlled by standard anti-hypertensive treatment (e.g., calcium antagonists) and may therefore not constitute a major safety concern [87]. Since blood pressure can be easily measured in clinical practice, this biomarker could be of great value as a tool for oncologists to assess and optimize antiangiogenic treatment. However, before any useful biomarker guided treatment optimization strategy can be developed a clear understanding of the dose-concentration-effect relationship is a prerequisite.

2 Objectives

This thesis aims at illustrating the concept of PK/PD modeling and simulation using biomarkers on the example of two projects with drugs from different therapeutic areas. In both cases drug concentration and biomarker data were obtained from clinical studies in healthy volunteers.

In the first project the noradrenergic response to venlafaxine (and O-desmethylvenlafaxine), measured by pupillography was subject to model development and, based on the modeling results, optimal pharmacodynamic sampling times for possible future studies were to be explored. Since venlafaxine is also available as an extended release formulation, the influence of a slower release on the PD response was to be assessed by deterministic simulations.

In the second project PK/PD models had to be developed to quantify changes of blood pressure, plasma concentrations of VEGF-A and VEGF-C, and sVEGFR-2 in relation to sunitinib (and SU12662) concentrations. In order to address the question whether a dose adjustment based on blood pressure measurements could be beneficial with respect to clinical outcome, a hypothetical clinical trial was simulated comparing a dose individualized regimen to the standard dose regimen.

Both projects discussed in this thesis have been previously published in part in international scientific journals:

Lindauer, A., Siepmann, T., Oertel, R. et al. Pharmacokinetic/Pharmacodynamic modelling of venlafaxine: pupillary light reflex as a test system for noradrenergic effects. Clin Pharmacokinet 2008; 47: 721-731

Lindauer, A., Di Gion, P., Kanefendt, F. et al. Pharmacokinetic/Pharmacodynamic modeling of biomarker response to sunitinib in healthy volunteers. Clin Pharmacol Ther 2010; 87: 601-608

3 Material and Methods

3.1 General Methods of PK/PD Data Analysis

3.1.1 Nonlinear Mixed Effects Modeling

The pharmacokinetic and pharmacodynamic data analyses described in this thesis were performed by means of nonlinear mixed effects modeling (NLME) implemented in NONMEM® (versions 6.0 and 6.2) [90]. This method is a special kind of nonlinear regression analysis where the observations (e.g., drug concentrations, biomarker measurements) are described by a mathematical function (i.e., a model) consisting of error-free independent variables (e.g., time, dose, covariates), the fixed effects, and variables that are subject to random error (e.g., between-subject variability, residual error), the random effects. Both effects are accounted for in the same model, therefore the term "mixed" effects modeling.

In contrast to the standard regression analysis, this approach provides the possibility to analyze data from different individuals at once by simultaneous estimation of the typical (i.e., average) model parameters and their associated variability. The method is also termed population PK/PD modeling, as it is especially useful for the analysis of variability among individuals in large patient populations.

NLME permits the distinction between different sources of variability associated with drug concentration or biomarker measurements. Model parameters may not only vary between different individuals (i.e., interindividual variability, IIV), but also within a particular subject from one occasion (e.g., day) to another (i.e., interoccasion variability, IOV). Finally, the discrepancy between observations and model predictions constitute the unexplained residual variability (i.e., residual error). A general mathematical expression of the NLME function is shown in equation 3-1:

$$Y = f(\theta, x, z, \Omega, K, \Sigma)$$
equation 3-1

where Y represents the vector of all observations in all individuals, the function f is the NLME model that contains the vector of typical population parameters (θ), the vector of fixed effects controlled by the investigator (x; e.g., time and dose) and, if applicable, the vector z, containing patient-specific covariates which are also treated as fixed effects in the model. The random effects are described by the matrices Ω, K and Σ comprising

interindividual, interoccasion and residual variability parameters, respectively. In the following expression a NLME model is illustrated for a pharmacokinetic one-compartment model with intravenous bolus administration:

$$C_{ji} = \underbrace{\frac{D}{\theta_V + \eta_{i,V} + \kappa_{q,V}} \cdot e^{\left(\frac{\theta_{CL} + \eta_{i,CL} + \kappa_{q,CL}}{\theta_V + \eta_{i,V} + \kappa_{q,V}} \cdot t_j\right)}}_{\hat{C}_{ji}} + \varepsilon_{ji} \qquad \text{equation 3-2}$$

where C_{ji} is the jth measured concentration in subject i at time t_j, D is the dose, θ_V and θ_{CL} are the typical volume of distribution and typical clearance in the population, respectively. The deviation of an individual value from the typical parameter value is described by η_i and the deviation from that at each occasion q, is denoted κ_q. ε_{ji} is the discrepancy between the individual predicted concentration ($\hat{C}_{ji}$) from the observation. η, κ and ε are random quantities with a mean value of 0 and the variances ω^2, π^2 and σ^2, respectively. Collectively, Ω, K and Σ are the matrices of all the estimable variability parameters.

The estimation algorithm implemented in NONMEM iteratively seeks for a set of model parameter values with the aim of maximizing the likelihood that the observations were derived from the model. Mathematically, the algorithm tries to find the global minimum of the extended least square objective function (OF$_{ELS}$, equation 3-3) [13]:

$$OF_{ELS} = \sum_{i=1}^{n} \left[\frac{(y_i - \hat{y}_i)^2}{var(y_i)} + \ln(var(y_i)) \right] \qquad \text{equation 3-3}$$

where y_i is the vector of the observations for subject i and $\hat{y}_i$ the vector of corresponding predictions, $var(y_i)$ is the variance matrix of y_i, which in fact is a function containing all the variability parameters of the model. The logarithm penalty term on the right-hand side of equation 3-3 prevents the objective function from minimizing to 0 as the variance parameters increase to infinity.

Since all random effects enter nonlinearly into the objective function, equation 3-3 has no closed-form solution and its minimum cannot be calculated analytically (as it would be the case for a simple linear regression model). In NONMEM a Taylor series approximation is used to account for this issue. A Taylor series is a high-order polynomial that approximates a function f at point x (i.e., f(x)) given the function value

and its derivatives ($\partial f(x)$) at another point x_0 [5]. In NONMEM the model function is linearized into a first-order polynomial of the function itself and its first partial derivatives with respect to the η's (etas) [90]. Thus, the first-order Taylor approximation of the (simplified) model from equation 3-2 evaluated at η_0 would be:

$$
\begin{aligned}
C_{ji} = f(...,\eta_0) + \frac{\partial f(...,\eta_0)}{\partial \eta_{i,V}} \cdot (\eta_{i,V} - \eta_{0,V}) \\
+ \frac{\partial f(...,\eta_0)}{\partial \eta_{i,CL}} \cdot (\eta_{i,CL} - \eta_{0,CL}) + \varepsilon_{ji}
\end{aligned}
\qquad \text{equation 3-4}
$$

where $f(...,\eta_0)$ is the function value for the jth concentration in the ith subject with the ηs set to η_0. The same applies to the partial derivates. Note that ε_{ji} now also contains the error resulting from the approximation. Two principal methods are used in NONMEM: the first-order (FO) method where the Taylor series is evaluated at $\eta_0=0$, and the more accurate FO conditional estimation (FOCE) method, where the approximation is done by setting η_0 to the vector of the Bayesian estimates of the η's. This means that at every iteration the estimates for all η's are computed conditionally on the current Ω matrix [5,90]. A further refinement is the use of the interaction option, allowing ε to be dependent on η, which is particularly important when the residual error increases proportionally to the observed value (i.e., proportional error model, see next section).

In this thesis only the first-order conditional estimation method (FOCE) with interaction was used. NONMEM runs were executed using Wings for NONMEM (version 6.14) [91] and compiled with the G77 Fortran compiler (version 2.95).

3.1.2   Model Development

Structural Model

A PK or PD model is usually developed in a step-wise manner, beginning with the simplest model proceeding to more complex ones. Here the word "complex" refers to the number of model parameters. At every step, that is, with every intermediate model, it has to be decided, based on objective and subjective criteria (see section 3.1.3), how to proceed with the model development (e.g., adding or excluding model parameters or covariates). Usually model building should start with the structural model including only few random effects parameters right from the beginning. More variability

parameters are then continuously added, and, if it is an objective of the analysis, covariates on model parameters are included [5].

The structural model should be able to characterize the central tendency of the observed data best. Different structural models were explored for the drugs that are subject to this thesis with details given in sections 3.2.5 and 3.2.6 for the venlafaxine example and sections 3.3.4 and 3.3.5 for the sunitinib example.

The combined PK/PD models were developed in a sequential manner. First the PK model was completed. Individual PK parameter estimates obtained from this step were then used as input (together with the PD data) for the development of the PD part of the models.

Interindividual Variability

Interindividual variability was generally modeled as an exponential relationship:

$$P_i = \theta \cdot e^{\eta_i}$$ equation 3-5

where P_i is the individual value of a model parameter (e.g., clearance), θ its typical value in the population and η_i is the difference between P_i and θ in the logarithmic domain. The interindividual variability is usually reported as a (geometric) coefficient of variation (CV) according to:

$$CV(\%) = 100 \cdot \sqrt{e^{\omega^2} - 1}$$ equation 3-6

For example, an estimate of ω^2 of 0.1, denoting the variance of the model parameter in the logarithmic domain, would translate to a CV of approximately 32%. The exponential parameterization has the advantage that individual parameter estimates cannot be negative. Moreover, PK parameters often follow a right-skewed (log-normal) distribution which is better captured with the exponential model.

Interindividual variability cannot always be estimated for every parameter in the model, especially when the number of subjects in the dataset is small. The decision if a variability parameter should be retained in the model or not, was mainly based on the estimated value itself and its contribution to the objective function value (OFV; see section 3.1.3.1). For example, if the estimated variance (or the CV) for a certain parameter was close to 0 it was removed from the model without any significant change of the OFV. It should be noted however, that this does not mean that the respective

parameter is free of variation. Rather it means that the given dataset does not contain sufficient information to support the quantification of the variability.

In the sunitinib project the correlation of variance parameters was also explored by estimating the off-diagonal elements of the covariance matrix Ω:

$$\Omega = \begin{bmatrix} \omega_{P1}^2 & \\ \omega_{P1,P2} & \omega_{P2}^2 \end{bmatrix} \qquad \text{equation 3-7}$$

where ω_{P1}^2 and ω_{P1}^2 are the variances of the parameter P1 and P2 and $\omega_{P1,P2}$ their covariance. The correlation coefficient (ρ) for the variances of the two parameters P1 and P2 is then calculated according to:

$$\rho = \frac{\omega_{P1,P2}}{\sqrt{\omega_{P1}^2 \cdot \omega_{P2}^2}} \qquad \text{equation 3-8}$$

The estimation of a full covariance matrix is a numerically complex operation and often leads to unstable models (e.g., models that do not converge or are very sensitive to initial estimates). Therefore the estimation of off-diagonal elements of the covariance matrix was only considered when: (i) a scatter plot matrix of the empirical Bayes estimates indicated a strong correlation between random effects; (ii) the correlation was mechanistically/physiologically plausible; and (iii) inclusion into the model significantly improved the OFV.

Interoccasion Variability

Interoccasion variability was only applicable to the sunitinib project where observations from more than one study day were available. Guided by the principle of parsimony it was decided to test for interoccasion variability only on the mean transit time, a parameter describing the delayed absorption of sunitinib. This decision was based on the visual inspection of the observed concentration vs. time plots for each subject, where the delay in the absorption phase obviously differed in magnitude from one study day to the other, within the same individual.

Similar to interindividual variability, an exponential relationship was applied for modeling interoccasion variability:

$$MTT_{iq} = \theta_{MTT} \cdot e^{\eta_i + \kappa_q}$$ equation 3-9

where MTT_{iq} is the mean transit time for the i-th subject on the q-th study day and θ_{MTT} describes the average value of this parameter in the study population. A CV for the interoccasion variability was calculated according to equation 3-6.

Residual Variability

Three different commonly used residual error models were applied in this thesis to account for the discrepancy between model predictions ($\hat{y}_{ji}$) and observations (y_{ji}):

    a) the additive model

$$y_{ji} = \hat{y}_{ji} + \varepsilon_{add}$$ equation 3-10

    b) the proportional model

$$y_{ji} = \hat{y}_{ji} \cdot (1 + \varepsilon_{prop})$$ equation 3-11

    c) the combined model

$$y_{ji} = \hat{y}_{ji} \cdot (1 + \varepsilon_{prop}) + \varepsilon_{add}$$ equation 3-12

where ε_{add} and ε_{prop} are random quantities with mean 0 and variances σ^2_{add} and σ^2_{prop}, respectively. Hence, $100 \cdot \sqrt{\sigma^2_{prop}}$ represents the coefficient of variation of the residual error (in %) and $\sqrt{\sigma^2_{add}}$ its standard deviation (same unit as the observations). The additive error model can usually be applied if the assumption of homoscedasticy holds (i.e., constant variance independent of the magnitude of the measurement). This is often the case for PD data when the range of measured values is narrow (e.g., blood pressure). If, however, the measured values span several orders of magnitude (e.g., drug concentrations) the error usually increases proportionally with increasing values. The combined error model, often seen in PK models, merges the former two models, hence being the most flexible approach.

3.1.3   Model Evaluation and Goodness-of-Fit

The assessment of how good a model fits to a given set of data is important in all model-based data analyses. The agreement between observations and model predictions

is evaluated by numerical and graphical tools. In the following sections the evaluation techniques that were used in this thesis are described. Since some of these methods are very time-consuming (e.g., bootstrap, visual predictive checks) they were not routinely applied to every single intermediate model but were reserved for the evaluation of key models and final models.

3.1.3.1 Metrics of Model Assessment

Objective Function Value

The value of the objective function (see section 3.1.1, equation 3-3) is a routine NONMEM output and serves as a metric to discriminate between competing models. Since the difference of the objective function value of two models (ΔOFV) is approximately χ^2-distributed, parametric statistics can be applied to calculate a p-value for a given ΔOFV [5]. For example, if two models differ in the number of model parameters by one (degree of freedom [df] = 1) a ΔOFV of at least 3.84 would be necessary for the models to be significantly different from each other (p <0.05). This method is also known as the likelihood ratio test (LRT). Table 3-1 shows some commonly used levels of significance along with their associated ΔOFV for different degrees of freedom.

Table 3-1 ΔOFV for various levels of significance (α) and degrees of freedom assuming a χ^2-distribution

Degrees of freedom	α=0.05	α=0.01	α=0.001
1	3.84	6.64	10.83
2	5.99	9.21	13.82
3	7.81	11.34	16.27
4	9.49	13.28	18.47

It should be noted that the LRT is strictly only valid for nested models, i.e. if one model is a hierarchical simplification of another [5]. A one-compartment model, for example is nested within a two-compartment model, whereas it is not a direct simplification of a model with nonlinear Michaelis-Menten elimination. However, in this thesis the ΔOFV

was also used for the assessment of non-nested models, although in such cases the LRT was never a single criterion for the discrimination between competing models.

Epsilon Shrinkage

Karlsson and Savic recently pointed to a problem that occurs especially in situations when individual data are sparse and lack sufficient information about model parameters [92]. Then individual predictions (IPRED) will "shrink" towards the actual observation. Goodness-of-fit plots of observations vs. IPRED will then suggest "a perfect fit" although the model may be misspecified, rendering this type of diagnostics useless to assess the model fit. A measure of informativeness of the individual predictions is ε-shrinkage. It is calculated as $100 \times (1-\sigma_{IWRES})$, where σ_{IWRES} stands for the standard deviation of the individual weighted residuals (IWRES). When ε-shrinkage is high (>20%) individual data are sparse in information and diagnostic plots using IPRED are of limited use [92].

3.1.3.2   Bootstrap Method

The bootstrap method, first described by Efron, is commonly seen in population PK data analyses as a tool to assess the precision of parameter estimates by calculating their nonparametric confidence intervals [93]. The procedure is a resampling technique where a sufficiently large number of new datasets is generated by randomly sampling with replacement individuals out of the original dataset. Parameter estimates are then obtained for each bootstrap dataset and summary statistics can be applied to the distribution of these estimates. In this thesis, whenever this method was applied, 1000 bootstrap datasets were generated and each was evaluated using the respective PK or PD model. With the results from those estimation procedures (i.e., "runs") where NONMEM was able to calculate the variance-covariance matrix (i.e., a successful covariance step), the 5th and 95th percentiles of the parameter distribution were derived representing the lower and the upper bound of a nonparametric 90% confidence interval. The bootstrap analysis was performed with PsN (Perl speaks NONMEM, versions 2.2.3 to 2.3.1) [94].

3.1.3.3 Standard Goodness-of-Fit Plots

The graphical assessment of a model fit is very important to detect model misspecification and to discriminate between competing models, especially in situations when numerical methods are not reliable or not applicable. The following goodness-of-fit plots were routinely inspected after every NONMEM run:

- Observations vs. IPRED and population predictions (PRED)
- Weighted residuals (WRES) vs. PRED
- WRES vs. time (or time after dose)
- Individual weighted residuals (IWRES) vs. IPRED

IWRES are not a standard output of NONMEM but can be easily obtained as shown in equation 3-13 for a combined residual error model:

$$\text{IWRES}_{ji} = \frac{(\text{OBS}_{ji} - \text{IPRED}_{ji})}{\sqrt{\sigma_{add}^2 + \sigma_{prop}^2 \cdot \text{IPRED}_{ji}^2}} \qquad \text{equation 3-13}$$

where IWRES_{ji} is the ith IWRES for the jth subject, OBS the observation (e.g., concentration), σ_{add} is the standard deviation and σ_{prop} the coefficient of variation of the additive and proportional components of the residual error model, respectively (see residual variability in section 3.1.2).

For key models and the final models, PsN was used to calculate conditional weighted residuals (CWRES), which were then plotted against PRED or time. Unlike WRES, which were always calculated by a first-order linearization around the population mean of the random model parameters even though FOCE was used as estimation method, CWRES in contrast were calculated by linearization at each individual's Bayesian estimates. Therefore, CWRES were thought to be more appropriate for model diagnostics when FOCE was the estimation method [92,95]. All goodness-of-fit plots were generated using the software Xpose (versions 4.0.1 to 4.0.3) [96].

3.1.3.4 Visual Predictive Check

The visual predictive check (VPC) is a simulation-based diagnostic tool increasingly used in order to assess if simulations from a model resemble the observations with which the model was developed [92,97]. A VPC is further useful to graphically assess how model simulations compare with data which were not used for model building (e.g., external validation, comparison with literature).

For the preparation of the VPCs 1000 simulations were performed with the final models under the original study design (e.g., dose, dosing interval, sampling times). With the 5th and 95th percentiles of the simulated values a 90% prediction interval was constructed and plotted along with the observations and the median of the simulated values [98]. Ideally, the median of the simulations should reflect the central tendency of the observations without any systematic deviation. Variability is well captured by the model if, at every sampling time point, 5% of the observations are above (below) the 95th (5th) percentile of the simulations. It is therefore recommended to plot also the respective percentiles of the observations and compare these with those obtained from the simulations [97]. However, since the number of subjects in either project was only 12 (i.e., maximal 12 observations per time point), the 5th and 95th percentiles were not regarded meaningful and were not calculated.

In the sunitinib example simulated and observed values of the biomarkers were normalized to their respective baseline values.

All VPCs shown in this thesis were generated using PsN and Xpose.

3.1.3.5   Sensitivity Analysis

In order to assess the influence and appropriateness of fixed parameters (i.e., model parameters that were not estimated but fixed to some predefined value), sensitivity analyses were performed. That is, each fixed model parameter value was changed in steps of 10% from -50% to +50% of its original value. The results were assessed in terms of changes of the estimated parameters and the OFV with respect to the original run. Differing from this procedure, R, the value for the relative potency of O-desmethylvenlafaxine compared to venlafaxine and R_{sl}, the relative contribution of the transduced signal with respect to the immediate signal of sunitinib's effect on blood pressure were changed from 0 to 1.0 by a step size of 0.1. Similarly, the value of K_d, the dissociation constant used in the sunitinib PD models, was changed from 1 to 10 by a step size of 1. The fraction of sunitinib transformed to SU12662 (f_m) was varied from 0.1 to 0.9 by a step size of 0.1.

3.1.4   Simulations

Most simulations performed in this thesis were stochastic simulations, either to perform VPCs (see section 3.1.3.4), to compare the models with data from literature (see section

3.3.6.1), or to predict the outcome of a dose individualization study (see section 3.3.6.2). For this kind of simulation, also known as Monte Carlo simulation, a number of sets of model parameters are randomly sampled from a multivariate distribution, determined by the typical parameter values and their associated variability. For each set of parameters the model response (e.g., drug or biomarker concentrations) is then calculated. This method permits inference not only on the typical model response (e.g., average concentration-time profile) but also on the expected variability in a population. All stochastic simulations were performed with NONMEM, except for the dose individualization study which was done with the R software (version 2.7.2) [99].

Deterministic simulations were performed to assess the influence of the mean absorption time (MAT) of venlafaxine on the pupillographic response and the plasma concentrations of venlafaxine and its metabolite. For this, the model code and all typical parameter values were entered into the software Berkeley Madonna (version 8.3.14) and the average model response of the amplitude was simulated for different values of MAT without taking into account parameter variability.

3.1.5 Statistical Analyses

For the descriptive presentation of the data and the results, different measures of central tendency (median, arithmetic or geometric mean) and dispersion (standard deviation, variance, coefficient of variation) were employed as appropriate. Calculations were usually performed using Microsoft® Excel 2002 or the R software.

For the statistical analysis of the survival data generated in the clinical trial simulation (see section 3.3.6.2) a Cox proportional hazard model was used. This model is frequently used for the statistical comparison of time-to-event data from different treatment groups (e.g., drug A vs. placebo). "Treatment group" is included as a dichotomous covariate (0=control, 1=treatment) and related to the hazard rate (equation 3-14). The hazard rate may be interpreted as an instantaneous rate of death at any time t:

$$h(t) = h_0(t) \cdot e^{(b \cdot group)}$$

equation 3-14

where $h_0(t)$ is the hazard rate of the control group (note: when group=0 then exp(0)=1); b is a regression coefficient. The hazard ratio (HR) can than be calculated according to:

$$HR = \frac{h(t)}{h_0(t)} = e^{(b)}$$ equation 3-15

A HR <1 means that the treatment is associated with an increased survival compared to the control group, whereas a value >1 means decreased survival.

A statistical test often applied to survival data is the log-rank test. Under the null hypothesis that the risk of death in two groups is the same (i.e., survival is not different), the expected number of events per group at each observed event time in ranked order is calculated. From the sums of the observed and the expected events (deaths) of each group (A and B) a test statistic Z can be derived:

$$Z = \frac{(O_A - E_A)^2}{E_A} + \frac{(O_B - E_B)^2}{E_B}$$ equation 3-16

where O_A and O_B are the sums of the observed number of events and E_A and E_B are the sums of the expected number of events. Z approximately follows a χ^2-distribution from which a p-value can be calculated.

3.2 Venlafaxine Study

3.2.1 Study Description

The study was designed as a randomized, double-blind, placebo-controlled crossover trial. The subjects received either 37.5 mg venlafaxine twice daily (manufactured as Trevilor® tablets by Wyeth, Münster, Germany; to preserve blinding tablets were pulverized and filled into hard gelatine capsules by the Pharmacy of the University Hospital Dresden, Germany) or placebo from day 1 to 7. From day 8 to 14 they received either 75 mg venlafaxine twice daily or placebo. After a 14-day washout phase the two groups were crossed over according to the protocol. A scheme of the study design, including sampling times, is shown in Figure 3-1. Subjects were not allowed to smoke or to consume alcohol or caffeine containing beverages during the study. The study was conducted at the facilities of the Institute of Clinical Pharmacology at the Medical Faculty of the University of Dresden under supervision of Prof. Dr. Dr. W. Kirch and Prof. Dr. M. Siepmann.

3.2.2 Subjects

Twelve healthy male volunteers, ageing between 23 and 32 years (mean ± SD: 26 ± 3 years), weighing between 67 and 85 kg (75 ± 6 kg) and between 176 and 192 cm (183 ± 5 cm) in height, were enrolled in the study. The subjects were included after a standard physical examination, routine clinical laboratory tests and a 12-lead ECG. The study was conducted according to the Declaration of Helsinki (Edinburgh Amendment 2000) and German regulations. Written informed consent from the subjects and approval from the University Hospital Ethics Committee (Dresden, Germany) were obtained.

3.2.3 Blood Sampling

Blood samples were taken from a cubital vein on day 14 immediately before the last dose of venlafaxine or placebo was given as well as 0.5, 2, 3, 4, 5, 7, 8, 10, 12, 14, 18 and 24 hours afterwards (Figure 3-1). Blood was left to clot for 90 min at room temperature, followed by centrifugation. The serum samples were then stored at -20°C until analysis.
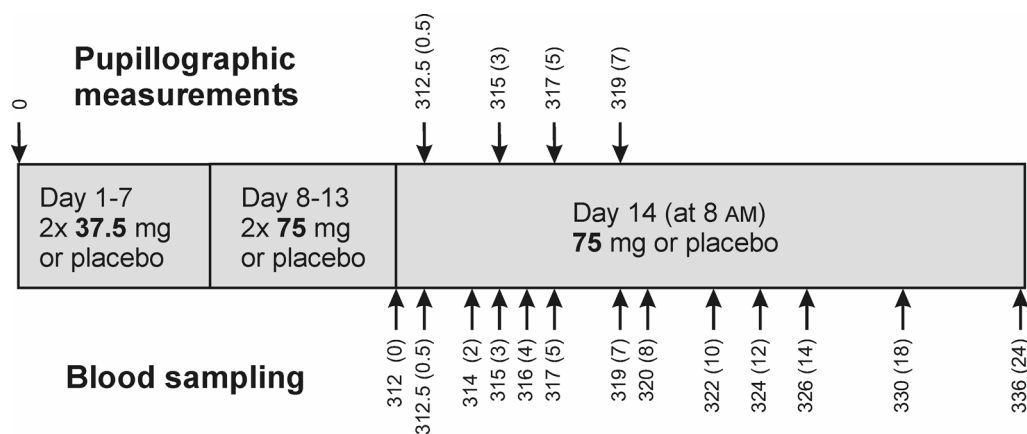
Figure 3-1 Scheduled time points of blood sampling and pupillographic measurement sessions. Time is given in hours. The numbers in parenthesis represent the time relative to dosing on day 14.

3.2.4   Analytical Methods

3.2.4.1   Determination of Venlafaxine and O-Desmethylvenlafaxine Concentrations

Concentrations of venlafaxine and O-desmethylvenlafaxine in serum were measured with a validated high-performance liquid chromatography assay with fluorescence detection at the Institute of Clinical Pharmacology at the Medical Faculty of the University of Dresden by Dr. Reinhard Oertel. The procedure was validated according to previously published method descriptions [100-102]. The lower limit of quantification was 28.1 nmol/L for venlafaxine and 29.6 nmol/L for O-desmethylvenlafaxine. Coefficients of variation expressing precision and relative errors expressing analytical accuracy ranged from 2.9 to 10.1% and from -3.1 to 3.1% for venlafaxine and from 2.6 to 5.7% and -6.0 to 4.6% for O-desmethylvenlafaxine, respectively.

3.2.4.2   Pupillography

Measurement of pupillary light reflex was done before the first dose on day 1 and 0.5, 3, 5, 7 hours after the last dose on day 14 of every treatment period (Figure 3-1). An infrared monocular pupillographic camera device (CIP™, AMTech, Weinheim, Germany) was used for recording of the pupillary light reflex. The procedure was described in more detail elsewhere [103]. In brief, in a shaded room a light flash of

200 ms duration was used to provoke miosis of the subject's pupil. The light-induced constriction and subsequent redilatation of the pupil was recorded by the camera device. The amplitude and 33% recovery time as response parameters were subject to the present analysis.

3.2.5 Pharmacokinetic Model

For the simultaneous estimation of venlafaxine and its major metabolite O-desmethylvenlafaxine a PK model previously described by Taft et al. [104] was adapted. This model includes a liver compartment accounting for the presystemic formation of O-desmethylvenlafaxine via the CYP2D6 enzyme system. According to a similar model developed for artemisinin [105], which also includes a liver compartment, the hepatic plasma flow (Q_H) was fixed to 0.63 L/h × body weight (in kg) and the volume of the liver compartment to 1 L. Different models describing the absorption phase were explored: first- and zero-order absorption with and without a time-lag parameter, as well as a system of serial transit compartments, previously reported for modeling the absorption kinetics of cyclosporine [106,107]. Mathematically this is a special case of the distribution function f(t) shown in equation 3-17:

$$f(t) = \frac{k_{tr}^N}{\Gamma(N)} \cdot t^{N-1} \cdot e^{(-k_{tr} \cdot t)}$$
equation 3-17

where N is the number of transit compartments, k_{tr} the transfer rate constant and $\Gamma(N)$ represents the gamma function of N. When N is an integer number the function f(t) is known as Erlang distribution function. The number of transfer compartments was set equal for all subjects and was estimated by successively introducing an additional transfer compartment into the model until the objective function value (OFV) did not improve anymore. The mean absorption time (MAT) was calculated as N/k_{tr}.

In principle, the fraction of venlafaxine metabolized to O-desmethylvenlafaxine (f_m) and the volume of distribution of venlafaxine (V_{VEN}) are not separately identifiable in the absence of data for other routes of elimination (e.g., concentrations in urine/feces). This was accounted for by fixing the volume of distribution of O-desmethylvenlafaxine (V_{ODV}) to 210 L a value that was reported in a previous study where O-desmethylvenlafaxine was administered intravenously to healthy subjects [107].

An exponential variance model was used to describe interindividual variability in the PK parameters except for f_m. Since this parameter is naturally constrained to lie between 0 and 1 a logit model was applied [108]:

$$f_{m,i} = \frac{1}{1 + e^{-\ln(f_{m,pop}/(1-f_{m,pop})) - \eta_i}}$$

<div align="right">equation 3-18</div>

$f_{m,i}$ denotes the parameter estimate for individual i, $f_{m,pop}$ is the typical value for f_m in the population and η_i represents a random quantity with mean 0 and variance ω^2. The coefficient of variation of the interindividual variability in $f_{m,pop}$ can be approximated by equation 3-19:

$$CV\% = (1 - f_{m,pop}) \cdot \omega \cdot 100$$

<div align="right">equation 3-19</div>

where ω denotes the standard deviation of η_i.

The residual variability for venlafaxine and O-desmethylvenlafaxine was estimated by two separate error models. Each error model consisted of a proportional and an additive component (i.e., a combined error model).

3.2.6   Pharmacodynamic Models

Prior to the model building, plots of pharmacodynamic effect vs. active concentration were generated to get a first impression of the behavior of the pharmacodynamic system. Based on preclinical data O-desmethylvenlafaxine was assumed to be half as potent as venlafaxine in inhibiting norepinephrine uptake [109]. Thus the active concentration was calculated as $0.5 \times C_{ODV} + C_{VEN}$. Different values for the relative potency of O-desmethylvenlafaxine were however tested as part of a sensitivity analysis.

Different structural pharmacodynamic models were explored: Linear and log-linear models, simple and sigmoid E_{max} models [8], indirect response models [110] and different kinds of tolerance models (see model development summary in Table 9-2 in the appendix) [9,111-117].

The interindividual variability in the PD parameters was described by an exponential error model. Additive, proportional and combined error models were tested for modeling the residual variability in the amplitude and the 33% recovery time.

3.2.7 Optimal Study Design and Simulations

The final PK/PD model for the amplitude (see section 4.1.2) was introduced in the D-optimal design software WinPOPT (version 1.2). The program evaluates the Fisher information matrix (FIM) of a given nonlinear mixed effects model and uses the determinant of this matrix as the optimization criterion (D-optimal). Since the inverse of the FIM is the covariance matrix of the model parameters, maximizing the determinant of the FIM results in improved precision of the parameter estimates (i.e., smaller standard errors) [118]. Two algorithms are available in the software, the exchange algorithm and simulated annealing. In this thesis only the exchange algorithm was used. On each iteration a single sampling time was exchanged with one from a list of possible sampling times (0.5, 1, 1.5, 2, 2.5, 3, 4, 5, 6, 7, 8, 9, 10, 11, 12 hours) that provides the same or a better value of the determinant of the FIM. Possible designs with 4 to 8 samples per subject were evaluated and the expected standard errors of the pharmacodynamic parameters as well as the determinant of the FIM were recorded. The baseline measurement at time 0 hours was always included and not subject to optimization. The number of subjects was always 12, receiving a single dose of 75 mg venlafaxine, except for the scenario with 5 sampling times, which was also evaluated for 24 subjects. The sampling times for a possible extended release formulation were calculated by setting the mean absorption time to 4 hours.

To numerically compare the different study designs, the relative efficiency (E_{rel}) was calculated according to:

$$E_{rel}(\%) = 100 * \sqrt[k]{\frac{D_{FIM,alternative}}{D_{FIM,reference}}} \qquad \text{equation 3-20}$$

where k is the number of evaluated model parameters, $D_{FIM,alternative}$ and $D_{FIM,reference}$ are the determinants of the FIMs for an alternative design and the reference design, respectively. The sampling schedule of the original venlafaxine study described in section 3.2.4.2 was applied to a single-dose study and chosen as the reference design (i.e., sampling at 0, 0.5, 3, 5, 7 hours).

To determine the influence of the venlafaxine formulation on the pharmacodynamic response, different values of mean absorption time (1, 2, 4, 8 hours) were used to simulate the typical response profile after a single dose of 75 mg.

3.3   Sunitinib Study

3.3.1   Study Description

The study was approved by the ethics committee of the Medical Faculty of the University of Cologne, Germany, and was conducted according to the Declaration of Helsinki and corresponding European and international guidelines. It was divided in a first part with 4 participants taking capsules containing 50 mg sunitinib (Sutent[®]; Pfizer Inc.) on each of 3 consecutive days (at 8:00 AM) and a later, second part with 8 subjects and drug administration on 5 consecutive days. Before the first drug administration subjects had to stay at the study site for 24 hours to evaluate possible diurnal changes of the drug-free (i.e., baseline) biomarker response. The rest of the study was conducted in an ambulatory manner at the facilities of the Department of Pharmacology of the Hospital of the University of Cologne under supervision of Prof. Dr. Uwe Fuhr.

3.3.1.1   Sampling Schedule

Blood samples were drawn on the day before the first dose was administered (day 0) at 8:00 AM, noon, 4:00 PM, 8:00 PM, midnight, 4:00 AM and 8:00 AM. After the first dose was given, blood sampling for the determination of plasma biomarker concentrations (i.e., VEGF-A, VEGF-C, soluble VEGFR-2) as well as sunitinib and SU12662 concentrations was carried out at 1, 2, 4, 6, 8, 10, 12, 24, 25, 36, 48, 49, 60, 72, 96, 120, 240, 288, 336, and 384 hours. In the second part additional blood sampling was performed 0.5, 24.5, 48.5, 72.5, 73, 84, 96.5, 97, 98, 100, 102, 104, 106, 108, 144, 168, and 432 hours after the first dose. Figure 3-2 provides a schematic representation of the dosing and sampling schedule. The samples were collected in EDTA tubes and immediately centrifuged for 15 min at 4 °C with 780 g in the first part and 1000 g in the second part of the study.
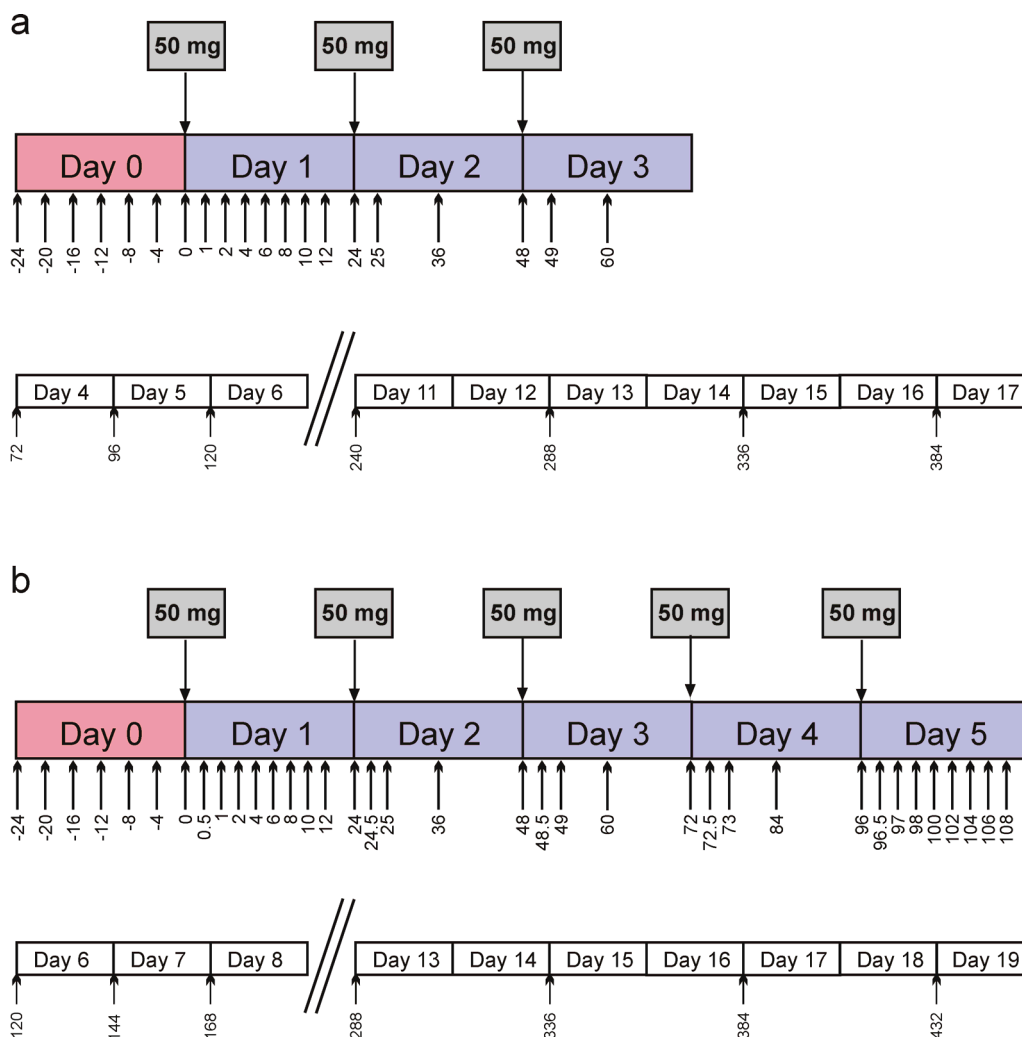
Figure 3-2   Blood sampling schedule in the first (**a**) and second (**b**) study part. Grey boxes indicate dosing events. Sampling times are given in hours relative to the first dosing event.

3.3.2   Subjects

Six healthy males and six healthy females (Caucasian, nonsmokers), ageing between 27 and 54 years (mean ± SD: 40 ± 5.5 years), weighing between 60 and 90 kg (72 ± 10.8 kg) and between 163 and 192 cm (175 ± 8 cm) in height, were included. All subjects gave their written informed consent prior to their participation.

3.3.3   Analytical Methods

3.3.3.1   Determination of Sunitinib and N-Desethylsunitinib

Sunitinib and SU12662 concentrations in human plasma were determined by high-performance liquid chromatography coupled with mass spectrometry (LC-MS/MS, Applied Biosystems/MDS Sciex API5000 LC/MS/MS) by Dr. Martina Kinzig at the Institute for Biomedical and Pharmaceutical Research (IMBP) under supervision of Prof. Dr. Fritz Sörgel. The method used d_5-sunitinib as an internal standard which was synthesized by Dr. Paul Elsinghorst under supervision of Prof. Dr. Michael Gütschow at the Institute of Pharmacy at the University of Bonn [119]. The response from calibration standards of sunitinib and SU12662 was linear from 0.06 to 100 ng/mL. The lower limit of quantification for plasma samples was 0.06 ng/mL for both analytes. Coefficients of variation (CV) expressing precision and relative errors (RE) expressing analytical accuracy ranged from 1.0 to 5.3% and +0.9 to +5.6% for sunitinib and from 2.9 to 3.9% and −2.2 to +3.9% for SU12662, respectively.

3.3.3.2   Determination of VEGF-A, VEGF-C and sVEGFR-2

Plasma concentrations of VEGF-A, VEGF-C and sVEGFR-2 were determined using commercially available enzyme-linked immunosorbent assay kits from R&D Systems (Minneapolis, USA). All assays were validated by the manufacturer for their use with plasma samples. The qualification of these assays, in terms of precision and accuracy, and the determination of biomarker levels in the samples were performed by Friederike Kanefendt and Cathleen Krambeer at the Institute of Pharmacy at the University of Bonn. Table 3-2 compares the precision and accuracy of the assays determined "in-house" to the manufacturer specifications. The detailed analytical procedure is described in the diploma thesis of Krambeer [120].

Table 3-2   Intra-assay precision and accuracy of the immunoassays

	Precision (CV)		Accuracy (RE)	
	Manufacturer	In-house	Manufacturer	In-house
VEGF-A (QuantiGlo®)	2.8 - 7.9%	1.5 - 6.4%	-2 - 10%	0.5 -15.3%
VEGF-C (Quantikine®)	3.5 - 6.6%	2.7 - 6.1%	-4 - 10%	-17.1 to -6.8%
sVEGFR-2 (Quantikine®)	2.9 - 4.2%	2.2 - 4.3%	-8 - 4%[a]	– [b]

a Determined in cell culture media.
b Could not be reliably determined in plasma.

CV: coefficient of variation; RE: relative error.

Accuracy of the sVEGFR-2 assay was not established in plasma by the manufacturer and failed to be reliably determined "in-house". Nevertheless, results obtained with this assay are valid as long as relative changes of this biomarker and not absolute values are of interest.

3.3.3.3   Blood Pressure

Blood pressure was measured with an automated device (Dinamap; Criticon, Tampa, USA) shortly before blood sampling and after the subjects had been resting for at least 5 min in a supine position.

3.3.4   Pharmacokinetic Model

Sunitinib and SU12662 pharmacokinetics were simultaneously estimated using a model that accounted for systemic and presystemic formation of the metabolite. The fraction of parent drug converted to metabolite (f_m) was set to 21%, a value previously reported [121].

Given that:

$$f_m = f_{m,pre} + (1 - f_{m,pre}) \cdot f_{m,sys}$$ equation 3-21

the ratio of the fraction formed presystemically ($f_{m,pre}$) to the fraction formed systemically ($f_{m,sys}$) is:

$$RPS = \frac{f_{m,pre}}{f_{m,sys}}$$ equation 3-22

Under the condition that $f_{m,pre}$, $f_{m,sys}$ and f_m are always <1 the above equations can be solved for $f_{m,pre}$, allowing the RPS being estimated as primary parameter:

$$f_{m,pre} = 0.5 + 0.5 \cdot RPS - 0.5 \cdot \sqrt{1 + 2 \cdot RPS + RPS^2 - 4 \cdot RPS \cdot f_m}$$ equation 3-23

The unknown bioavailability of sunitinib is the product of the fraction of a dose that is absorbed from the gut (f_a) and the fraction not metabolized presystemically (1- $f_{m,pre}$). Since no PK information from intravenously administered sunitinib was available f_a could not be estimated and was fixed to 1.

Like in the venlafaxine project, it was explored if the inclusion of a transit compartment model of absorption would improve the fit [122]. However, differing from the procedure described in section 3.2.5 the number of transit compartments was not

constrained to an integer value but was estimated as a model parameter. For both sunitinib and SU12662 one and two distribution compartments were tested. The residual variability was estimated separately for sunitinib and SU12662 using a combined error model.

3.3.5   Pharmacodynamic Models

For all biomarkers, possible diurnal baseline changes were evaluated by one or two cosine functions based on data from the 24 hours before the first dose was given (day 0). First, it was tested if a model describing time-dependent baseline values improved the model fit with data from day 0 only. In the affirmative, it was included in the PD model and was only retained if it also significantly improved the model fit on the whole dataset.

To describe the concentration-effect relationship of the different biomarkers a mechanism-based approach was applied, linking the drug-specific part (i.e., drug-receptor interaction) to the biological system-specific part (i.e., biomarker signal) with a unique transducer function for each biomarker (Figure 3-3). Danhof et al. extensively reviewed this approach in a recent publication [123].

Since for sunitinib and SU12662 equal potency has been reported [62], the active moiety used in the model was the sum of unbound sunitinib and SU12662 concentrations (active unbound concentration, AC_{ub}). To calculate the AC_{ub} 95 and 90 % protein binding were assumed for sunitinib and SU12662, respectively [59].

The drug-specific part was described by a simple hyperbolic function (Figure 3-3 and equation 3-24) relating the AC_{ub} to the fractional tyrosine kinase inhibition (INH):

$$INH = \frac{AC_{ub}}{K_d + AC_{ub}}$$ equation 3-24

The dissociation constant K_d was fixed to 4 ng/ml. Mendel et al. [124] reported this value for the VEGF-dependent inhibition of VEGFR-2 tyrosine kinase phosphorylation by sunitinib *in vitro*. Different transducer functions (e.g., linear, hyperbolic, power) relating the INH to the measured biomarker signal were explored during model development.
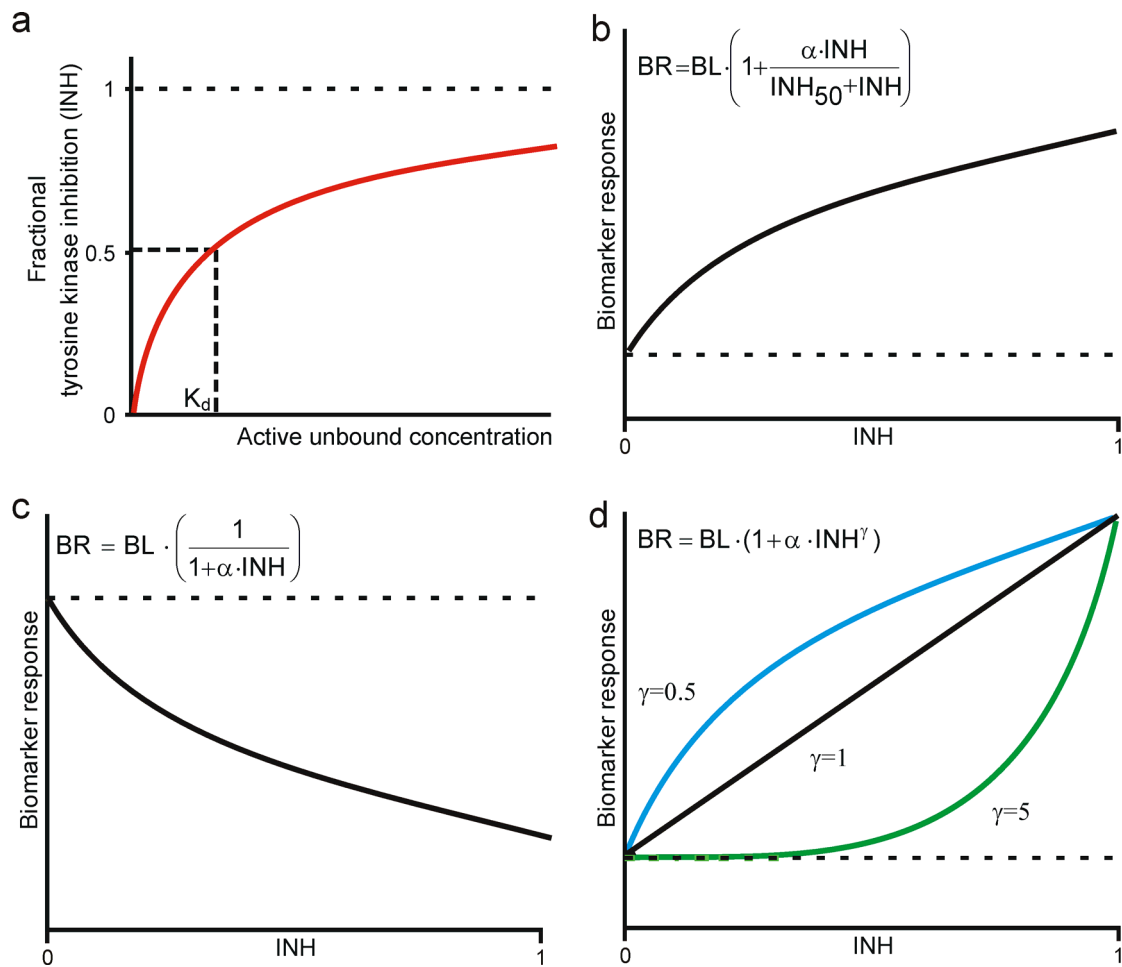
Figure 3-3 Relationship between drug concentration and biomarker response in a mechanism-based pharmacodynamic model. The drug-specific tyrosine kinase inhibition (**a**) is linked to the system-specific biomarker response by a transducer function. **b** Hyperbolic relationship, **c** inverse linear relationship, **d** power function. Note that when γ equals 1 the relationship is linear. The dotted line represents the baseline value of the biomarker.

K_d: dissociation constant; BR: biomarker response; BL: baseline; α: intrinsic activity parameter; INH_{50}: INH that elicits 50% of the maximal biomarker response; γ: exponent of the power function.

Increasing systolic and diastolic blood pressure values were modeled simultaneously each with a separate additive residual error model. Because of the simultaneous mechanisms of action that are discussed for this effect (see section 1.4.2) [87], it was tested if the inclusion of a second, slower mechanism could improve the model fit.

A possible time delay in VEGF-A response relative to drug concentration was tested for by including a transduction component in the model [125]. Differences in VEGF-A levels between subjects in the first part and the second part of the study, caused by two

different centrifugation speeds at which plasma samples were generated, were accounted for by including the study part as a covariate on baseline VEGF-A levels (BL_{VEGF-A}, equation 3-25):

$$BL_{VEGF-A,PART1} = BL_{VEGF-A} \cdot \theta_{PART1}^{IND} \qquad \text{equation 3-25}$$

where θ_{PART1} represents a factor adjusting for systematic differences in VEGF-A concentrations between the two study parts and IND is an indicator variable taking a value of 1 for subjects in the first part and 0 otherwise.

Changes in sVEGFR-2 concentrations were described by an indirect response model [110] with the INH affecting the zero-order release rate (K_{in}) of this biomarker. Proportional residual error models were applied for VEGF-A and sVEGFR-2.

3.3.6   Simulations

3.3.6.1   Comparison with Literature

To compare predictions from the pharmacodynamic models with previously reported biomarker data, 1000 individuals receiving a typical sunitinib treatment (1 cycle: 50 mg/day over 4 weeks, then 2 weeks off treatment) were simulated. Two treatment cycles were simulated to compare predicted blood pressure with blood pressure vs. time profiles from a study in 7 normotensive patients with metastatic renal cell carcinoma (mRCC) [74]. To compare model-predicted variability with the standard deviations (SD) shown in the original graph, a 68% prediction interval (approximately equal to the interval embraced by ±1 SD) of the simulated data was calculated.

Four cycles were simulated for the comparison of predicted changes in circulating biomarkers with the biomarker response reported in studies with patients suffering from breast cancer [75], mRCC [76,77], and gastrointestinal stromal tumor (GIST) [78].

For all simulations the final model parameter estimates were used, except that the mean systolic and diastolic baseline blood pressure values were set to 120 and 72.3 mmHg (the baseline values from the Azizi-study [74]), respectively, to compensate for baseline differences between the subjects in the present study and the patients in the report.

The biomarker data were graphically extracted from biomarker vs. time plots in the above mentioned publications using the measurement tool included in Adobe Acrobat Pro, version 9.1.2 (Adobe Systems, San Jose, USA).

3.3.6.2 Clinical Trial Simulation: Dose Individualization Based on Blood Pressure Increase

To explore the hypothesis that dose adjustments based on individual blood pressure measurements could be beneficial in terms of clinical outcome, various clinical trial scenarios were simulated comparing a standard dose group with a group where the dose was adjusted based on individual blood pressure measurements. Since the present study was conducted in healthy volunteers, a model for clinical outcome could obviously not be developed with the data at hand. However, such a model relating sunitinib exposure (i.e., AUC) to an outcome measurement (overall survival) has recently been published by Houk et al. [126] They used a parametric Weibull distribution function (equation 3-26) to describe the survival data of 146 patients with mRCC.

$$S(t) = e^{\left[-\ln 2 \cdot \left(\frac{t}{\varphi} \right)^{\gamma} \right]} \qquad \text{equation 3-26}$$

where S(t) is the survival function giving the proportion of patients alive at time t, γ is a shape parameter and φ is the median survival time, modeled as a function of exposure: φ=baseline+slope×exposure. The following parameter estimates were reported by Houk et al. and used for the simulations in the present thesis: γ: 1.78, baseline: 110 days, slope: 485 days/mg·h/L. The probability of dying in an interval of length t_{inter} is calculated by multiplying the hazard rate h(t) with t_{int} as shown in the following equation [127]:

$$P(\text{death})_{int} = h(t) \cdot t_{int} = \frac{PDF(t)}{S(t)} \cdot t_{int} = \ln 2 \cdot \frac{\gamma}{t} \cdot \left(\frac{t}{\varphi} \right)^{\gamma} \cdot t_{int} \qquad \text{equation 3-27}$$

where PDF(t) is the probability density function of the survival function from equation 3-26 at time t. As a measurement of exposure they used the average daily steady-state AUC of sunitinib during a treatment cycle (AUC_{daily}) calculated according to equation 3-30 (the authors stated that similar results were obtained using the AUC of the total drug [sunitinib+metabolite], in their final model, however, they only used the AUC_{daily} of sunitinb).

During the treatment with sunitinib patients often suffer from side effects with fatigue being the most dominant in clinical practice. Severe fatigue often requires a dose reduction and should therefore be considered in a realistic simulation scenario. A

logistic regression model relating the frequency of grade 3 or 4 fatigue (according to Common Terminology Criteria for Adverse Events of the National Cancer Institute version 3.0) to sunitinib exposure was developed by the Pharmacometrics Department of the FDA during the approval process of sunitinib [128]. Their analysis included data from 516 patients with different tumor types who were treated with sunitinb in clinical trials. According to this report, the probability of occurrence of grade 3/4 fatigue P(fatigue) is related to the sum of sunitinib and SU12662 exposure (AUC_{sum}) as shown in equation 3-28:

$$P(\text{fatigue}) \quad = \frac{1}{1 + e^{-(0.5144 \cdot AUC_{sum} - 3.2164)}} \qquad \text{equation 3-28}$$

From the above equation it can be calculated that for each unit increase of AUC_{sum} the probability of occurrence of severe fatigue increases 1.7-fold (i.e., odds ratio). This model only predicts the total probability of experiencing severe fatigue during the entire study duration and not the incidence of fatigue in one treatment cycle. This, however, was important to properly simulate dose reduction events per cycle. Assuming that the risk of suffering from fatigue is the same in every treatment cycle, P(fatigue) can be split into smaller probabilities of equal size. The 516 patients used in the FDA analysis were treated for approximately 17 cycles, thus the probability of having a fatigue event in one cycle P(fatigue,cyc) is:

$$P(\text{fatigue,cyc}) = 1 - \sqrt[17]{1 - P(\text{fatigue})} \qquad \text{equation 3-29}$$

Houk et al. showed in their analysis that the risk of experiencing fatigue increases during the treatment with sunitinib, reaching a maximum probability (plateau) already after one treatment cycle [126]. Thus, assuming equal probability of fatigue in every cycle (including the first one) may only produce a minor overestimation of the occurrence of fatigue.

From the final PK and blood pressure model (see section 4.2.1 and 4.2.2.1) individual parameters were simulated for 75 virtual patients per treatment group. The individual clearance of sunitinib ($CL/F_{sunitinib}$) and SU12662 ($CL/f_{a,SU12662}$) were used to calculate AUC_{daily} (equation 3-30) and AUC_{sum} (equation 3-31). The fraction of the dose converted to SU12662 was fixed to 0.21 as described in section 3.3.4.

$$AUC_{daily} = \frac{Dose}{CL / F_{sunitinib}} \cdot \frac{days\ on\ treatment\ (28)}{total\ days\ per\ cycle\ (42)}$$

equation 3-30

$$AUC_{sum} = \frac{Dose}{CL / F_{sunitinib}} + \frac{f_m \cdot Dose}{CL / f_{a,SU12662}}$$

equation 3-31

To calculate diastolic blood pressure at steady state, first the active unbound concentration at steady state was calculated according to equation 3-32:

$$AC_{ub}^{ss} = f_{ub,sunitinib} \cdot \frac{Dose}{CL / F_{sunitinib} \cdot 24} + f_{ub,SU12662} \cdot \frac{f_m \cdot Dose}{CL / f_{a,SU12662} \cdot 24}$$

equation 3-32

The fractional tyrosine kinase inhibition at steady state (INH_{ss}) was then calculated as previously shown in equation 3-24. After 28 days of treatment not only the pharmacokinetic system can be assumed to having reached equilibrium but also the pharmacodynamic system. The time-delay component included in the final blood pressure model was therefore not considered in these simulations and diastolic blood pressure at day 28 was calculated from the final blood pressure model (equation 4-6), setting the immediate signal and the transduced signal both equal to INH_{ss}. It was further assumed that blood pressure measurements were always performed at the same time of day and circadian variations in diastolic blood pressure were not taken into account. Since diastolic and systolic blood pressure are highly correlated and diastolic blood pressure is closely related to vascular resistance, only the diastolic value was considered in this simulation study.

The study duration in the virtual trials was 960 days (20 treatment cycles). The cycle length was 6 weeks (42 days) according to the approved 4-weeks-on/2-weeks-off treatment schedule. At the end of every 4-weeks-on treatment period a "clinical assessment" was scheduled where diastolic blood pressure and the probabilities of death and severe fatigue were calculated for every individual based on the current dose he received. The individual probabilities of death or experiencing fatigue in a given cycle were used to generate a dichotomous variable with a value of 1 for "alive" or "fatigue" and 0 for "dead" or "no fatigue". For example, if the probability of experiencing fatigue for a given individual was 0.10, a random draw from a virtual urn containing 10 balls

marked "fatigue" and 90 balls marked "no fatigue" was made. In mathematical terms, this is sampling at random from a binomial distribution. Figure 3-4 illustrates the treatment schedule.
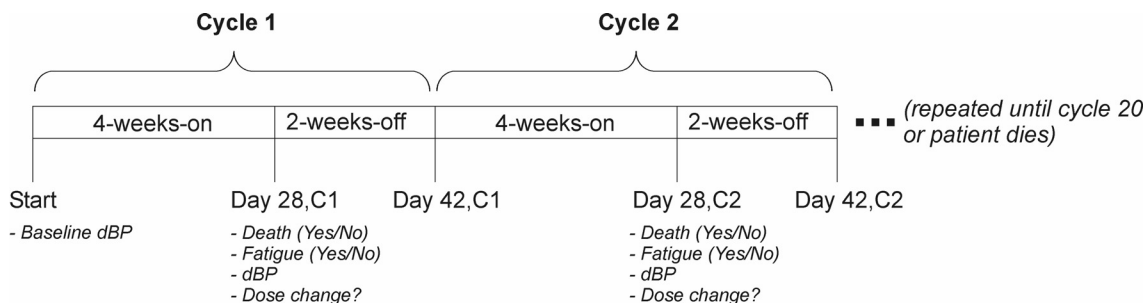
Figure 3-4 Treatment schedule used for the virtual trial. Whether a patient died or experienced fatigue since the last assessment was calculated from the individual probabilities as explained in the text. The dose for the next cycle was changed according to the algorithm shown in Figure 3-5.

dBP: diastolic blood pressure.

Then a decision was made if and how the dose should be adjusted for the subsequent cycle. The starting dose for both groups was 50 mg/day and, in accordance with the Sutent® prescribing information [129], dose adjustments were only allowed between 25 mg/day and 87.5 mg/day. In both groups the dose was reduced by 12.5 mg if severe fatigue occurred. In the individualized dose group the dose was augmented by 12.5 mg if the increase in diastolic blood pressure (relative to the pretreatment value) did not reach a predefined target.

Initially, a 16% increase in diastolic blood pressure was chosen as a target, corresponding to an INH_{ss} of 0.55. However, other target values ranging from 11.6% to 20.3% were also explored (see below). To make the simulations more realistic, it was also considered that the rise in blood pressure may reach values demanding intervention with an antihypertensive drug. This was assumed to occur when the simulated diastolic blood pressure was greater than 100 mmHg. In this case, no further dose increment was allowed for the rest of the study. Dose reductions, however, remained possible. This treatment algorithm for the individualized dose group is illustrated in Figure 3-5.
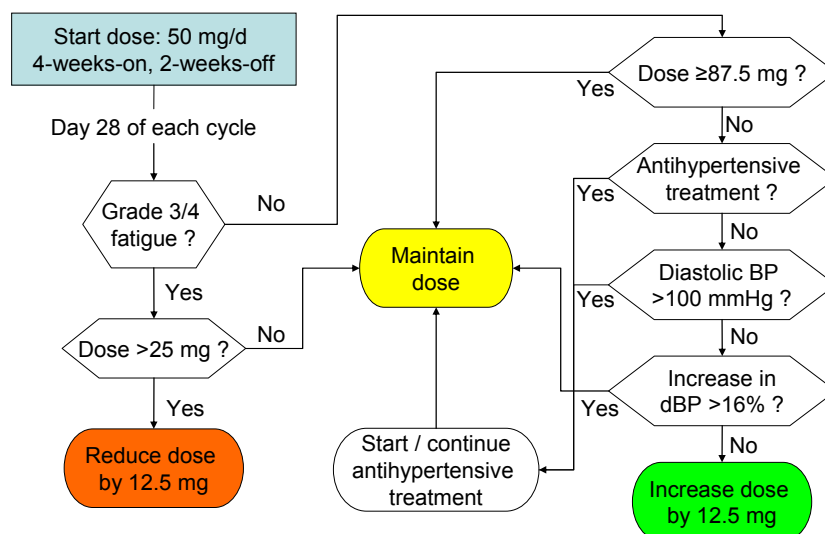
Figure 3-5   Treatment algorithm used for the simulation of a clinical trial with blood pressure controlled dose adjustments.

dBP: diastolic blood pressure.

The following modifications of the initial study design were also investigated:

- Different number of patients per group (25, 50, 100, 150, 200, 250)
- Different target values for the increase in diastolic blood pressure (11.6%, 13.0%, 14.5%, 17.4%, 18.9%, 20.3%; corresponding to INH_{ss} values of 0.40, 0.45, 0.50, 0.60, 0.65, 0.70)

Median time to death and frequency of severe fatigue were recorded as outcome parameters of the simulated trials. Each scenario was repeatedly simulated 500 times. In each of the 500 trial replicates a Cox proportional hazard model was applied to calculate the hazard ratio and the log-rank p-value, analyzing the difference in the median time to death (i.e., overall survival) between the two groups. The statistical power to detect a significant difference between the two groups was then calculated as the percentage of trial replicates with p <0.05. The 2.5th and 97.5th percentiles of the distribution of an outcome parameter across the trial replicates were derived, representing the lower and the upper bound of a 95% confidence interval. The last dose level a patient received at the end of the study (or at the time of his death) and the frequency of antihypertensive treatment was also recorded.

The simulations were performed with R (version 2.7.2) [99]. The code can be found in the appendix (Code 9-8).

4 Results

4.1 Venlafaxine Study

4.1.1 Pharmacokinetic Model

Plasma concentration-time data of venlafaxine and its metabolite were successfully described by a model with one-compartment disposition for both analytes (Figure 4-1). Inclusion of additional disposition compartments did not improve the model fit. The absorption process described by a system of 3 transit compartments was superior to other tested absorption models, including first- and zero-order absorption with and without a lag-time parameter. The application of an absorption model where the number of transit compartments is an estimable parameter (like in the sunitinib project) was not feasible in the present analysis due to excessive NONMEM runtimes.

Important steps of the model development are summarized in Table 9-1 in the appendix.
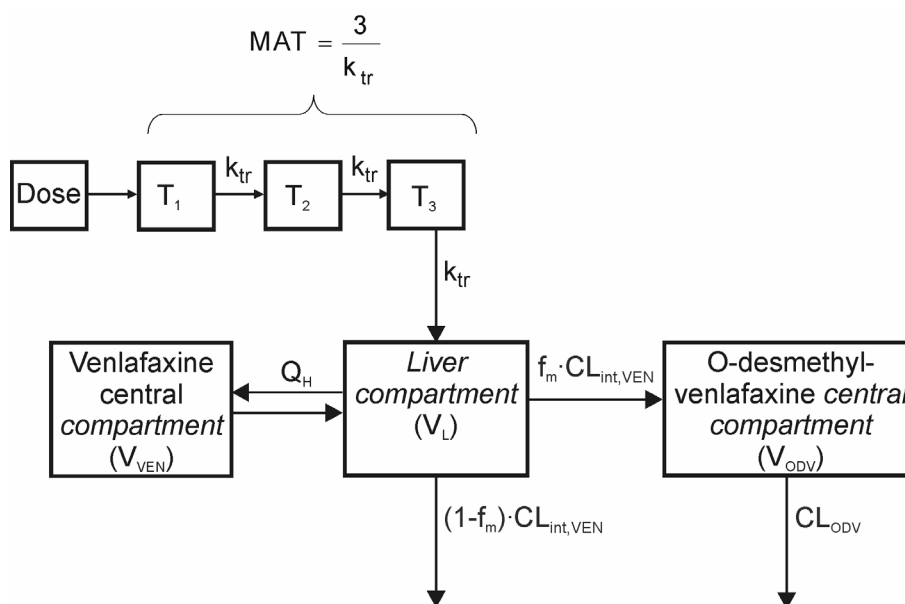
Figure 4-1 Pharmacokinetic model for the simultaneous prediction of venlafaxine and O-desmethylvenlafaxine concentrations. After oral administration venlafaxine passes the 3 transit compartments of absorption (T_1, T_2, T_3) and enters the liver where it is metabolized to O-desmethylvenlafaxine.

k_{tr}: transit rate constant; MAT: mean absorption time; V_{VEN}: volume of distribution of venlafaxine's central compartment; V_{ODV}: volume of distribution of O-desmethylvenlafaxine's central compartment; V_L: volume of the liver compartment; f_m: fraction of venlafaxine metabolized to O-desmethylvenlafaxine; $CL_{int,VEN}$: intrinsic clearance of venlafaxine; CL_{ODV}: clearance of O-desmethylvenlafaxine; Q_H: liver plasma flow.

Although it was previously shown, that about 5% of venlafaxine is renally excreted [50,130], this fact was neglected during the model building process, since the introduction of a renal clearance parameter did not improve the model fit. The model performed well in terms of precision of the parameter estimates, as suggested by the relatively narrow bootstrap confidence intervals (Table 4-1). Only $CL_{int,VEN}$ and its interindividual variability showed a wider confidence interval. This is likely due to the fact that one subject had a very high clearance of venlafaxine compared to the population mean (652 L/h vs. 99.9 L/h). It was only possible to estimate interindividual variability in MAT, $CL_{int,VEN}$, and f_m. Inclusion of more variability parameters did not improve the model fit (see summary of the model development in Table 9-1 in the appendix). This is not uncommon in nonlinear mixed-effects modeling when the number of subjects is small while the number of model parameters is high.

Table 4-1 Pharmacokinetic parameter estimates and bootstrap confidence intervals

Parameter	Estimate (90% CI)	IIV, CV% (90% CI)
V_{VEN} (L)	178 (164 - 203)	-
$CL_{int,VEN}$ (L/h)	99.9 (69.9 - 150)	94.8 (46.1 - 146.4)
f_m	0.746 (0.613 - 0.855)	34.5 (20.4 - 47.5)
CL_{ODV} (L/h)	17.7 (16.8 - 18.9)	-
MAT (h)	1.03 (0.843 - 1.24)	38.9 (17.0 - 50.9)
$\sigma_{prop,VEN}$ (%)	18.5 (12.2 - 29.7)	-
$\sigma_{add,VEN}$ (nmol/L)	26.4 (10.0 - 38.6)	-
$\sigma_{prop,ODV}$ (%)	8.86 (6.51 - 11.9)	-
$\sigma_{add,ODV}$ (nmol/L)	54.8 (20.8 - 79.3)	-

IIV: interindividual variability; CV: coefficient of variation; V_{VEN}: venlafaxine's volume of distribution; $CL_{int,VEN}$: intrinsic clearance of venlafaxine; f_m: fraction of venlafaxine metabolized to O-desmethylvenlafaxine; CL_{ODV}: clearance of O-desmethylvenlafaxine; MAT: mean absorption time; σ_{prop}: proportional residual variability (CV); σ_{add}: additive residual variability (standard deviation).

The sensitivity analysis (Figure 9-5, appendix) revealed that changing the value of Q_H caused V_{VEN} to vary between 110 and 228 L but led at the same time to higher OFVs compared to the original run. Setting the QH at a value hat corresponds to the hepatic blood flow (1.2 L/h × bodyweight) resulted in an estimate of V_{VEN} of 258 L and an increase of the OFV by 12 units. Varying the volume of the liver compartment from 0.5

to 1.5 L did neither affect the parameter estimates nor the OFV (Figure 9-6, appendix). When changing the fixed value for V_{ODV} the OFV increased and the estimates for CL_{ODV} and f_m varied between 9 to 21 L/h and 0.34 to 0.87, respectively (Figure 9-7, appendix).

The visual predictive checks for venlafaxine and O-desmethylvenlafaxine are shown in Figure 4-2. The majority of the observations were located within the prediction interval and there is no systematic misspecification.
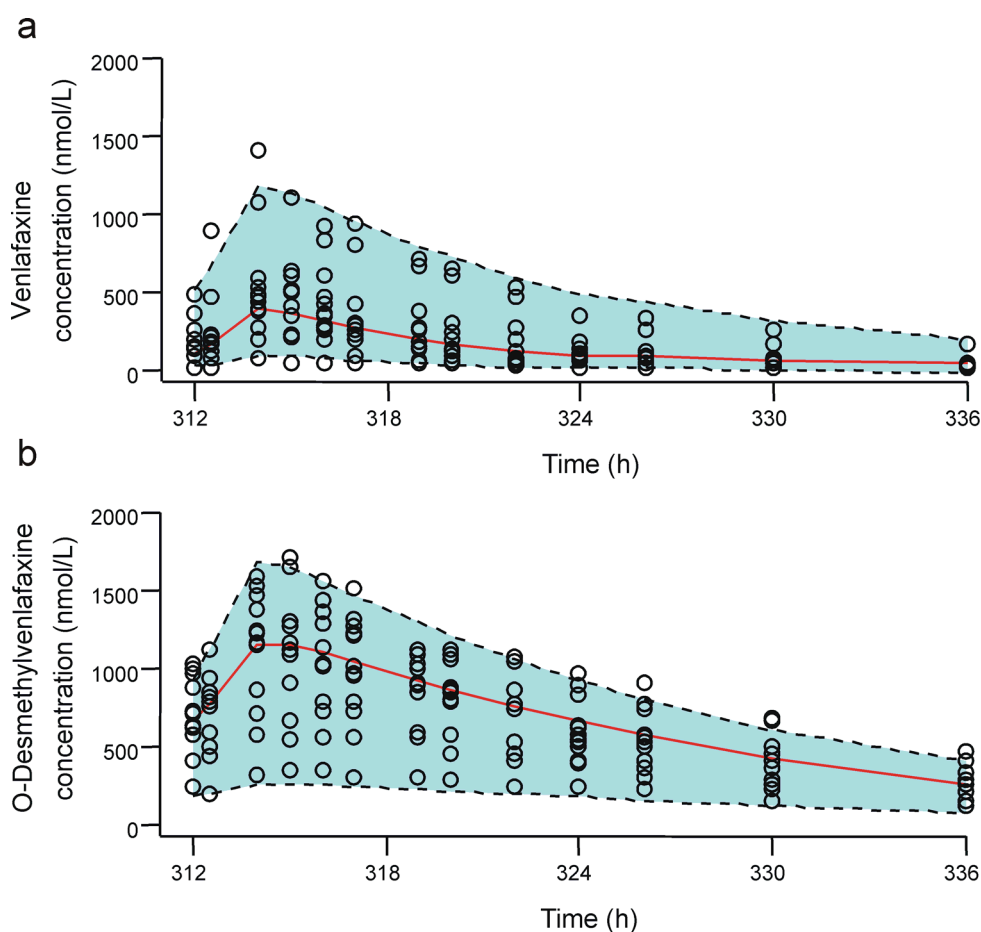
Figure 4-2 Visual predictive check for (**a**) venlafaxine and (**b**) O-desmethylvenlafaxine. The 5th and 95th percentiles (dashed lines) and the median (solid red line) obtained from 1000 simulations are shown together with the actual observations (black circles).

The goodness-of-fit plots shown in the appendix (Figure 9-1 and Figure 9-2) also demonstrate that the model described the data reasonably well. No obvious model misspecification was detected.

The NONMEM code of the PK model is provided in the appendix (Code 9-1).

Table 4-2 compares pharmacokinetic parameters calculated with the present model with values previously reported in the literature.

Table 4-2 Comparison of estimated pharmacokinetic parameters with literature values

Parameter[a]	NONMEM[b] n=12	Effexor® Prescribing Information[46][c]	Klamerus et al.[51][c] n=18	Troy et al.[130][c] n=18
V_{VEN}/F/BW (L/kg)	8.0 (65.9%)	7.5 (49.3%)	8.1 (37.0%)	8.3 (47.0%)
$CL_{int,VEN}$/BW (L/h/kg)	1.3 (97.0%)	1.3 (46.1%)	1.73 (56.1%)	2.1 (67.3%)
V_{ODV} /f_m/BW (L/kg)	4.5 (44.7%)	5.7 (31.5%)	4.6 (23.9%)	6.0 (61.7%)
CL_{ODV}/f_m/BW (L/h/kg)	0.4 (44.7%)	0.4 (50.0%)	0.3 (21.9%)	0.4 (41.7%)

a   Estimates were normalized to body weight (BW) for comparison reasons only.
b   Values are expressed as geometric mean (geometric coefficient of variation, CV) and were
     calculated from individual Bayes estimates.
c   Values are expressed as arithmetic mean (CV).

V_{VEN}: venlafaxine's volume of distribution; F: bioavailability; $CL_{int,VEN}$: intrinsic clearance of venlafaxine; f_m: fraction of venlafaxine metabolized to O-desmethylvenlafaxine; V_{ODV}: O-desmethylvenlafaxine's volume of distribution; CL_{ODV}: clearance of O-desmethylvenlafaxine.

Mean parameter values were very similar to previous findings except for the variability in $CL_{int,VEN}$ which strongly depends on the composition of the study population in terms of their metabolic performance. For the purpose of comparability, the pharmacokinetic parameters in Table 4-2 are presented per kg of body weight. Since exponential models were used in this study to describe the interindividual variability in the parameters this study, the geometric means and associated coefficients of variations are presented.

The hepatic extraction ratio of venlafaxine (E_H) can be calculated as follows:

$$E_H = \frac{CL_{int,VEN}}{(Q_H + CL_{int,VEN})}$$
equation 4-1

resulting in a value of 68% (for a person weighing 75 kg).

The fraction of venlafaxine metabolized to O-desmethylvenlafaxine (f_m) was estimated to be 75% with an interindividual variability of 35% (CV). Results from a mass balance study with radioactive marked venlafaxine showed that at least 60% of absorbed venlafaxine is transformed to O-desmethylvenlafaxine [50].

4.1.2 Pharmacodynamic Models

There was no clear hint from the placebo period of this trial (Figure 4-3 **b** and **d**) - nor from other studies investigating the effects of various antidepressants (i.e., venlafaxine, paroxetine, desipramine and reboxetine) on pupillary light reflex for up to six weeks - that this measure varies over time without administration of active drug [58]. The data from the placebo period of the present study were therefore not further considered in the analysis.

Shortly after administration of the drug, the amplitude was found to be decreased and the 33% recovery time was reduced compared to their respective baseline values (Figure 4-3 **a** and **c**).
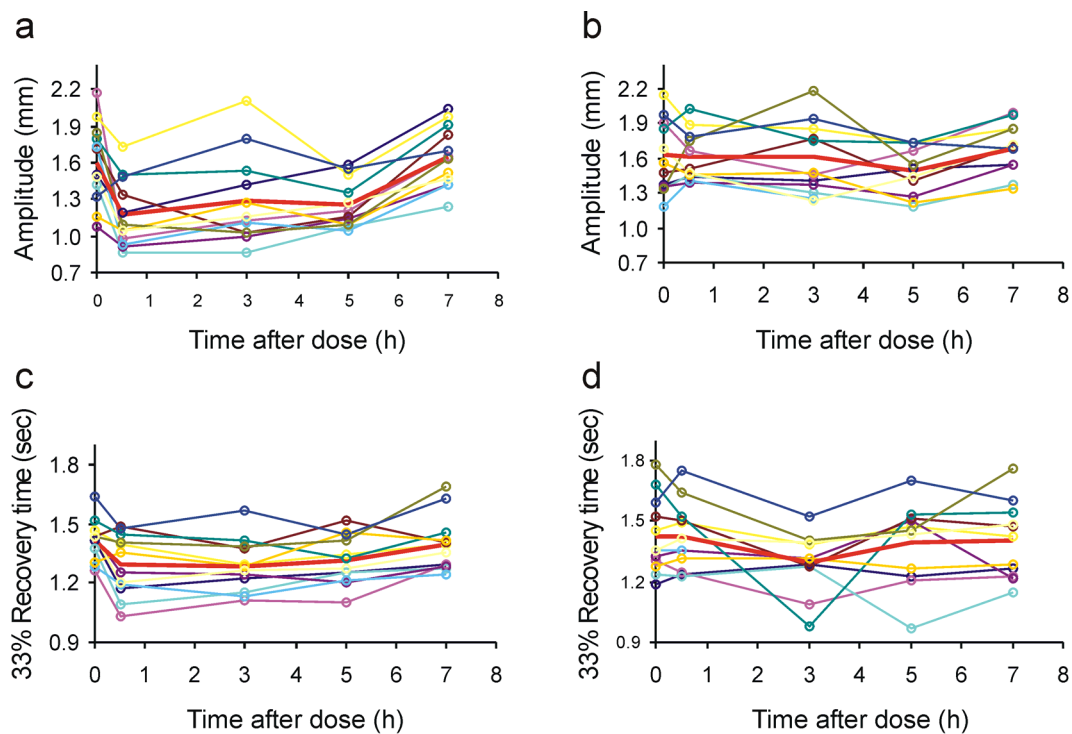
Figure 4-3   Individual time course of the amplitude and 33% recovery time after administration of venlafaxine (**a** and **c**) and during the placebo period (**b** and **d**). The thick red line represents the mean response.

The maximum decrease in the amplitude and the maximum reduction of the 33% recovery time were estimated to occur about 1 hour after administration, whereas the peak concentration of the active drug was about 2-3 hours after administration.

In Figure 4-4 the mean amplitude and the mean 33% recovery time are plotted against mean plasma concentrations of the active moiety. A decrease of the effect over time, despite equal plasma concentrations, can be seen. This phenomenon is known as proteresis and is indicative of the development of acute tolerance to the drug regarding the amplitude and the 33% recovery time.
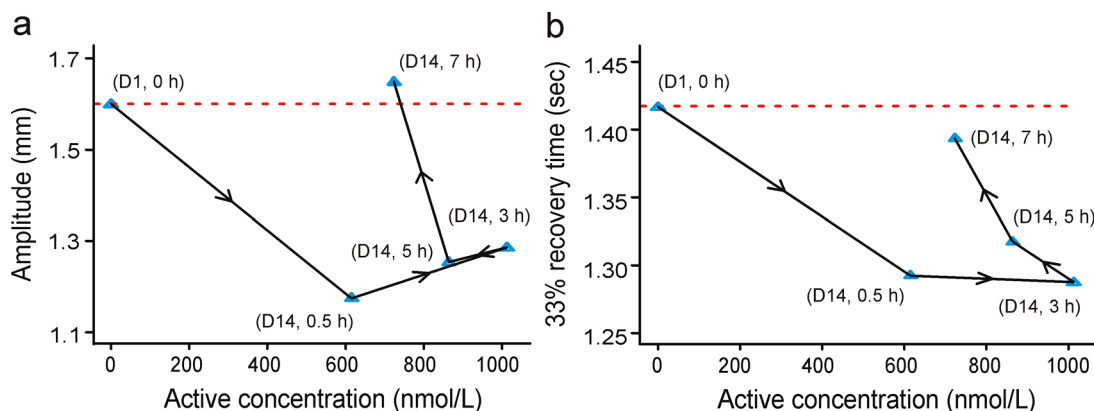
Figure 4-4   Mean pharmacodynamic effect vs. mean plasma concentration (blue triangles) of the active moiety (i.e., $C_{VEN} + 0.5 \times C_{ODV}$) for (**a**) amplitude and (**b**) 33% recovery time. The arrows represent the progression of time, the red dotted lines indicate the mean baseline effect. The sampling times are also shown.

D1: Day 1; D14: day 14.

This behavior was best described by a modified version of a model that Porchet et al. [116] used for the analysis of the effect of nicotine on the heart rate. The same model was used for the amplitude and the 33% recovery time. Other PD models that were tested (linear and log-linear models, simple and sigmoid E_{max} models, indirect response models and different kinds of tolerance models) did not converge successfully and/or resulted in imprecise parameter estimates and higher OFVs (see summary of the model development in Table 9-2 and Table 9-3 in the appendix).

The model is similar to the effect compartment model developed by Sheiner et al. [131], including an additional compartment, referred to here as the "tolerance" compartment. In this tolerance compartment, a hypothetical mediator M is generated, which acts as a contrary force opposing the effects of venlafaxine and O-desmethylvenlafaxine. The rate of change of the concentration of the mediator (C_M) in the tolerance compartment can be expressed as in equation 4-2:

$$\frac{dC_M}{dt} = k_{1tol} \cdot (R \cdot C_{ODV} + C_{VEN}) - k_{tol0} \cdot C_M \qquad \text{equation 4-2}$$

where R is the relative potency of O-desmethylvenlafaxine (fixed to 0.5); k_{1tol} is the first-order rate constant at which the concentration of M in the tolerance compartment rises, driven by the concentration of venlafaxine and O-desmethylvenlafaxine; and k_{tol0} is the rate constant at which the concentration of M declines.

Since k_{1tol} and k_{tol0} are not separately identifiable they were set equal ($k_{1tol}=k_{tol0}=k_{tol}$). Thus k_{tol} describes the rate of appearance or disappearance of tolerance, whichever is the slower process, and represents the delay in the development of tolerance. Finally, the observed effect (E, amplitude or 33% recovery time) is described by a linear relationship:

$$E = BL - S_E \cdot (R \cdot C_{ODV} + C_{VEN}) + S_T \cdot C_M \qquad \text{equation 4-3}$$

where BL denotes the baseline effect, S_E is the slope (i.e., the potency) of the drug effect model and S_T is the slope of the tolerance model. Note that S_E and S_T contribute with different signs to the overall effect. Model parameters were precisely estimated as shown in Table 4-3.

The visual predictive checks for the amplitude and the 33% recovery time are shown in Figure 4-5. The majority of the observations were located within the prediction interval. No systematic misspecification was seen for the 33% recovery time. The amplitude however, tended to be slightly underestimated at later time points after administration of the drug. Goodness-of-fit plots shown in the appendix (Figure 9-3 and Figure 9-4) support this finding.

The NONMEM codes of the final model for the amplitude and the 33% recovery time are also provided in the appendix (Code 9-2 and Code 9-3).

The sensitivity analysis (Figure 9-8 and Figure 9-9 in the appendix) showed that when setting R at values of 0 to 0.4, the OFV and the residual variability in both the amplitude and the 33% recovery time increased. Values of R between 0.6 and 1 affected neither the OFV nor the residual variability relevantly. Fixing R at 1, that is, assuming equal potency of venlafaxine and O-desmethylvenlafaxine, reduced the estimates for the S_E and S_T by about 20%, while the k_{tol} changed by only about 10%. Thus fixing R at 0.5 is not supposed to introduce much bias in the parameter estimates.

Table 4-3   Parameter estimates and bootstrap confidence intervals for pharmacodynamic model

Parameter	Estimate (90% CI)	IIV, %CV (90% CI)
Amplitude		
$BL_{amplitude}$ (µm)	1600 (1490 - 1740)	11.6 (5.79 - 15.6)
S_E (µm·L/nmol)	1.86 (1.48 - 2.54)	-
S_T (µm·L/nmol)	1.52 (1.32 - 2.13)	-
K_{tol} (1/h)	1.38 (0.74 - 2.53)	-
$t_{1/2tol}$ (min)	30.1 (16.4 - 56.2)	-
σ_{prop} (%)	16.2 (13.4 - 17.8)	-
33% Recovery time		
$BL_{recovery}$ (msec)	1420 (1370 - 1470)	6.80 (4.54 - 8.46)
S_E (msec·L/nmol)	0.497 (0.372 - 0.834)	-
S_T (msec·L/nmol)	0.376 (0.256 - 0.695)	-
k_{tol} (1/h)	1.04 (0.631 - 2.00)	-
$t_{1/2tol}$ (min)	40.0 (20.8 - 65.9)	-
σ_{prop} (%)	4.97 (3.99 - 5.76)	-

IIV: interindividual variability; CV: coefficient of variation; BL: baseline value; S_E: slope of the effect model; S_T: slope of the tolerance model; k_{tol}: rate constant of development or disappearance of tolerance (i.e., tolerance delay); $t_{1/2tol}$: half-life of development or disappearance of tolerance (=$ln2/k_{tol}$); σ_{prop}: proportional residual variability (CV).
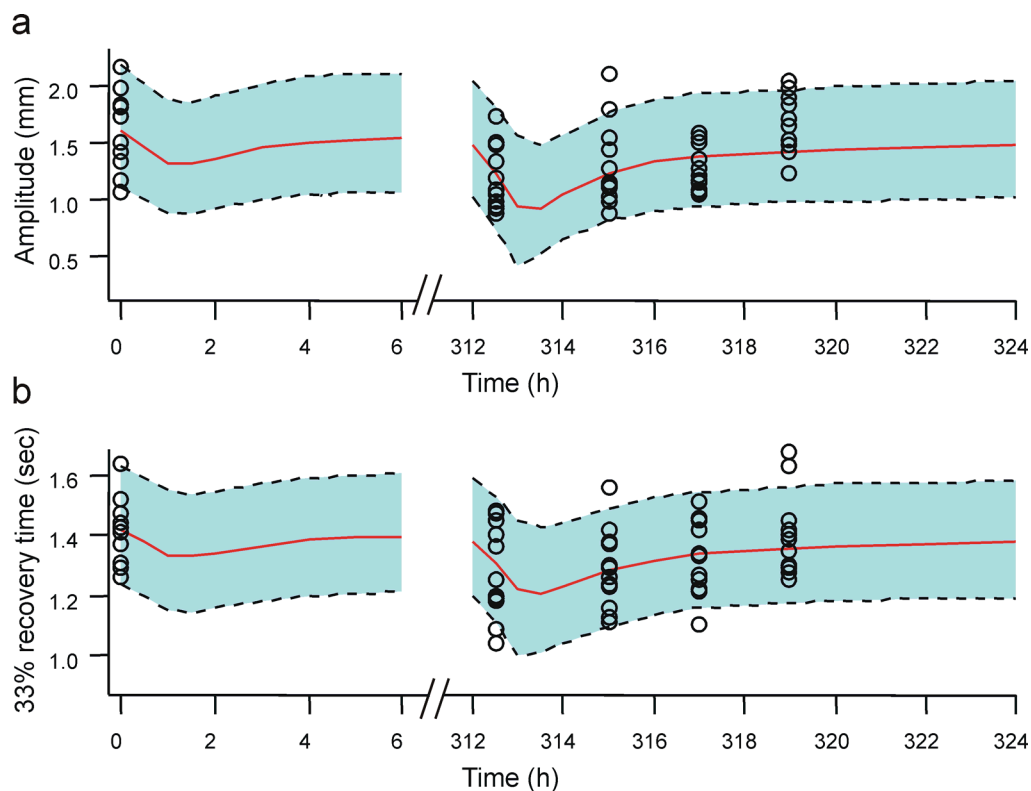
Figure 4-5 Visual predictive checks for (**a**) amplitude and (**b**) 33% recovery time. The open circles are the observations. The 5th and 95th percentiles (dashed lines) and the median (solid red line) obtained from 1000 simulations are shown together with the actual observations (black circles). Note the break in the x-axes.

4.1.3 Optimal Study Design

All tested sampling schedules for a possible single-dose study on the pupillographic response (amplitude) to immediate-released venlafaxine were more efficient than the reference design and the original sampling design with sampling at steady state (Table 4-4). The original design of the venlafaxine study, with samples obtained at steady state, was only marginally superior to the single-dose reference design which used the same sampling times relative to dosing. The predicted relative standard errors (RSE) of the fixed effects parameters for optimized schedules with 5 to 8 measurements per subject were lower than 20%. Even a design with only 4 pupillographic measurements per subject would be approximately 19% more efficient and would result in more precise parameter estimates than the reference schedule with 5 samples.

Table 4-4   Predicted performance of different sampling schedules

Number of Samples	Sampling times	Predicted relative standard errors (%)					
		BL	S_E	S_T	k_{tol}	IIV(BL)	E_{rel} (%)
5	0, 0.5, 3, 5, 7 *(Reference design)*	3.44	28.5	33.0	25.9	42.3	100.0
5	0, 312.5, 315, 317, 319 *(original sampling times, dosing at 312 h)*	3.44	27.4	31.9	24.9	42.4	104.8
8	0, 0.5, 1.5, 2.5, 3, 5, 6, 7	3.43	15.0	16.5	14.4	41.6	150.6
7	0, 0.5, 1.5, 2.5, 3, 5, 6	3.43	15.6	16.9	15.4	41.7	144.3
6	0, 0.5, 1.5, 3, 5, 6	3.43	16.0	17.6	17.0	41.7	137.1
5	0, 0.5, 1.5, 3, 6	3.43	16.2	17.8	17.8	41.8	126.6
4	0, 2, 3, 6	3.44	19.0	21.1	20.8	42.1	119.2
5 (24 subj.)	0, 0.5, 1.5, 3, 6	2.43	11.5	12.6	12.6	29.6	253.2
5 (MAT=4)	0, 2, 5, 11, 12	3.44	46.8	56.0	43.5	42.0	63.2

BL: baseline value; S_E: slope of the effect model; S_T: slope of the tolerance model; k_{tol}: rate constant of development and disappearance of tolerance; IIV(BL): interindividual variability in BL; E_{rel}: relative efficiency of a sampling schedule with respect to the original schedule, MAT: mean absorption time.

The baseline response (BL) would be precisely estimated (RSE: <4%) in all designs, since this parameter is mostly determined by the measurement at 0 hours. The precision with which the interindividual variability in BL can be estimated depends on the number of subjects studied. Doubling the number of subjects to 24 reduced the predicted RSE of the IIV(BL) from 42% to 30% and would be two-times more efficient. As might have been expected, optimal sampling times for an extended release formulation were at later time points than for an immediate release formulation. However, in this scenario pharmacodynamic parameters (except BL) would be estimated with only poor precision (RSE: >40%).

4.1.4   Influence of the Absorption Time on the Response

A slower absorption (i.e., longer MAT) had a considerable impact on the typical response vs. time profiles. Figure 4-6 shows how different values of the MAT influence the plasma concentration-time curves of venlafaxine and O-desmethylvenlafaxine.
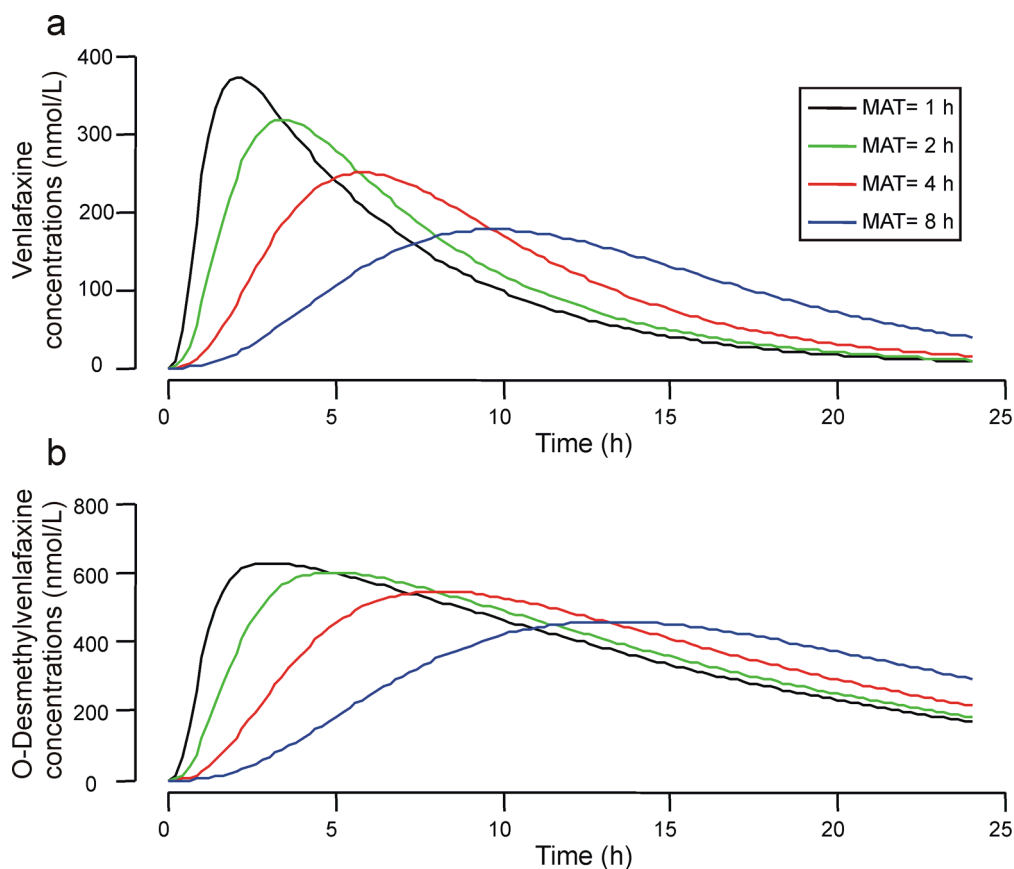
Figure 4-6   Typical concentration-time profiles of venlafaxine (**a**) and O-desmethylvenlafaxine (**b**) simulated with different values of the mean absorption time (MAT). The liberation rate of an extended release formulation of venlafaxine approximately corresponds to a MAT of 4 to 8 hours.

Changes in the concentration-time profile of the drug directly affect the pharmacodynamic response parameters (Figure 4-7). Obviously, the longer the MAT the smaller is the peak response and that the maximum response is shifted towards later time points.
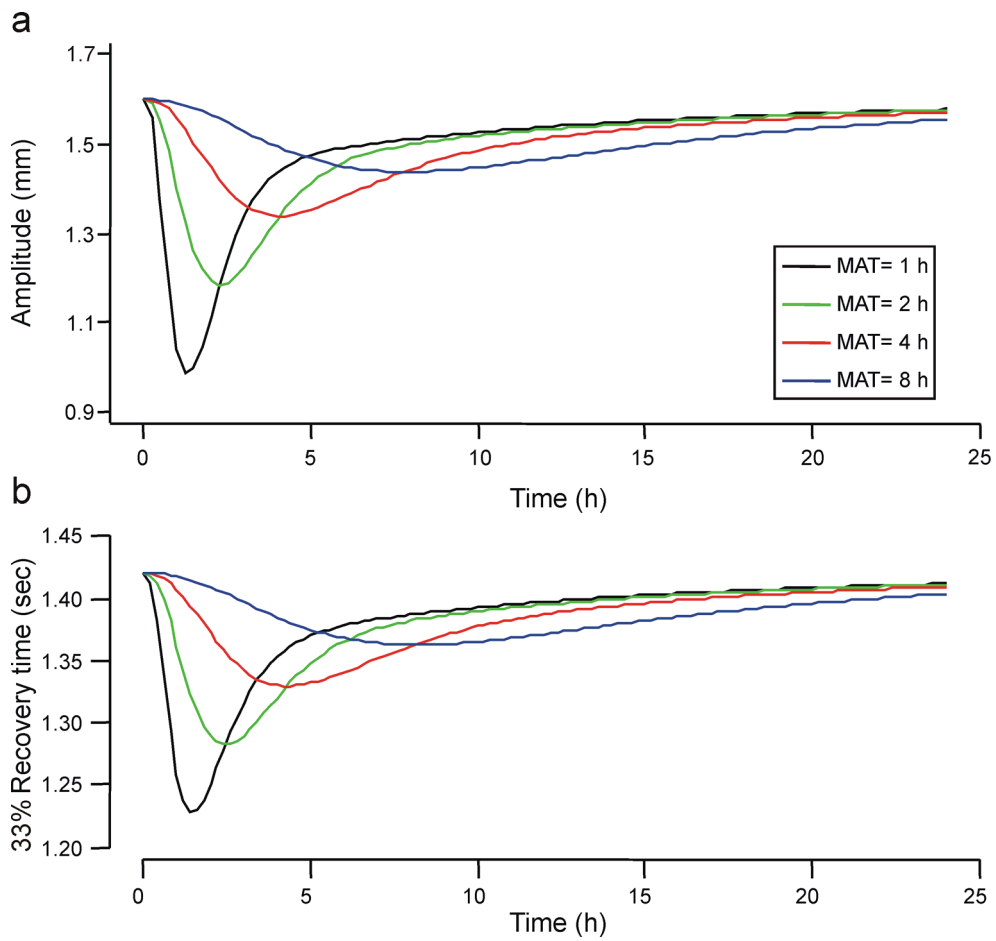
Figure 4-7   Typical amplitude (**a**) and 33% recovery time (**b**) response simulated with different values of the mean absorption time (MAT). The liberation rate of an extended release formulation of venlafaxine approximately corresponds to a MAT of 4 to 8 hours.

4.2 Sunitinib Study

4.2.1 Pharmacokinetic Model

The final pharmacokinetic model (Figure 4-8) included a one- and two-compartment disposition for SU12662 and sunitinib, respectively. Inclusion of the second disposition compartment for sunitinib reduced the objective function value (OFV) significantly by 114 units (p <0.001), whereas an additional compartment for SU12662 did not improve the model fit. Important steps of the model building process are summarized in Table 9-4 in the appendix.

$$MTT = \frac{N+1}{k_{tr}}$$
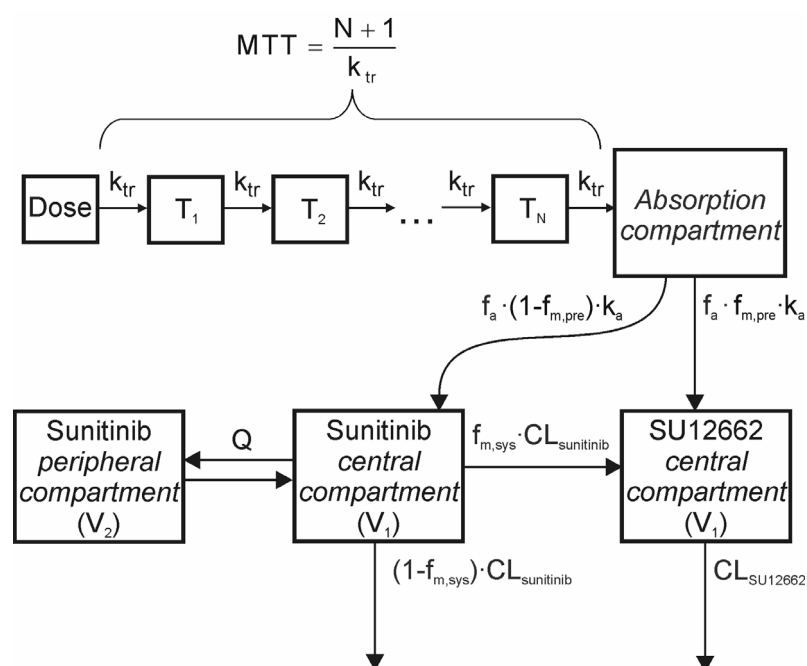
Figure 4-8 Pharmacokinetic model for the simultaneous prediction of sunitinib and SU12662 concentrations. After oral administration sunitinib passes the transit compartments T_1 to T_N mimicking delayed absorption. The number of transit compartments (N) and the mean transit time (MTT) were estimated as model parameters. The transit rate constant (k_{tr}) is a secondary parameter. From the absorption compartment sunitinb enters systemic circulation unchanged or is metabolized to its major active metabolite SU12662. f_a is the fraction of drug that is absorbed from the gut; $f_{m,pre}$ and $f_{m,sys}$ are the fractions of sunitinib metabolized to SU12662 either systemically or presystemically.

CL: clearance; Q: intercompartmental clearance; V: volume of distribution.

Random effects of apparent volumes and clearances for both sunitinib and SU12662 were all highly correlated and estimation of covariances between these parameters significantly reduced the objective function (ΔOFV: 91 units, p <0.001). The ratio of presystemic to systemic metabolite formation was 1.91, indicating that metabolite

formation is mainly attributable to a first-pass effect. Accounting for delayed absorption with a system of transit compartments considerably improved the fit compared to a model with immediate first-order absorption (ΔOFV: 564 units). Although the estimation of the interindividual variability in the mean transit time had no impact on the fit, inclusion of interoccasion variability in this parameter reduced the OFV by 74 units. The sensitivity analysis (Figure 9-16, appendix) showed that setting f_m to different values had no important influence on the OFV or estimated model parameters - except, of course, on the volume of distribution and the clearance of SU12662, demonstrating that these parameters are not separately identifiable.

No systematic misspecification was evident from the VPCs for sunitinib and SU12662 plasma concentrations (Figure 4-9) or from the goodness-of-fit plots (Figure 9-10 and Figure 9-11, appendix).
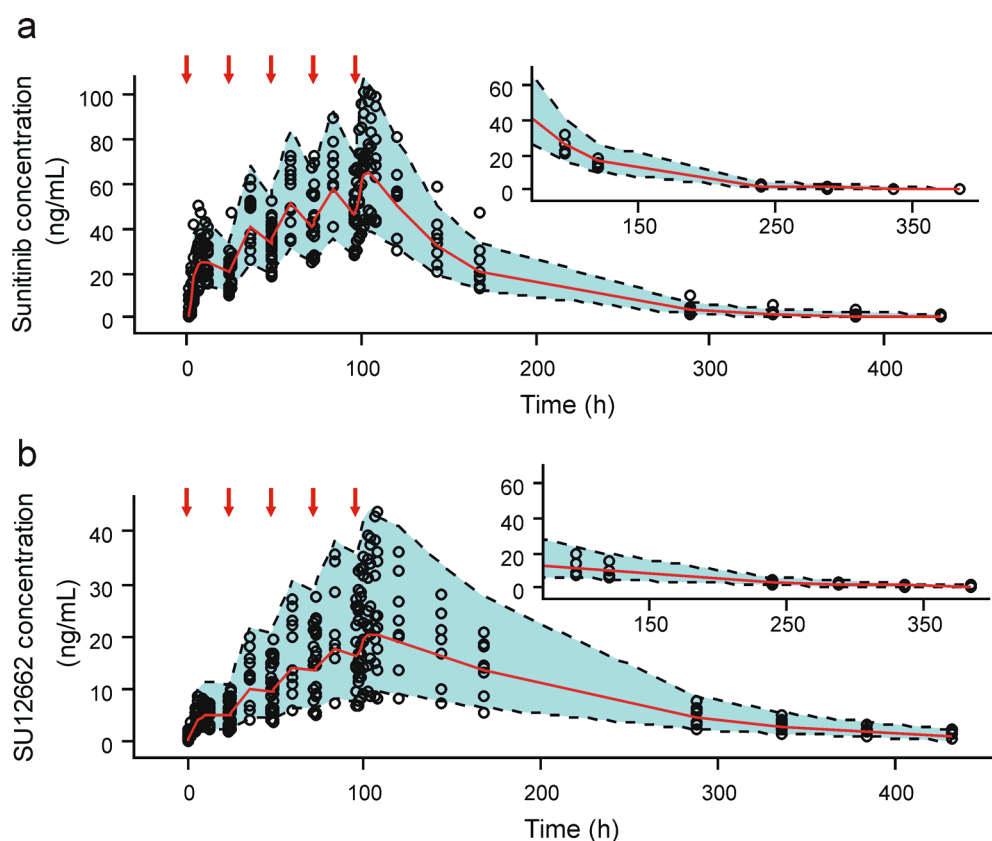
Figure 4-9   Visual predictive checks (VPCs) for (**a**) sunitinib and (**b**) SU12662 plasma concentrations. The 5th and 95th percentiles (dashed lines) and the median (solid red line) obtained from 1000 simulations are shown together with the actual observations (black circles). For subjects who only received 3 doses the VPCs for time points >72 h are shown separately. The arrows indicate dosing events.

Pharmacokinetic parameter estimates and their bootstrap confidence intervals are summarized in Table 4-5.

Table 4-5 Parameter estimates and their bootstrap confidence intervals (CI) from the pharmacokinetic model

Parameter	Estimate (90% CI)	IIV, %CV (90% CI)
RPS	1.91 (1.66 - 4.60)	-
MTT (h)	1.48 (1.25 - 2.06)	$-^a$
N	1.46 (0.88 - 1.87)	61 (28 - 82)
k_a (h^{-1})	0.54 (0.48 - 0.66)	26 (1.7 - 39)
$CL/F_{sunitinib}$ (L/h)	32.4 (28.8 - 37.8)	28 (20 - 36)
$V_1/F_{sunitinib}$ (L)	1720 (1397 - 2003)	33 (24 - 43)
$Q/F_{sunitinib}$ (L/h)	3.3 (2.5 - 15.3)	-
$V_2/F_{sunitinib}$ (L)	221 (190 - 386)	-
$CL/f_{a,SU12662}$ (L/h)	14.6 (12 -18)	43 (35 - 66)
$V_1/f_{a,SU12662}$ (L)	1410 (1141 - 1855)	47 (38 - 66)
Correlations		
$\rho(CL/F_{sunitinib}, V_1/F_{sunitinib})$	0.88 (0.80 - 0.96)	-
$\rho(CL/F_{sunitinib}, CL/f_{a,SU12662})$	0.70 (0.50 - 0.93)	-
$\rho(CL/F_{sunitinib}, V_1/f_{a,SU12662})$	0.67 (0.41 - 0.93)	-
$\rho(V_1/F_{sunitinib}, CL/f_{a,SU12662})$	0.90 (0.84 - 0.99)	-
$\rho(V_1/F_{sunitinib}, V_1/f_{a,SU12662})$	0.90 (0.93 - 0.99)	-
$\rho(CL/f_{a,SU12662}, V_1/f_{a,SU12662})$	0.99 (0.99 - 1.00)	-
Residual error		
$\sigma_{add,sunitinib}$ (ng/mL)	0.07 (0.02 - 0.17)	-
$\sigma_{prop,sunitinib}$ (%)	11 (8.8 - 12)	-
$\sigma_{add,SU12662}$ (ng/mL)	0.36 (0.13 - 0.39)	-
$\sigma_{prop,SU12662}$ (%)	11 (9.3 - 13)	-

IIV: interindividual variability; CV: coefficient of variation (%); RPS: ratio of presystemic to systemic metabolite formation; MTT: mean transit time; N: number of transit compartments; k_a: absorption rate constant; CL: clearance; V_1: volume of distribution of the central compartment; Q: intercompartmental clearance; V_2: volume of distribution of the peripheral compartment; F: bioavailability ($f_a \cdot [1-f_{m,pre}]$); f_a: fraction of absorbed dose (fixed to 1); ρ: correlation coefficient; σ_{add}: additive residual variability (standard deviation); σ_{prop}: proportional residual variability (CV).

a Interoccasion variability in MTT was estimated at 111% (90%CI: 77 - 138).

The NONMEM code of the final model is provided in the appendix (Code 9-4).

4.2.2   Pharmacodynamic Models

4.2.2.1   Blood pressure

A time-dependent variation in baseline systolic and diastolic blood pressure ($BL(T)_{systolic,diastolic}$) was found to be best described by a function including two cosine terms (equation 4-4) previously used by Hempel et al. [132]:

$$BL(T)_{systolic,diastolic} = BL(24)_{systolic,diastolic}$$

$$\cdot \left[1 + \left(AMP_1 \cdot \cos\left(\frac{T \cdot 2\pi}{24} - PS_1 \right) + AMP_2 \cdot \cos\left(\frac{T \cdot 2\pi}{12} - PS_2 \right) \right) \right] \quad \begin{array}{c} \text{equation} \\ \text{4-4} \end{array}$$

where $BL(24)_{systolic,diastolic}$ is the mean systolic or diastolic blood pressure during a 24-hour period, AMP_1 and AMP_2 are the amplitudes of each cosine term, PS_1 and PS_2 are the phase shifts of the functions relative to time (T) determining when a maximum or minimum occurs. The periods of the two cosine terms were 24 and 12 hours, respectively. The estimate for PS_1 was close to zero and fixed to this value in the final model with no impact on the OFV. Based on individual parameter estimates, blood pressure was calculated to be 2.2 to 8.1% higher in the evening (~10:00 PM) and ~2.4 to 8.3% lower in the afternoon (~2:00 PM) compared to the individual $BL(24)_{systolic,diastolic}$ estimate. At 8:00 AM the relative deviation from the individual $BL(24)_{systolic,diastolic}$ value ranged from -3 to +3%. Figure 4-10 shows the predicted diastolic blood pressure during 24 hours for the subjects in the present study.
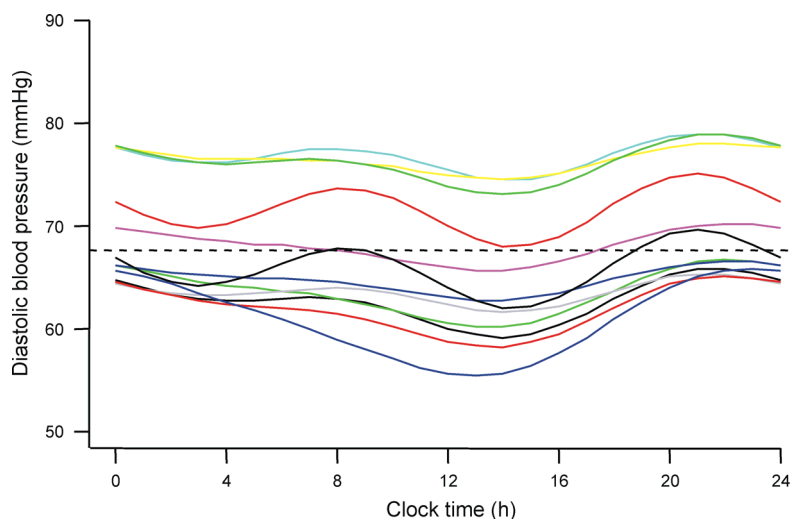
Figure 4-10   Individual predictions of diastolic blood pressure of the 12 subjects during a 24-hour (drug-free) interval. The dashed line marks the average 24-hour baseline diastolic blood pressure in this population.

Estimation of separate amplitudes or phase shifts for systolic and diastolic blood pressure did not improve the fit or resulted in unstable models (see Table 9-5 in the appendix).

The increase in systolic and diastolic blood pressure observed after sunitinib administration (Figure 4-11), was found to be well described by equation 4-5 and equation 4-6 including an immediate signal (ISIG), which was set equal to the fractional tyrosine kinase inhibition (INH, see section 3.3.5) and a slower, transduced signal (TSIG).
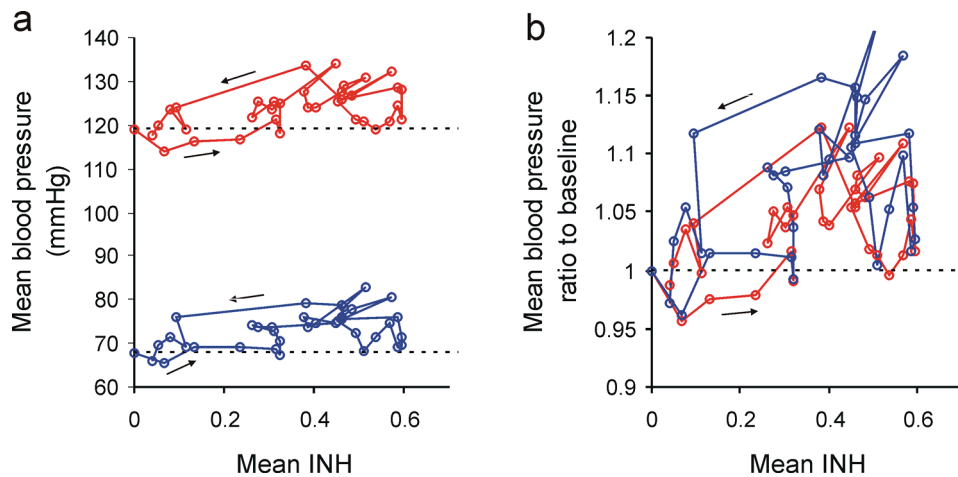
Figure 4-11 Mean systolic (red) and diastolic (blue) blood pressure vs. mean fractional tyrosine kinase inhibition (INH) (**a**). On the right-hand side (**b**) the blood pressure response is presented as ratio to baseline (i.e., the mean of all measurements on day 0). The arrows indicate the progression of time; the dashed line marks the baseline blood pressure.

$$\frac{dTSIG}{dt} = \frac{1}{\tau_{BP}} \cdot (INH - TSIG)$$

equation 4-5

$$BP_{systolic,diastolic} = BL(T)_{systolic,diastolic} \cdot \left[1 + \alpha_{systolic,diastolic} \cdot (ISIG + R_{sl} \cdot TSIG)\right]$$

equation 4-6

where $\alpha_{systolic,diastolic}$ is the intrinsic activity denoting the power of the drug to produce a response in diastolic or systolic blood pressure and τ_{BP} is the transduction time describing the time delay for the slower signal. R_{sl} denotes the proportional contribution of this slower signal to the overall effect. It was estimated to be close to 1 and finally fixed to this value without affecting the OFV. In fact, the sensitivity analysis showed,

that setting R_{sl} to values <1 led to higher OFVs (Figure 9-17, appendix). Of the fixed-effects parameters only τ_{BP} was sensitive to changes in R_{sl} which appears logical given that both parameters describe the transduced signal and may be correlated. Setting the dissociation constant K_d to values >4 ng/mL had almost no effect on the OFV or the random-effects parameters. $\alpha_{systolic}$, $\alpha_{diastolic}$ and τ_{BP} changed by 20-30% for every unit change of K_d (Figure 9-18, appendix).

τ_{BP} was estimated to be 121 h showing a considerably delayed response to the slower process. Although the inclusion of this parameter was associated with a significant reduction of the OFV of 13 units (p <0.001), its 90% confidence interval (CI), however, was fairly wide (12.2–541 h). Estimates and 90% CIs for all other parameters are given in Table 4-6.

Table 4-6 Parameter estimates and their bootstrap confidence intervals (CI) from the sunitinib blood pressure models

Parameter	Estimate (90% CI)	IIV, %CV (90% CI)
$BL(24)_{systolic}$ (mmHg)	118 (115 - 121)	6.7(4.6 - 7.7)
$BL(24)_{diastolic}$ (mmHg)	67.6 (65.1 - 70.5)	8.7 (6.3 - 9.6)
AMP_1	0.025 (0.014 - 0.036)	75 (32 - 137)
PS_1	0 *fixed*	-
AMP_2	-0.016 (-0.023 to -0.006)	78 (36 - 200)
PS_2	1.4 (1.1 - 1.6)	-
$\alpha_{systolic}$	0.078 (0.035 - 0.142)	135 (65 - 257)
$\alpha_{diastolic}$	0.145 (0.082 - 0.221)	71 (42 - 104)
R_{sl}	1 *fixed*	-
τ_{BP} (h)	121 (12.2 - 541)	-
Correlations		
$\rho(BL(24)_{systolic}, BL(24)_{diastolic})$	0.70 (0.49 - 0.92)	-
$\rho(\alpha_{systolic}, \alpha_{diastolic})$	0.88 (0.29 - 0.98)	-
Residual error		
$\sigma_{add,systolic}$ (mmHg)	7.4 (6.6 - 8.1)	-
$\sigma_{add,diastolic}$ (mmHg)	6.6 (5.9 - 7.1)	-

IIV: interindividual variability; CV: coefficient of variation; $BL(24)_{systolic,diastolic}$: average systolic or diastolic blood pressure over 24 hours; BL: baseline value; $AMP_{1,2}$: amplitude of the first or second cosine term; $PS_{1,2}$: phase shift of the first or second cosine term; α: intrinsic activity parameter; R_{sl}: relative contribution of the transduced signal to the effect; τ: transduction time; ρ: correlation coefficient; σ_{add}: additive residual variability (standard deviation).

The visual predictive checks (Figure 4-12) demonstrate that the model predicted the observed data reasonably well. Variability, however, appears to be slightly overestimated especially at later time points. Goodness-of-fit plots, shown in the appendix, support this finding (Figure 9-12 and Figure 9-13).
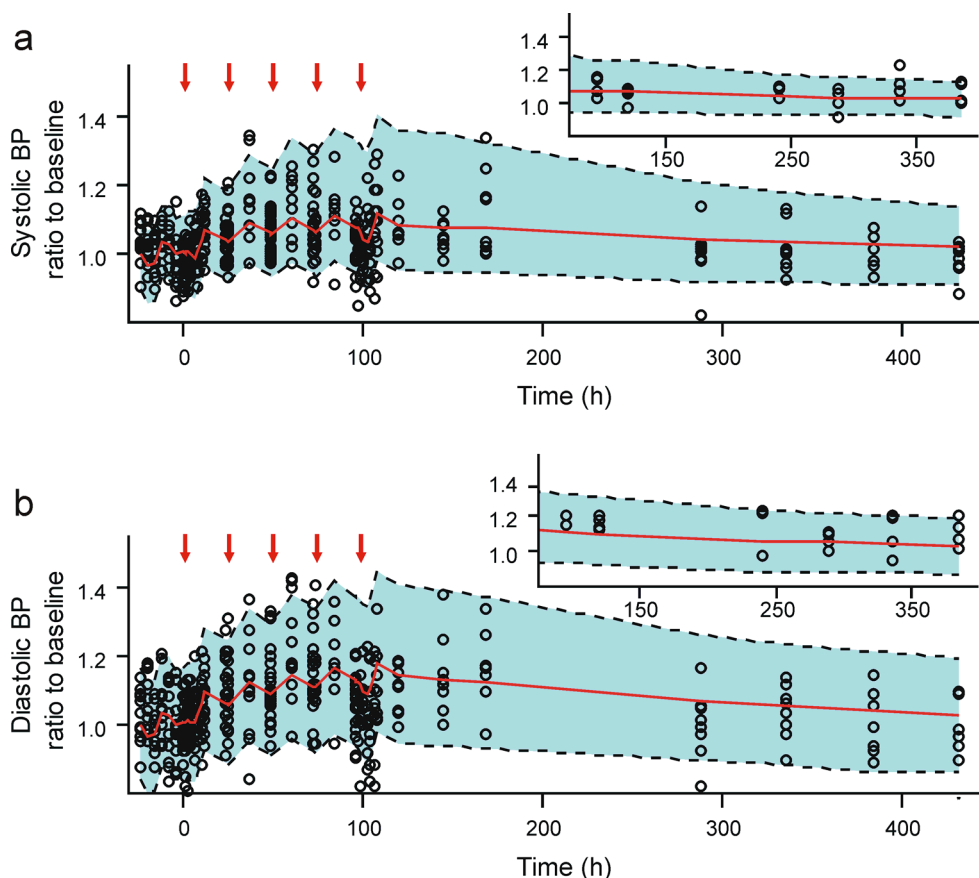
Figure 4-12   Visual predictive checks (VPCs) for (**a**) systolic and (**b**) diastolic blood pressure. The 5th and 95th percentiles (dashed lines) and the median (solid red line) obtained from 1000 simulations are shown together with the actual observations (black circles) normalized to their respective baseline estimates. For subjects who only received 3 doses the VPCs for time points >72 h are shown separately. The arrows indicate dosing events.

The NONMEM code of the final blood pressure model is provided in the appendix (Code 9-5).

4.2.2.2   VEGF-A

None of the tested cosine models for diurnal variations in VEGF-A levels were significantly different from the mean baseline value.

From Figure 4-13 it is evident that the relationship between the fractional tyrosine kinase inhibition (INH) and VEGF-A concentrations is not linear.
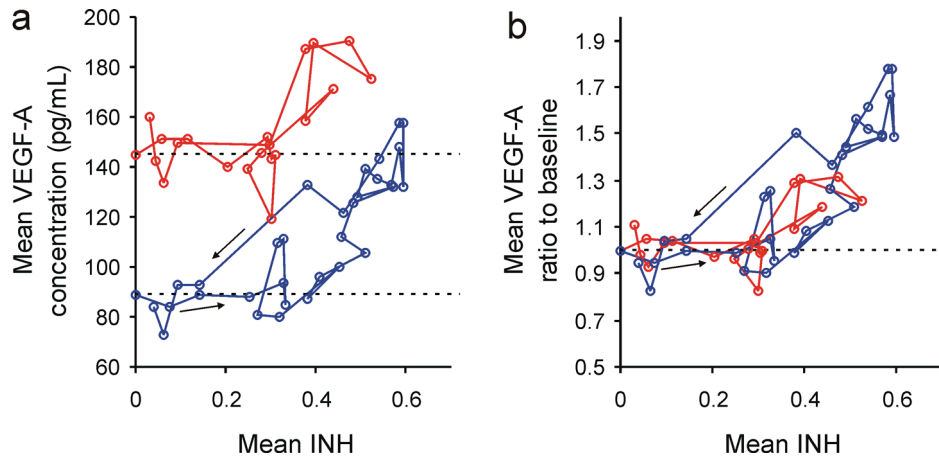
Figure 4-13   Mean VEGF-A concentrations vs. mean fractional tyrosine kinase inhibition (INH) grouped by study part (Part 1: red, Part 2: blue). In **b** the VEGF-A concentrations are normalized to the baseline concentration (i.e., the mean of all measurements on day 0). The arrows indicate the progression of time; the dashed line marks the baseline.

A power function including a signal transduction component was found to best describe this relationship (equation 4-7 and equation 4-8). A summary of the model building process is provided in Table 9-6 in the appendix.

$$\frac{dTSIG}{dt} = \frac{1}{\tau_{VEGF-A}} \cdot \left(INH^{\gamma} - TSIG \right)$$

equation 4-7

$$VEGF-A = BL_{VEGF-A} \cdot (1 + \alpha_{VEGF-A} \cdot TSIG)$$

equation 4-8

where α_{VEGF-A} is the intrinsic activity and γ is a shape parameter describing the signal modification during the transduction process (see Figure 3-3); TSIG denotes the transduced signal and τ_{VEGF-A} the transduction time. Exclusion of γ from the model (i.e., fixing it to 1) worsened the OFV by 85 units. The inclusion of a signal transduction function to account for a time delay in VEGF-A response improved the OFV by 73

units. The signaling process of VEGF-A was slightly delayed as indicated by a transduction time of only ~12 hours in a typical subject. However, in two subjects individual estimates of τ_{VEGF-A} were considerably longer (85 and 327 h) explaining the high interindividual variability (CV: 373%) associated with this parameter. The baseline estimate of VEGF-A (BL_{VEGF-A}) in the first part of the study was 1.76 times higher than in the second part (p <0.05). This is most likely due to the differences in the centrifugation speed (780 g in the first, and 1000 g in the second part) at which plasma samples were prepared. The sensitivity analysis (Figure 9-19, appendix) is not very conclusive. The values of τ_{VEGF-A}, the interindividual variability (IIV) in τ_{VEGF-A} and α_{VEGF-A} are quite sensitive to changes in K_d, however, without a consistent pattern. This may be due to the relatively low precision with which these parameters could be estimated (i.e., wide confidence intervals, see Table 4-7).

Table 4-7   Parameter estimates and their bootstrap confidence intervals (CI) from the sunitinib VEGF-A model

Parameter	Estimate (90% CI)	IIV, %CV (90% CI)
BL_{VEGF-A} (pg/ml)	80.1 (66.1 - 99.6)	33 (14 - 41)
θ_{PART1} on BL_{VEGF-A}	1.76 (1.35 - 2.27)	-
γ	4.3 (3.4 - 6.7)	-
α_{VEGF-A}	10.2 (5.1 - 57)	68 (29 - 99)
τ_{VEGF-A} (h)	11.8 (3.4 - 45.4)	373 (94 - 2143)
Residual error		
$\sigma_{prop,VEGF-A}$ (%)	18 (17 - 20)	-

IIV: interindividual variability; CV: coefficient of variation; BL: baseline value; θ_{PART1}: baseline adjustment for subjects from the first part of the study; γ: shape parameter; α: intrinsic activity parameter; τ: transduction time; σ_{prop}: proportional residual variability (CV).

The visual predictive check (Figure 4-14) indicated some overestimation of the variability between 30 and 100 hours after the first dose. Overall, however, the model fitted reasonably well to the observed data, which is also supported by the goodness-of-fit plots shown in the appendix (Figure 9-14).

The NONMEM code of the VEGF-A model is provided in the appendix (Code 9-6).
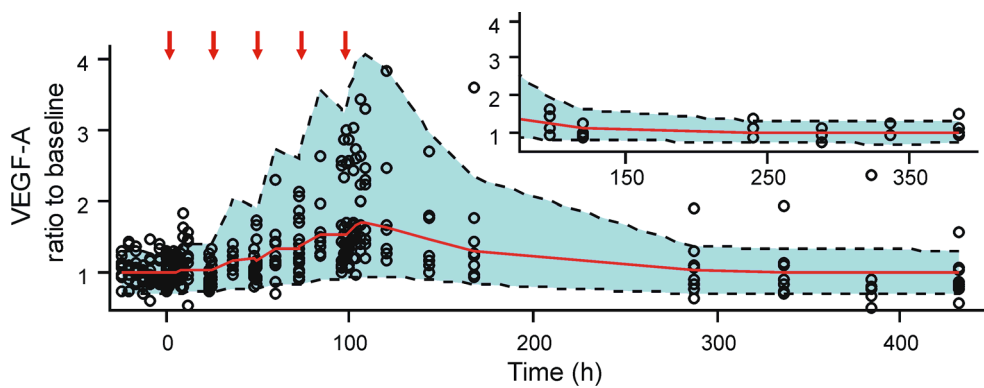
Figure 4-14   Visual predictive check for VEGF-A. The 5th and 95th percentiles (dashed lines) and the median (solid line) obtained from 1000 simulations are shown together with the actual observations (black circles) normalized to their respective baseline estimates. For subjects who only received 3 doses the VPC for time points >72 h is shown separately. The arrows indicate dosing events.

4.2.2.3   VEGF-C

VEGF-C concentrations did not show any consistent change over time (Figure 4-15), nor were they related to the fractional tyrosine kinase inhibition (Figure 4-16). The development of a PK/PD model was therefore not considered for this biomarker. From Figure 4-16 (**a**) it is evident that plasma concentrations differed between the two study parts. As with VEGF-A, the different centrifugation speeds are likely to be responsible for this observation.
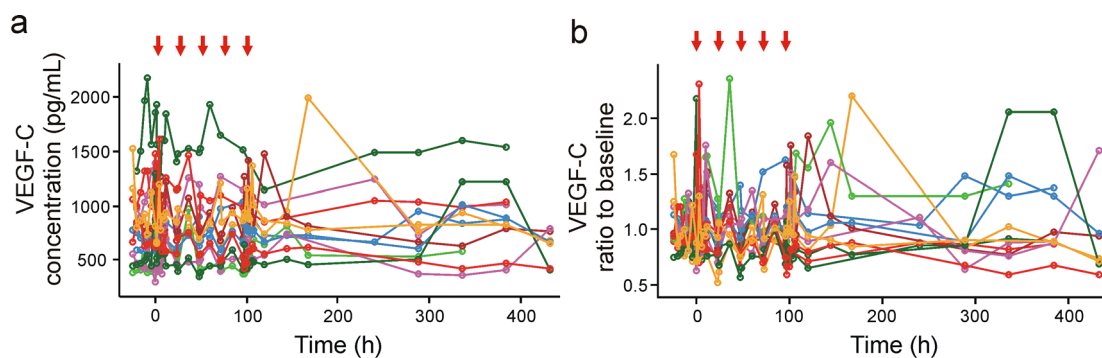
Figure 4-15   Individual VEGF-C concentrations plotted against time (**a**). The right panel (**b**) shows the VEGF-C concentrations normalized to the baseline concentration (i.e., the mean of all measurements on day 0). The arrows indicate dosing events.
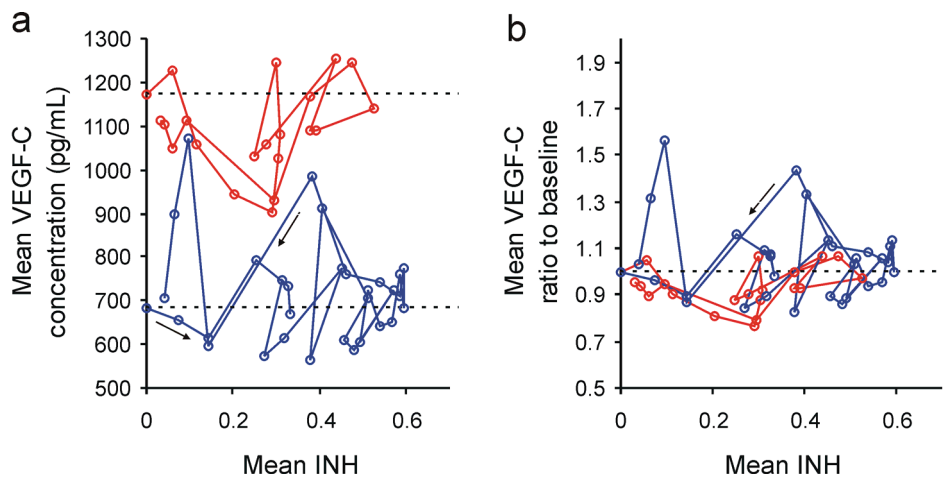
Figure 4-16 Mean VEGF-C concentrations vs. mean fractional tyrosine kinase inhibition (INH) grouped by study part (Part 1: red, Part 2: blue). In **b** the VEGF-C concentrations are normalized to the baseline concentration (i.e., the mean of all measurements on day 0). The arrows indicate the progression of time; the dashed line marks the baseline.

4.2.2.4   sVEGFR-2

Inclusion of a cosine function describing diurnal variation in baseline sVEGFR-2 levels did not improve the model fit.

An indirect response model (equation 4-9) with the fractional tyrosine kinase inhibition (INH) reducing the zero-order release rate (K_{in}) of sVEGFR-2 best described the data:

$$\frac{dsVEGFR-2}{dt} = K_{in} \cdot \left[\frac{1}{(1 + \alpha_{sVEGFR-2} \cdot INH)} \right] - k_{out} \cdot sVEGFR-2 \qquad \text{equation 4-9}$$

where $\alpha_{sVEGFR-2}$ is the intrinsic activity and K_{in} was assumed to equal $BL_{sVEGFR-2} \times k_{out}$.

Other functional relationships were also tested and are summarized in Table 9-7 in the appendix.

The first-order rate constant k_{out} may be interpreted as the elimination rate constant of sVEGFR-2 from plasma. Hence, the typical half-life ($\ln2/k_{out}$) of this soluble receptor was ~4 days. The delayed response of sVEGFR-2 is evident from Figure 4-17 where mean concentrations are plotted against the INH – the clockwise hysteresis loop indicates that the response is time-dependent.
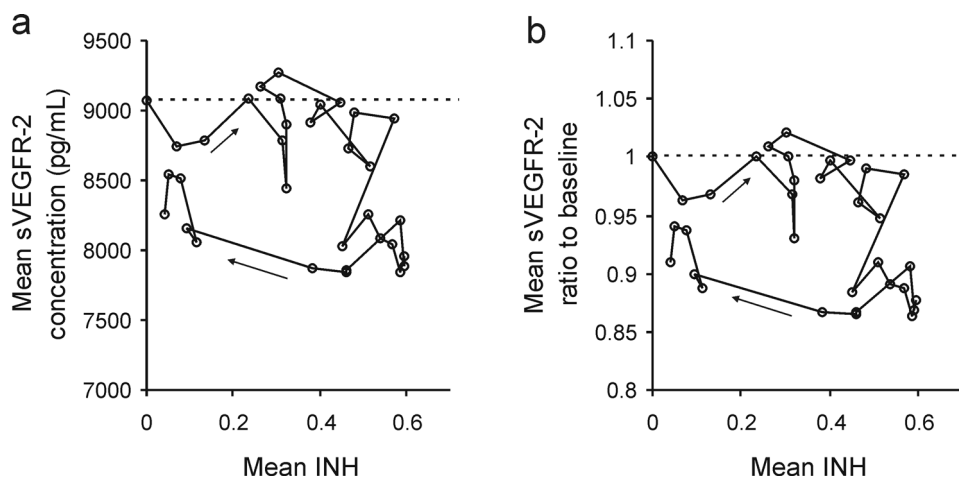
Figure 4-17   Mean VEGFR-2 concentrations vs. mean fractional tyrosine kinase
inhibition (INH). In **b** the VEGFR-2 concentrations are normalized to
the baseline concentration (i.e., the mean of all measurements on day
0). The arrows indicate the progression of time; the dashed line marks
the baseline.

The sensitivity analysis (Figure 9-20, in the appendix) showed that setting the
dissociation constant (K_d) to different values had only little impact on most of the
parameter estimates. Only $\alpha_{sVEGFR-2}$ changed by about 20% for every unit change in K_d.
This, however, is not surprising, since $\alpha_{sVEGFR-2}$ and K_d are interdependent parameters
that are not separately identifiable. Values of K_d <4 ng/mL increased the OFV, whereas
with greater values of K_d the OFV slightly decreased.

The visual predictive check (Figure 4-18) shows that the median prediction matches the
observed concentrations and that the variability was reasonably described. Standard
goodness-of-fit plots are provided in the appendix (Figure 9-15). Parameter estimates
and 90% CIs are presented in Table 4-8.
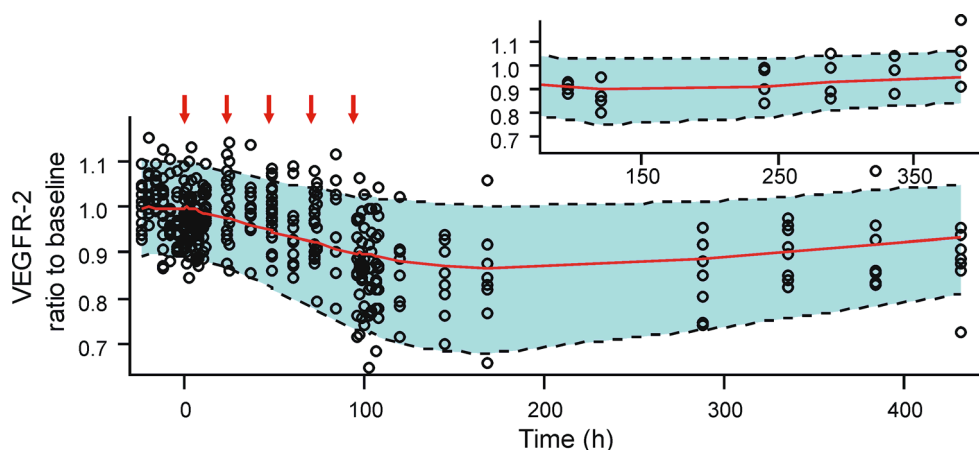
Figure 4-18 Visual predictive check for VEGF-A. The 5th and 95th percentiles (dashed lines) and the median (solid red line) obtained from 1000 simulations are shown together with the actual observations (black circles) normalized to their respective baseline estimates. For subjects who only received 3 doses the VPC for time points >72 h is shown separately. The arrows indicate dosing events.

Table 4-8 Parameter estimates and their bootstrap confidence intervals (CI) from the sVEGFR-2 model

Parameter	Estimate (90% CI)	IIV, %CV (90% CI)
$BL_{sVEGFR-2}$ (pg/mL)	9060 (8620 - 9470)	10 (5.3 - 13)
$\alpha_{sVEGFR-2}$	0.50 (0.28 - 0.80)	70 (18 - 200)
$k_{out,sVEGFR-2}$ (d^{-1})	0.175 (0.103 - 0.259)	66 (21 - 131)
Residual error		
$\sigma_{prop,sVEGFR-2}$ (%)	6.5 (6.2 - 6.9)	-

IIV: interindividual variability; CV: coefficient of variation; BL: baseline value; α: intrinsic activity parameter; k_{out}: rate of loss of biomarker response; σ_{prop}: proportional residual variability (CV).

The NONMEM code can be found in the appendix (Code 9-7).

4.2.3 Comparison with Data from Literature

The average predictions from the blood pressure model matched closely the data reported by Azizi et al. [74] for the normotensive mRCC patients (Figure 4-19). The variability in the simulated values is, however, higher than in the original report. In Figure 4-20 the mean predicted changes in VEGF-A and sVEGFR-2 levels are compared with data from previously reported investigations in cancer patients [75-78].

The present models predicted consistently smaller mean changes in VEGF-A or sVEGFR-2 levels from baseline compared to average observations in cancer patients.
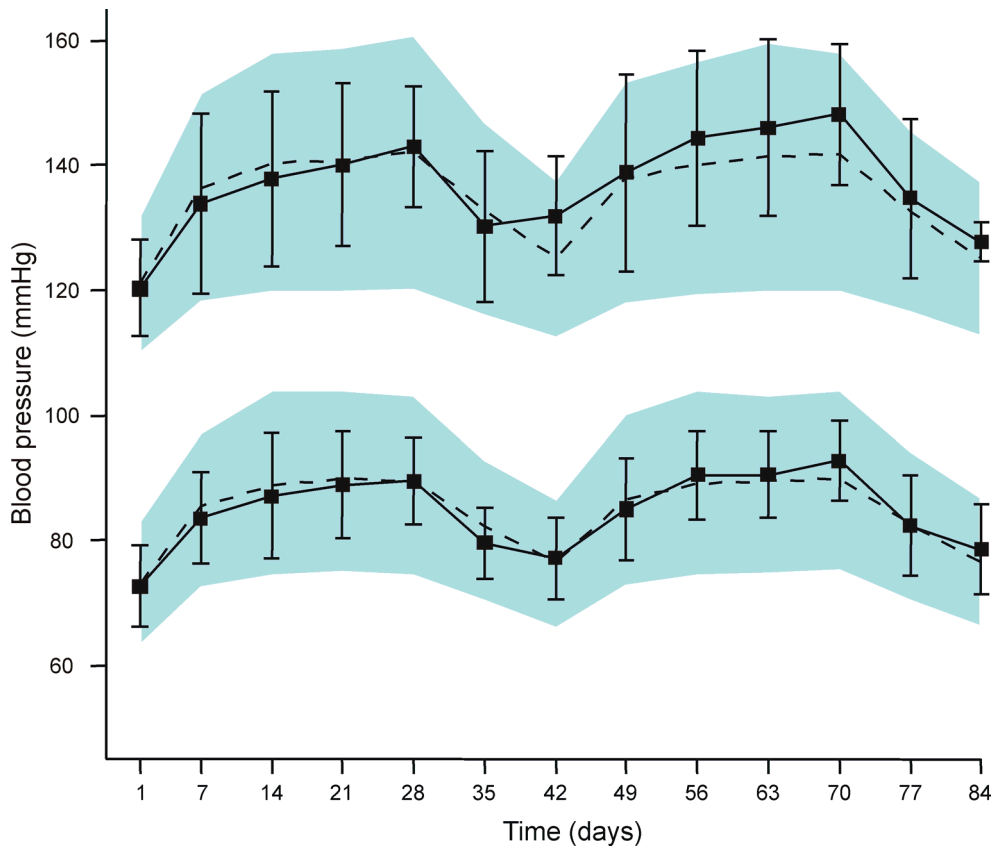
Figure 4-19   Comparison of model-simulated time courses of the blood pressure response with data extracted from graphs in a previous publication. The mean values (dashed line) and the 68% prediction interval (blue area) of simulated systolic and diastolic blood pressure are compared to mean values (filled squares) and standard deviation (SD) (vertical bars) reported by Azizi et al. [74].
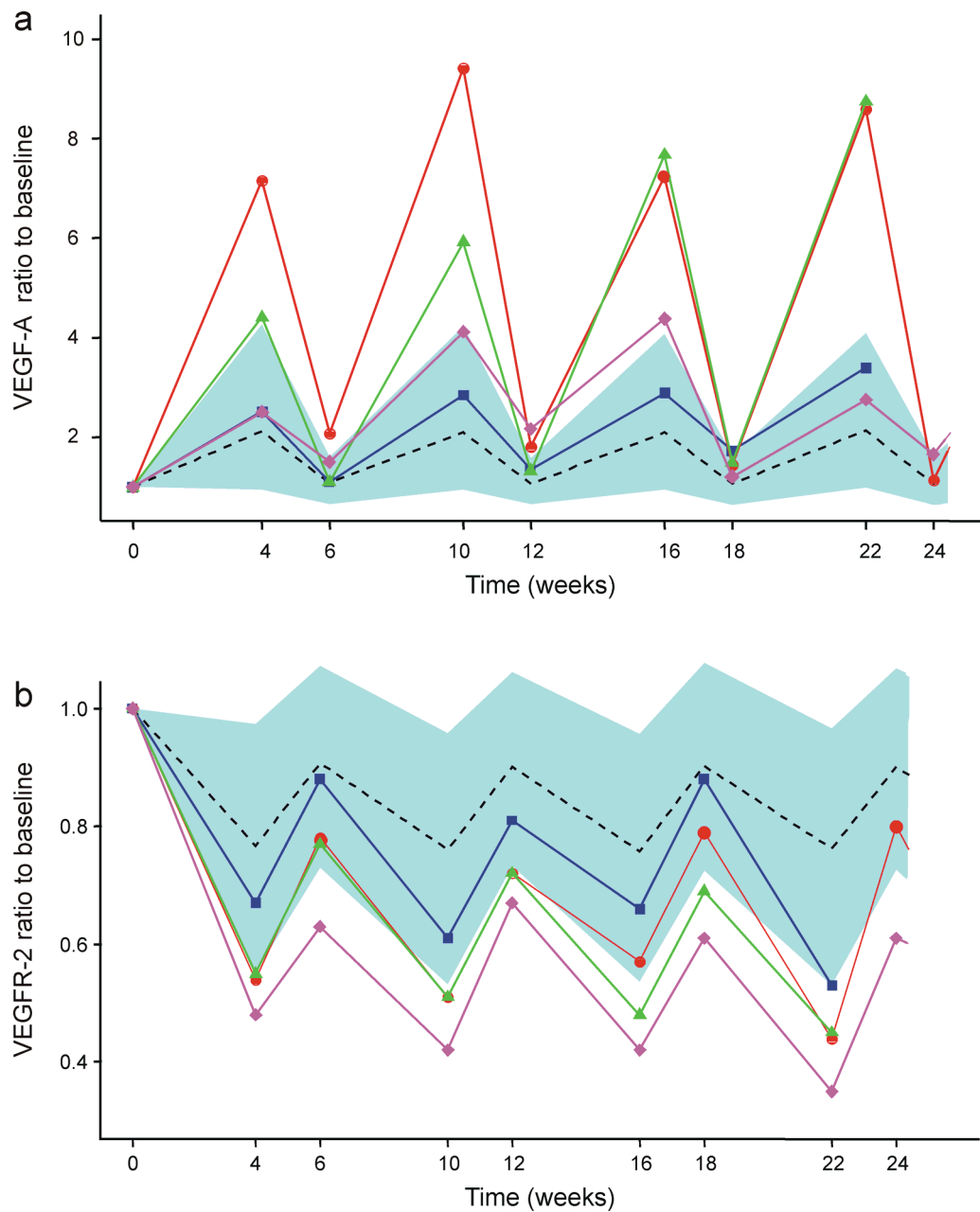
Figure 4-20 Simulated mean changes (dashed lines) of (**a**) VEGF-A, and (**b**) sVEGF-2 levels are shown together with mean changes reported in studies in patients with GIST (——■—, Norden-Zfoni et al. [78]), breast cancer (——●—, Burstein et al. [75]), and mRCC (——▲—, Deprimo et al. [76] and ——◆—, Kontovinis et al. [77]). The blue area represents the 90% prediction interval of the simulations. For the sake of clarity and because a measure of variability (e.g., SD) was not provided in all studies, no error bars are shown.

4.2.4   Clinical Trial Simulation

In the initial simulation scenario, with 75 patients per group and a target increase of diastolic blood pressure of 16%, the median overall survival (OS) in the standard dose group was 574 days (95% CI, 490 - 700) and 784 days (95% CI, 616 - 826) in the individualized dose group (hazard ratio: 0.64 [95% CI, 0.40 – 0.92], power: 62.2% [95% CI, 57.8 – 66.4]). The incidence of grade 3/4 fatigue was 10.7% (95% CI, 4.0 – 17.0) in the standard dose group and 17.3% (95% CI, 10.6 - 26.7) in the individualized dose group. In the standard dose group 24.0% (95% CI, 15.3 – 33.3) of the patients needed antihypertensive treatment compared to 28% (95% CI, 17.3 – 37.3) in the individualized dose group. The distribution of the dose levels patients received in their final treatment cycle is shown in Figure 4-21. Almost half of the patients in the individual dose group ended up with the highest dose allowed of 87.5 mg.
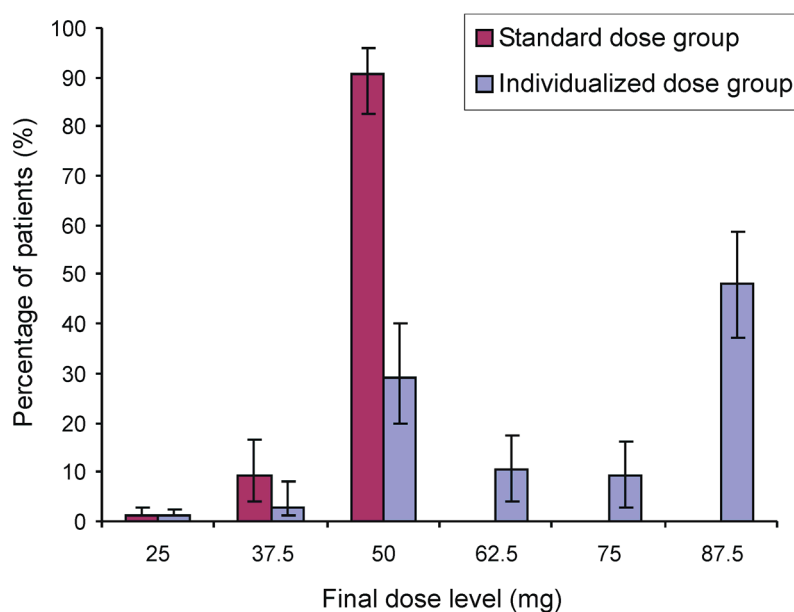
Figure 4-21   Frequency distribution of the final dose level the patients received in the trial. The error bars represent the 95% confidence interval.

Figure 4-22 shows the simulated survival curves. Statistical power to detect a significantly longer median OS in relation to the number of patients studied or the target blood pressure increase are shown in Figure 4-23. Table 4-9 summarizes the simulation results for different values of the target increase in diastolic blood pressure.
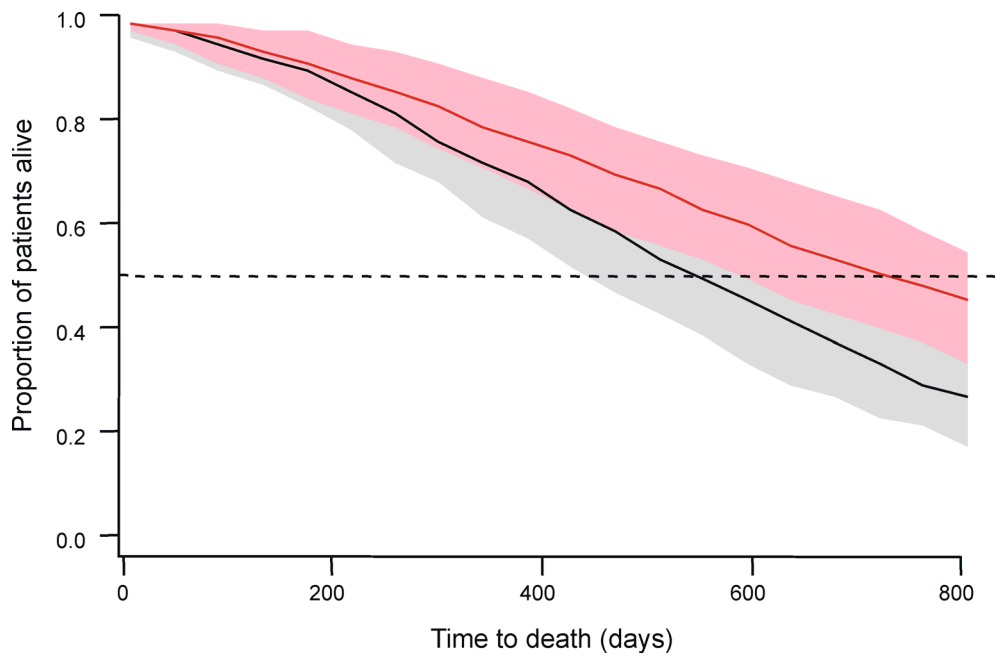
Figure 4-22 Simulated median survival curves in patients with mRCC for the standard treatment group (black solid line) and the individualized dose group (red line). The shaded areas are the 95% confidence intervals around the respective survival curves.
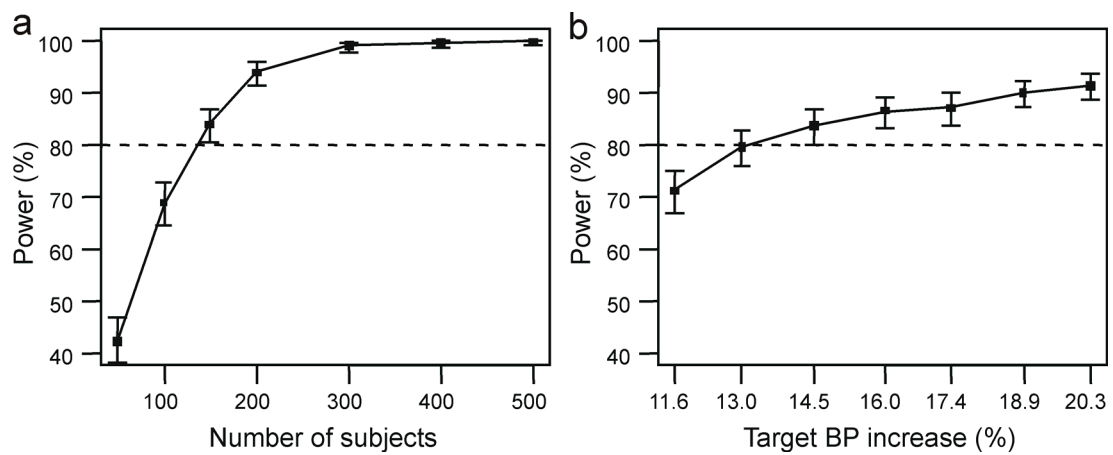
Figure 4-23 Statistical power to detect a significantly longer median overall survival in relation to the total number of patients studied (**a**, target dBP increase fixed to 16%) or target dBP increase (**b**, number of patients fixed to 150). Vertical bars represent the 95% confidence intervals. dBP: diastolic blood pressure.

Table 4-9   Impact of target blood pressure on the overall survival and the incidence
                of fatigue

Target blood pressure increase (%)	Median overall survival (days)		Incidence of grade 3/4 fatigue (%)	
	Individualized dose group	**Standard dose group**	**Individualized dose group**	**Standard dose group**
11.6	742	574	17.3	10.7
13.0	742	574	17.3	10.7
14.5	742	574	17.3	10.7
16.0	784	574	17.3	10.7
17.4	784	574	18.7	10.7
18.9	784	574	18.7	10.7
20.3	784	574	18.7	10.7

5 Discussion

5.1 Venlafaxine Study

5.1.1 Pharmacokinetic Model

The pharmacokinetic model adequately described the plasma concentration-time profiles of venlafaxine and O-desmethylvenlafaxine and was able to account for the presystemic formation of this metabolite in the liver (i.e., first-pass effect). This could be achieved by integrating a physiological body compartment, the liver, and using liver plasma flow and liver volume as fixed physiological parameters. Taft et al. [104] were the first who applied such a model to describe venlafaxine and O-desmethylvenlafaxine plasma concentrations. The present model is a modification of the one they used and differs mainly in two aspects. First, a system of transit compartments was applied to account for a delayed absorption of venlafaxine. It was recently demonstrated that this approach gives mathematically more stable models and also provides more precise parameter estimates as, for example, the inclusion of an absorption lag-time [122]. Second, in contrast to Taft et al. [104], who fixed the fraction metabolized (f_m) to a value obtained from literature in order to estimate the volume of distribution of O-desmethylvenlafaxine (V_{ODV}) and its clearance (CL_{ODV}), in the present work V_{ODV} was fixed to 210 L, in order to estimate f_m and its interindividual variability. Because venlafaxine is exclusively metabolized to O-desmethylvenlafaxine via the CYP2D6 enzyme system, which is subject to genetic polymorphism [133], it seemed reasonable that f_m varies more between healthy subjects than V_{ODV} and CL_{ODV}. A disadvantage of this approach is that the interindividual variability in f_m cannot be fully separated from the variability in V_{ODV} and CL_{ODV}. This means that the estimate for the interindividual variability in f_m (CV: 34.5%) also contains the variability in V_{ODV} and CL_{ODV} to some (unknown) extent. However, this weakness apparently did not lead to erroneous results since parameter estimates from the present model are consistent with values previously reported (Table 4-2).

Numerous researchers have described the highly variable metabolism of venlafaxine due to CYP2D6 polymorphism [133-139]. Consistent with these findings, a high value for the interindividual variability in the intrinsic clearance of venlafaxine ($CL_{int(VEN)}$; CV: 94.8%) was estimated in the present work.

Another feature of the model is its ability to estimate the hepatic extraction ratio E_H, which was calculated to be 68% and is indicative for a moderate to high extraction drug. Based on the results from a crossover trial with orally and intravenously administered venlafaxine, Patat et al. [49] calculated an E_H of 55 to 60%.

Although several assumptions had to be made for model building (e.g., fixing Q_H, V_{ODV}, and the volume of the liver compartment) precise and reasonable parameter estimates could be obtained. All assumptions are physiologically reasonable and are based on previous findings. A sensitivity analysis showed that changing the value of fixed parameters had either no relevant influence on other model parameters or worsened the model fit in terms of OFV. Setting the Q_H, for example, at a value corresponding to the hepatic blood flow (1.2 L/h/kg) worsened the model fit in terms of the OFV. This is interesting, since the hepatic elimination of drugs is usually limited by the hepatic blood flow [140]. During the passage through the liver, drug molecules associated with or distributed into blood cells normally redistribute rapidly back into the plasma when concentrations decline there due to metabolism. In the case of venlafaxine, an explanation could be that the distribution of this drug from erythrocytes to the plasma is very slow. Then the hepatic clearance may not exceed the hepatic plasma flow.

Nevertheless, the present study endorses the conclusion drawn by Taft et al. [104], that this kind of semi-physiological model provides useful information on the disposition of drugs that undergo hepatic metabolism.

5.1.2   Pharmacodynamic Models

The shortening of the 33% recovery time of the pupillary light reflex induced by venlafaxine and O-desmethylvenlafaxine is presumably reflecting sympathetic potentiation in the iris due to the inhibition of norepinephrine (NE) reuptake from the synaptic gap. Venlafaxine and O-desmethylvenlafaxine have no relevant affinity to muscarinergic receptors of the iris [54]. Therefore, the decrease in the amplitude of the pupillary light reflex induced by venlafaxine and O-desmethylvenlafaxine is assumed to be caused by NE-mediated inhibition of central parasympathetic (Edinger-Westphal) neurons, again due to NE reuptake blockade [58].

In the present analysis, a smaller effect (i.e., the shortening of the 33% recovery time and the decrease of the amplitude) was observed at the end of a dosing interval than at the beginning, despite equal plasma concentrations of the active drug (Figure 4-4). This

indicates the development of acute tolerance of the pharmacodynamic response. In general, there are several possible mechanisms for the development of tolerance: counter-regulation by an endogenous substance, receptor desensitization, receptor downregulation, and depletion of an endogenous precursor pool. In this case, the most likely explanation for the acute tolerance is rapid desensitization of β-adrenoceptors, since it has been demonstrated *in vivo* that a single administration of venlafaxine and O-desmethylvenlafaxine led to reduced cyclic adenosine monophosphate (cAMP) response to isoproterenol in the pineal gland of rats [141]. Franklin et al. later confirmed this result and showed that the reduction of responsiveness is not due to a decrease in NE concentration (similar to a precursor pool depletion) but most likely a result of β-adrenoceptor desensitization [142].

Models, similar to the one applied here, including a tolerance compartment have already successfully been used to describe the effect of nicotine on heart rate [116], the antinociceptive effect of morphine [115], and the effect of caffeine on blood pressure [117]. It is, of course, a simplification of the true underlying mechanism, which is undoubtedly more complex. However, more mechanistic models (e.g., negative feedback model [113], precursor pool model [112]) were tested but did not show superiority in terms of model fit. Moreover, because more complex models need more parameters to be estimated, they resulted in imprecise estimates due to overparameterization.

Nevertheless, the model is justified by its ability to describe the concentration-effect relationship and the time course of the effect of venlafaxine and O-desmethylvenlafaxine on the pupillary light reflex parameters, amplitude and 33% recovery time. An interesting parameter that can be derived from the analysis is the half-life of development or disappearance of tolerance ($t_{1/2tol}$). The estimates of $t_{1/2tol}$ were similar for both amplitude and 33% recovery time (30 min and 40 min, respectively) and suggest that after about 3 hours (~5 half-lives), full sensitivity to venlafaxine should be regained.

It could be argued that a predose value for the PD measurements at day 14 should have been determined and used for model building instead of, or in addition to, the baseline value at day 0. However, the last PD measurements on day 14 (7 hours after the last dose and 5 hours before the end of the dosing interval) did not differ from their baseline

values at day 1 ([mean±SD] 1.64 ± 0.25 vs. 1.60 ± 0.33 mm for amplitude and 1.39 ± 0.14 vs. 1.42 ± 0.10 sec for 33% recovery time). This indicates that the drug effect returns to baseline within a dosing interval of 12 hours and no "accumulation" of the drug effect occurs. Thus, it is unlikely that inclusion of predose PD values at day 14 would have altered the modeling results much.

No PK and PD measurements after the first dose were performed, since the aim of the present study was to investigate the time course of the effect of venlafaxine and O-desmethylvenlafaxine under steady-state conditions, as this was considered to be of more clinical relevance. However, PK and PD measurements after a single dose of venlafaxine and the influence of different doses could be studied in future trials in order to characterize the kinetic complexities of the tolerance phenomenon in more detail by developing a more mechanistic model.

5.1.3   Optimal Study Design

As an example of the utility of model-based data analysis, the model for the amplitude was used for the optimization of pupillographic measurement times. The single-dose reference design was only slightly inferior to the original design used in the venlafaxine study where sampling was performed at steady-state (same sampling times relative to the preceding dose event). In this case, sampling at steady state offers no relevant advantage over sampling after the first administration.

All optimal sampling schedules with 4 to 8 measurements per subject were more efficient than the reference design with 5 measurements per subject. Most interestingly, designs with the same number of samples per subject or even one less outperformed the reference design. This demonstrates the importance of selecting the most informative sampling times in order to obtain precise parameter estimates in later analysis. The exploration of different sampling schedules permits the rational planning of future studies taking into account costs and other limitations. In the case of a single-dose study with 12 subjects it could be shown that a schedule with 8 samples would only slightly improve parameter precision compared to an optimal design with 5 samples per subject. However, if the (precise) determination of interindividual variability is an objective, than more subjects would have to be included.

5.1.4 Influence of Absorption Time on the Response

Since venlafaxine is also offered as an extended release formulation (Effexor XR®), it was of interest how a slower release (represented by a longer mean absorption time, MAT) would influence the pharmacodynamic response.

Simulations showed that a longer MAT would lead to reduced maximal plasma concentrations of venlafaxine and O-desmethylvenlafaxine occurring later in time. Correspondingly, the peak response of the amplitude and the 33% recovery time would also be smaller and would be shifted towards later time points. This is of importance, as the response is weaker for a longer MAT, it may happen that in a study with the extended release formulation the pupillographic response is not easily distinguishable from the placebo response. Furthermore, sampling times optimal for a study with the immediate release formulation would be inadequate for slow-released venlafaxine (see Table 4-4).

5.2   Sunitinib Study

5.2.1   Pharmacokinetic Model

Plasma concentration-time profiles for sunitinib and SU12662 were successfully described by a pharmacokinetic model simultaneously accounting for presystemic and systemic metabolite formation. This type of model was previously used for a variety of drugs that undergo a significant first-pass metabolism [143-145], but had not been used for sunitinb. Volume and clearance estimates from the model compare well to previous reports in healthy volunteers [146]. The high correlations that were estimated for random effects on apparent volume and clearance terms of sunitinib and SU12662 (correlation coefficients ranging from 0.67 to 0.99) reflect the interdependence of these parameters caused by the fraction absorbed (f_a) and the fraction metabolized (f_m) as common, however unknown, sources of variability. Accounting for delayed absorption greatly improved the model fit. However, its impact on steady-state concentrations may be negligible, given the long half-lives of sunitinib and SU12662 (~55 and ~73 h, respectively) in relation to the mean transit time (MTT) of only ~1.5 h. Likewise, the interoccasion variability in the MTT, although substantial (CV: 111%), is not expected to affect plasma concentrations at equilibrium.

5.2.2   Pharmacodynamic Models

A mechanism-based approach that permits the separation between drug-specific (tyrosine kinase inhibition) and biological system-specific components (biomarker signal) was successfully applied to relate drug concentrations to biomarker response.

The drug-specific part of the model consisted of a function relating free drug concentration to VEGFR-2 tyrosine kinase inhibition based on *in vitro* data for protein binding [59] and kinase inhibition [124]. An important assumption was that all measured biomarker effects are triggered solely by the inhibition of the VEGFR-2 tyrosine kinase. Although sunitinib targets several other tyrosine kinases (see section 1.4.1), for the biomarkers studied here, it is likely that this assumption holds true, since signaling via VEGFR-2 is predominantly responsible for angiogenesis, and similar effects on biomarkers had been described also for other drugs targeting VEGFR-2 [71].

A limitation of the present study was the small number of subjects leading to less precise estimates of interindividual variability parameters. Moreover, for ethical reasons,

only up to five doses of sunitinib were given. However, because of the long half-lives of sunitinib and SU12662 steady state is not reached until ~12 days after treatment start. This might explain, why parameters describing a time delay (τ_{BP}, τ_{VEGF-A}, $k_{out,sVEGFR-2}$) could not be estimated precisely.

5.2.2.1 Blood Pressure

The dual mechanism of action that was incorporated in the blood pressure model is compatible with the theory of how hypertension is caused by antiangiogenic therapy: (i) reduction in endothelial nitric oxide synthase (eNOS) expression which is controlled by VEGF signaling [147], and (ii) vascular rarefaction [85], that is, a decrease in perfused microvessels and a reduction in capillary density both controlling peripheral vascular resistance. A reduction in eNOS expression and the subsequent decline in nitric oxide production are likely to be more rapid than functional and morphological alterations to the vasculature. It is intriguing how closely model simulations compare to the observations that Azizi et al. reported for patient with metastatic renal cell carcinoma (mRCC) (Figure 4-19) [74]. Thus, drug effects on blood pressure may not be decisively influenced by this disease.

It is known that blood pressure is subject to diurnal variations [148] and accounting for a circadian rhythm improved the model fit in the present analysis. Therefore, for future studies it may be advisable to either account for diurnal blood pressure changes by a model, or to obtain measurements always at the same time of day.

5.2.2.2 Circulating Biomarkers

A relatively quick rise in VEGF-A concentrations was observed and a slow decline in sVEGFR-2 levels. Given the short plasma half-life of VEGF-A of ~13 min [149], it was assumed that the small delay in VEGF-A response is likely due to a slow signal transduction process, rather than rate-limiting elimination from plasma. By contrast, the calculated half-life for sVEGFR-2 of ~4 days is of the same order as the half-life (~7 days) that was reported for VEGF-trap, a soluble analogue of VEGFR-1 [149]. Thus, rate-limiting elimination may likely be the reason for the delayed sVEGFR-2 response.

Subjects in the first part of the study had significantly higher VEGF-A and VEGF-C levels than subjects in the second part. This is very likely due to the different centrifugation speeds used for sample preparation in the two parts. VEGF-A (and

VEGF-C) is present within platelets, thus at lower rotation speeds more platelets remain in the plasma supernatant and any VEGF-A (or –C) released from these will also be measured [150-152]. This difference, however, could be successfully accounted for by including "study part" as a covariate on the baseline estimate for VEGF-A (BL_{VEGF-A}). VEGFR-2 concentrations were not affected by this difference.

No changes in VEGF-C levels in relation to sunitinib concentrations were observed in this study. The reason for this is not quite clear, since in a study with mRCC patients a 23% reduction in VEGF-C levels during the first cycle was reported [153]. It might be, that changes of VEGF-C levels are not directly related to tyrosine kinase inhibition but rather occur secondary to effects on a tumor and are therefore not observable in healthy subjects. An alternative explanation could be that the effect on VEGF-C might be too weak to be obvious after only 5 doses of sunitinib.

5.2.3   Comparison with Data from Literature

The simulations suggested that the change in VEGF-A levels from baseline is smaller in healthy subjects than in cancer patients (Figure 4-19 a). Moreover, changes in this biomarker seem to be more pronounced in patients with mRCC or breast cancer than with GIST. Similarly, changes in simulated sVEGFR-2 levels were smaller than observations in patients, with GIST patients exhibiting the least fold-change (Figure 4-19 b). It may be concluded that VEGF-A released from tumor cells adds substantially to VEGF-A derived from other body cells. Likewise, the inhibition of sVEGFR-2 release into circulation by sunitinib may be more affected in tumor tissue than in healthy ones. This would be in accordance with preclinical observations in tumor-bearing and healthy mice [73]. Moreover, it appears that the magnitude of biomarker release (or inhibition of release) depends on the type of tumor.

This is in line with the theory that mRCC is more susceptible to angiogenesis inhibition than is GIST [80]. In GIST, sunitinib's affinity to KIT seems to be of higher relevance for the antitumor effect than inhibition of angiogenesis [81]. In this context it is important to note, that VEGF receptors are also overexpressed in breast cancer tissue [154].

5.2.4 Clinical Trial Simulation

The results from the clinical trial simulations showed that adjusting the dose based on individual diastolic blood pressure measurements could relevantly prolong overall survival (OS). However, the benefit of the estimated 210 days of longer survival comes at the cost of a higher risk to suffer from severe fatigue. Since fatigue is a manageable and reversible side effect this may be clinically acceptable. Variation of the target increase in diastolic blood pressure suggested, that an increase of 16%, may be the most useful target. Higher target values only led to an increased incidence of severe fatigue but did not prolong survival any further.

With clinical trial simulations it is possible to estimate the probability that a trial will be successful and the influence of different design factors (e.g., study size) on this probability can be investigated. This was done by repeatedly simulating the trial and counting the number of times the null hypothesis (no difference between the two groups) was declared false. This number divided by the total number of simulation replicates represents the statistical power of the trial [16].

Not surprisingly, the statistical power to demonstrate a significant difference in OS was related to the number of patients studied. Figure 4-23 suggests that about 125 patients per group may be needed to achieve a power greater than 80%. However, it should be noted that the results from the power analysis may be overly optimistic since important factors such as dropouts, noncompliance, occurrence of adverse events others than fatigue leading to dose reductions, treatment interruption, death unrelated to tumor etc., were not considered in the present simulations. In fact, in a large phase III trial a reduction of the dose was necessary in about 50% of the patients [155].

The purpose of this clinical trial simulation was to give an impression of the potential that dose individualization of sunitinb may have and to show the usefulness of modeling and simulation as a tool to explore this. More exhaustive simulations including the above-mentioned factors will be required when a real clinical trial is to be planned. Especially a (logistic regression) model relating the probability of having a dose reduction or a treatment interruption to some measure of drug exposure would be useful. Despite the limitations of this simulation study, the benefit of dose individualization based on blood pressure measurements is obvious and in line with previous findings. Several retrospective analyses showed that elevated blood pressure has the potential to

be predictive for treatment outcome with antiangiogenic agents [79,156,157]. Rixe et al. [79], found that hypertension of >grade 2 was an independent predictor for a better clinical response in patients with mRCC treated with sunitinib. Moreover, a tremendous survival benefit was observed in phase II studies of axitinib, a selective inhibitor of VEGF receptors 1, 2, and 3, where patients with recorded diastolic blood pressure ≥90 mmHg lived about 90 weeks (!) longer than patients without blood pressure increase [158]. This probably led to the decision to apply a special dose-titration scheme based on blood pressure control for the phase III program of this drug [70,158]. Although not published yet, it is very likely that the company developing axitinib (Pfizer Inc.) used modeling and simulation techniques to support this decision.

6 Conclusions and Perspectives

Although the two drugs sunitinib and venlafaxine come from unrelated therapeutic fields, oncology and central nervous system diseases, the approach of PK/PD modeling and simulation using biomarkers could be successfully applied to both of them. In fact, these two therapeutic areas are among the ones with the highest failure rates of drug development programs. Most likely this is due to the lack of robust and early responding biomarkers, capable of quantifying efficacy in proof-of-concept studies [159].

Even though a correlation between pupillary light reflex parameters and the clinical effect of antidepressant drugs has not been established yet, pupillography has the potential of generating biomarkers that are useful in the clinical development of this kind of drugs. In this thesis it was shown, that light reflex parameters changed in a concentration-dependent manner, and parameters describing venlafaxine's pharmacological potency (S_E) were derived from PK/PD models. Given this, a company investigating on norepinephrine reuptake inhibitors could conduct a small crossover study in healthy subjects where different doses of the candidate drug(s), placebo and the marketed competitor are administered. The results would indicate the most potent candidate, permit early comparison with the competitor, and facilitate dose selection for the phase II studies. All this is extremely valuable information, obtained from only one, relatively inexpensive study in a short period of time.

If pupillographic response could ultimately be related to clinical response, this biomarker may also be used for dose adjustments early in the course of the treatment. For instance, a pupillographic assessment could be scheduled a few days after treatment initiation and a dose adjustment would be made according to the results, instead of waiting several weeks until changes of clinical symptoms are observed.

The data used in this thesis originated from small studies in healthy volunteers, excluding the possibility to establish a relationship between biomarker response and clinical outcome. The models developed in here may, however, serve as a starting point for further investigations in patients where establishing such a relationship is an objective. One such starting point is the planning of sampling times at which biomarker observations should ideally be scheduled in a clinical study. PK/PD models can be used

for this task as it was illustrated in the venlafaxine project. Informative sampling times are a prerequisite for a meaningful analysis of biomarker data. Furthermore, simulations can be used to assess how a different formulation (e.g., extended release) would influence the PD response.

In the sunitinib project simulations suggested that the circulating biomarkers behave differently in healthy subjects and patients and that the biomarker response may also depend on the tumor entity. It would be interesting to conduct a population PK/PD meta-analysis on biomarker data from studies in patients with different tumor entities. The present models would provide the basis with "tumor type" being investigated as a covariate on, for example, the intrinsic activity parameters α_{VEGF-A} or $\alpha_{sVEGFR-2}$. In patients, biomarker response may not be constant over weeks and months of treatment. Indeed, in a study with continuous daily sunitinib administration, VEGF-A levels kept increasing over 4 months of treatment without reaching a plateau [81]. This, however, could be easily incorporated in a model and might reflect disease progression. With biomarker data from large patient populations the influence of additional patient specific covariates on biomarker response, such as age, sex, disease state, tumor size, concurrent medication, previous treatment etc., could be explored, thus gaining more insight into the complexities of the disease and the biomarker response itself. In the end, this may help to earlier identify patients not responding to the drug and would give some guidance how treatment should be continued (e.g., dose increase, switch to another drug of the same class, change drug class, etc.).

The predictive value of circulating biomarkers with respect to the outcome of an antiangiogenic therapy is still a matter of debate [160,161]. Evidence for blood pressure as a predictor of clinical response, however, is much stronger [79,158,160,162,163]. In this thesis simulations were performed combining the developed blood pressure model with a published survival model and a model accounting for the risk of severe fatigue. The results suggested that individualizing the dose of sunitinib based on blood pressure measurements has the potential to prolong survival by 7 months. The real value of this kind of dose individualization has to be confirmed prospectively, like it is currently done for axitinib [70], before it can be routinely applied in clinical practice. However, it was exemplified how modeling and simulation could be used for the planning of such a prospective clinical trial.

In summary, biomarkers are of great utility for the development of new drugs and the optimization of drug treatment. They can be used to support the selection of the most effective (and least toxic) candidate compound, are helpful in finding the most appropriate dose or dosing schedule, and may support regulatory approval. This will make the development process more efficient and important new drugs will be available earlier.

In clinical practice biomarkers offer the possibility to adjust treatment modalities based on the patients' individual biomarker response, providing the physician with a potent tool to improve drug treatment

PK/PD modeling and simulation will play a central role in biomarker research, establishing the link between dose and biomarker response. This will help us to understand the complexities of a pharmacological response in a quantitative way.

7 Summary

In this thesis the concept of pharmacokinetic/pharmacodynamic modeling using biomarkers for the description of concentration-effect relationships was illustrated on the example of two projects with drugs from different therapeutic areas.

As first example venlafaxine, an antidepressant selectively inhibiting serotonin and norepinephrine reuptake from the synaptic gap, was investigated. The inhibition of norepinephrine uptake is assumed to enhance antidepressant efficacy when venlafaxine is given at higher therapeutic doses. Therefore the investigation of the concentration-response relationship of noradrenergic effects is of clinical interest. A useful test system to measure noradrenergic response is pupillography since the pupillary light reflex is controlled, in part, by the sympathetic nervous system. In a randomized-controlled crossover trial, 12 healthy volunteers received placebo or up to 75 mg venlafaxine twice daily for 14 days. On day 14 blood samples were drawn to determine serum concentrations of venlafaxine and its major active metabolite O-desmethylvenlafaxine. Together with data from serial pupillographic measurements in these volunteers, a pharmacokinetic/pharmacodynamic (PK/PD) model was developed to describe the time course of the noradrenergic response.

The PK part of the model was simultaneously fit to venlafaxine and O-desmethylvenlafaxine concentration-time data, yielding precise parameter estimates that are similar to published results. A rapid development of tolerance of the pupillary light reflex parameters, amplitude and 33% recovery time, was seen, most probably due to desensitization of β-adrenoceptors. This was successfully accounted for in the PD part of the model. The half-life of development and regression of tolerance was estimated to be 30 min for the amplitude and 40 min for the 33% recovery time.

As examples of possible applications of the model, optimal pupillographic sampling times for a hypothetical single-dose study were calculated based on the modeling results. Using simulations it was investigated how an oral formulation with a slower drug release (extended release) would influence the PD response-time profile.

In the second project sunitinib, a multitargeted tyrosine kinase inhibitor with antiangiogenic properties, was investigated. The effects on blood pressure, plasma concentrations of vascular endothelial growth factor A and C (VEGF-A and -C) and its

soluble receptor-2 (sVEGFR-2) in response to administration of 50 mg sunitinib on 3 to 5 consecutive days were studied in 12 healthy volunteers. PK/PD models were developed to quantify changes of these biomarkers in relation to plasma concentrations of sunitinib and its active metabolite.

Increasing blood pressure and VEGF-A levels were observed shortly after the first dose while a decrease in sVEGFR-2 occurred with substantial delay. No concentration-dependent changes of VEGF-C levels were observed in this study. The models predicted a percent change (relative to baseline) in systolic and diastolic blood pressure, VEGF-A, and sVEGFR-2 levels, of 10%, 18%, 124%, and -24% respectively, for a typical subject after 4 weeks of sunitinib treatment with 50 mg/day. Simulated blood pressure-time courses excellently compared to published patient data, whereas changes in circulating biomarkers were greater in patients than simulations suggested for healthy subjects. With the model for blood pressure changes, and published models for survival and incidence of fatigue, clinical trials were simulated showing that blood pressure-guided dose individualization could potentially prolong the median survival time by 210 days, compared to the standard dosing regimen.

The approach of PK/PD modeling and simulation using biomarkers was successfully applied in both projects and more insight into the concentration-response relationship of venlafaxine and sunitinib was obtained. Biomarkers will play an increasingly important role in drug development and pharmacotherapy. They will guide important decisions regarding candidate selection, dose finding and regulatory approval and will improve our understanding of complex diseases like cancer and mental disorders. Modeling and simulation are extremely useful tools to fully exploit the potential of biomarkers in this context.

8 References

(1) Dost, FH. Der Blutspiegel - Kinetik der Konzentrationsabläufe in der Kreislaufflüssigkeit. Leipzig, Thieme, 1953.

(2) Nelson, E. Kinetics of drug absorption, distribution, metabolism, and excretion. J Pharm Sci 1961; 50: 181-192.

(3) Teorell, T. Kinetics of distribution of substances administered to the body. I. The extravascular modes of administration. Arch Int Pharmacodyn Ther 1937; 57: 205-225.

(4) Teorell, T. Kinetics of distribution of substances administered to the body. II. The intravascular modes of administration. Arch Int Pharmacodyn Ther 1937; 57: 226-240.

(5) Bonate, PL. Pharmacokinetic-Pharmacodynamic Modeling and Simulation. New York, NY, Springer, 2006.

(6) Ariens, E. Affinity and intrinsic activity in the theory of competitive inhibition. I. Problems and theory. Arch Int Pharmacodyn Ther 1954; 99: 32-49.

(7) Stephenson, R. A modification of receptor theory. Br J Pharmacol Chemother 1956; 11: 379-393.

(8) Holford, NH, Sheiner, LB. Kinetics of pharmacologic response. Pharmacol Ther 1982; 16: 143-166.

(9) Mager, DE, Wyska, E, Jusko, WJ. Diversity of Mechanism-Based Pharmacodynamic Models. Drug Metab Dispos 2003; 31: 510-518.

(10) Sun, YN, Dubois, DC, Almon, RR et al. Fourth-generation model for corticosteroid pharmacodynamics: A model for methylprednisolone effects on receptor/gene-mediated glucocorticoid receptor down-regulation and tyrosine aminotransferase induction in rat liver. J Pharmacokinet Biopharm 1998; 26: 289-317.

(11) Aldrich, J. R.A. Fisher and the making of maximum likelihood 1912-1922. Stat Sci 1997; 12: 162-176.

(12) Sheiner, BL, Beal, SL. Evaluation of methods for estimating population pharmacokinetic parameters. II. Biexponential model and experimental pharmacokinetic data. J Pharmacokinet Biopharm 1981; 9: 635-651.

(13) Sheiner, LB, Beal, SL. Evaluation of methods for estimating population pharmacokinetics parameters. I. Michaelis-Menten model: routine clinical pharmacokinetic data. J Pharmacokinet Biopharm 1980; 8: 553-571.

(14) Sheiner, LB, Beal, SL. Evaluation of methods for estimating population pharmacokinetic parameters. III. Monoexponential model: routine clinical pharmacokinetic data. J Pharmacokinet Biopharm 1983; 11: 303-319.

(15) Sheiner, LB, Rosenberg, B, Marathe, VV. Estimation of population characteristics of pharmacokinetic parameters from routine clinical data. J Pharmacokinet Biopharm 1977; 5: 445-479.

(16) Ette, EI, Williams, PJ (eds.). Pharmacometrics. Hoboken, NJ, John Wiley & Sons, 2007.

(17) Munos, B. Lessons from 60 years of pharmaceutical innovation. Nat Rev Drug Discov 2009; 8: 959-968.

(18) US Department of Health and Human Services, Food and Drug Administration. Innovation or stagnation? Challenge and opportunity on the critical path to new medical products. 2007. URL: http://www.fda.gov/oc/initiatives/criticalpath/whitepaper.pdf

(19) Stanski, DR, Rowland, M, Sheiner, LB. Getting the Dose Right: report from the Tenth European Federation of Pharmaceutical Sciences (EUFEPS) conference on optimizing drug development. J Pharmacokinet Pharmacodyn 2005; 32: 199-211.

(20) Sheiner, LB. Learning versus confirming in clinical drug development. Clin Pharmacol Ther 1997; 61: 275-291.

(21) Holford, NH, Kimko, HC, Monteleone, JP et al. Simulation of clinical trials. Annu Rev Pharmacol Toxicol 2000; 40: 209-234.

(22) Duffull, SB, Mentre, F, Aarons, L. Optimal Design of a Population Pharmacodynamic Experiment for Ivabradine. Pharm Res 2001; 18: 83-89.

(23) Chien, JY, Friedrich, S, Heathman, MA et al. Pharmacokinetics/Pharmacodynamics and the stages of drug development: role of modeling and simulation. AAPS J 2005; 7: E544-E559.

(24) Committee for Medicinal Products for Human Use, European Medicines Agency. Guideline on strategies to identify and mitigate risks for first-in-human clinical trials with investigational medicinal products. 2007. URL: http://www.ema.europa.eu/htms/human/humanguidelines/efficacy.htm

(25) Mandema, JW, Hermann, D, Wang, W et al. Model-based development of gemcabene, a new lipid-altering agent. AAPS J 2005; 7: E513-E522.

(26) Lalonde, RL, Kowalski, KG, Hutmacher, MM et al. Model-based Drug Development. Clin Pharmacol Ther 2007; 82: 21-32.

(27) Miller, R, Ewy, W, Corrigan, BW et al. How modeling and simulation have enhanced decision making in new drug development. J Pharmacokinet Pharmacodyn 2005; 32: 185-197.

(28) Samara, E, Granneman, R. Role of population pharmacokinetics in drug development - A pharmaceutical industry perspective. Clin Pharmacokinet 1997; 32: 294-312.

(29) Olson, SC, Bockbrader, H, Boyd, RA et al. Impact of population pharmacokinetic-pharmacodynamic analyses on the drug development process - Experience at Parke-Davis. Clin Pharmacokinet 2000; 38: 449-459.

(30) Kowalski, KG, Olson, S, Remmers, AE et al. Modeling and simulation to support dose selection and clinical development of SC-75416, a selective COX-2 inhibitor for the treatment of acute and chronic pain. Clin Pharmacol Ther 2008; 83: 857-866.

(31) Bhattaram, VA, Booth, BP, Ramchandani, RP et al. Impact of pharmacometrics on drug approval and labeling decisions: a survey of 42 new drug applications. AAPS J 2005; 7: E503-E512.

(32) US Department of Health and Human Services, Food and Drug Administration. Guidance for Industry - End-of-Phase 2A Meetings. 2009. URL: http://www.fda.gov/downloads/Drugs/GuidanceComplianceRegulatoryInformation/Guidances/ucm079690.pdf

(33) PricewaterhouseCoopers. Pharma 2020: VirtualR&D - Which path will you take? 2008. URL: http://www.pwc.com/gx/en/pharma-life-sciences/pharma-2020/pharma2020-virtual-rd-which-path-will-you-take.jhtml

(34) Cross, J, Lee, H, Westelinck, A et al. Postmarketing drug dosage changes of 499 FDA-approved new molecular entities, 1980-1999. Pharmacoepidemiol Drug Saf 2002; 11: 439-446.

(35) Pharmazeutische Zeitung. Neue Arzneistoffe. 2010. URL: http://www.pharmazeutische-zeitung.de/index.php?id=2670

(36) Mar Fernandez de Gatta MD, Victoria, CM, Ardanuy, R et al. Evaluation of population pharmacokinetic models for amikacin dosage individualization in critically ill patients. J Pharm Pharmacol 2009; 61: 759-766.

(37) Leader, WG, Chandler, MH, Castiglia, M. Pharmacokinetic optimisation of vancomycin therapy. Clin Pharmacokinet 1995; 28: 327-342.

(38) Chrystyn, H, Mulley, BA, Peake, MD. The accuracy of a pharmacokinetic theophylline predictor using once daily dosing. Br J Clin Pharmacol 1987; 24: 301-307.

(39) Jelliffe, RW, Schumitzky, A, Bayard, D et al. Model-based, goal-oriented, individualised drug therapy. Linkage of population modelling, new 'multiple

model' dosage design, bayesian feedback and individualised target goals. Clin Pharmacokinet 1998; 34: 57-77.

(40) Wallin, JE, Friberg, LE, Karlsson, MO. A tool for neutrophil guided dose adaptation in chemotherapy. Comput Methods Programs Biomed 2009; 93: 283-291.

(41) Harris, S. Riding the wave. 2010. URL: http://pharmexec.findpharma.com/pharmexec/Strategy/Riding-the-Wave/ArticleStandard/Article/detail/674795?contextCategoryId=48158

(42) Biomarkers Definitions Working Group. Biomarkers and surrogate endpoints: Preferred definitions and conceptual framework. Clin Pharmacol Ther 2001; 69: 89-95.

(43) Colburn, WA, Lee, JW. Biomarkers, validation and pharmacokinetic-pharmacodynamic modelling. Clin Pharmacokinet 2003; 42: 997-1022.

(44) International Conference on Harmonization. Statistical Principles for Clincial Trials. 1998. URL: http://www.ich.org/cache/compo/475-272-1.html#E9

(45) Lathia, CD, Amakye, D, Dai, W et al. The value, qualification, and regulatory use of surrogate end points in drug development. Clin Pharmacol Ther 2009; 86: 32-43.

(46) Wyeth Pharmaceuticals Inc. Effexor Prescribing Information. 2010. URL: http://www.accessdata.fda.gov/drugsatfda_docs/label/2010/020151s056s057lbl.pdf

(47) Simon, JS, Aguiar, LM, Kunz, NR et al. Extended-release venlafaxine in relapse prevention for patients with major depressive disorder. J Psychiatr Res 2004; 38: 249-257.

(48) Fritze, J, Schneider, B, Weber, B. Venlafaxin ist kein SSRI, sondern ein SNRI, und das ist relevant. Psychoneuro 2003; 29: 240-244.

(49) Patat, A, Troy, S, Burke, J et al. Absolute bioavailability and electroencephalographic effects of conventional and extended-release formulations of venlafaxine in healthy subjects. J Clin Pharmacol 1998; 38: 256-267.

(50) Howell, SR, Husbands, GE, Scatina, JA et al. Metabolic disposition of 14C-venlafaxine in mouse, rat, dog, rhesus monkey and man. Xenobiotica 1993; 23: 349-359.

(51) Klamerus, KJ, Maloney, K, Rudolph, RL et al. Introduction of a composite parameter to the pharmacokinetics of venlafaxine and its active O-desmethyl metabolite. J Clin Pharmacol 1992; 32: 716-724.

(52) Muth, EA, Haskins, JT, Moyer, JA et al. Antidepressant biochemical profile of the novel bicyclic compound Wy-45,030, an ethyl cyclohexanol derivative. Biochem Pharmacol 1986; 35: 4493-4497.

(53) Harvey, AT, Rudolph, RL, Preskorn, SH. Evidence of the Dual Mechanisms of Action of Venlafaxine. Arch Gen Psychiatry 2000; 57: 503-509.

(54) Lecrubier, Y. Clinical utility of venlafaxine in comparison with other antidepressants. Int Clin Psychopharmacol 1995; 10 Suppl 2: 29-35.

(55) Redrobe, JP, Bourin, M, Colombel, MC et al. Dose-dependent noradrenergic and serotonergic properties of venlafaxine in animal models indicative of antidepressant activity. Psychopharmacology 1998; 138: 1-8.

(56) Thompson, C. Onset of action of antidepressants: results of different analyses. Hum Psychopharmacol 2002; 17 Suppl 1: S27-S32.

(57) White, TL, Depue, RA. Differential Association of Traits of Fear and Anxiety With Norepinephrine- and Dark-Induced Pupil Reactivity. J Pers Soc Psychol 1999; 77: 863-877.

(58) Bitsios, P, Szabadi, E, Bradshaw, CM. Comparison of the effects of venlafaxine, paroxetine and desipramine on the pupillary light reflex in man. Psychopharmacology 1999; 143: 286-292.

(59) Rini, BI. Sunitinib. Expert Opin Pharmacother 2007; 8: 2359-2369.

(60) Goodman, VL, Rock, EP, Dagher, R et al. Approval summary: Sunitinib for the treatment of imatinib refractory or intolerant gastrointestinal stromal tumors and advanced renal cell carcinoma. Clin Cancer Res 2007; 13: 1367-1373.

(61) Sherman, L, Peng, G, Patyna, S et al. Open-label, single-dose, phase I study evaluating the mass balance and pharmacokinetics (PKs) of sunitinib (SU) in healthy male subjects [abstract 731]. 14th European Cancer Conference; 2007 Sep 23-27, Barcelona, Spain. Eur J Cancer Supplements 2007; 5 (Suppl. 4): 116

(62) Faivre, S, Demetri, G, Sargent, W et al. Molecular basis for sunitinib efficacy and future clinical development. Nat Rev Drug Discov 2007; 6: 734-745.

(63) Chow, LQM, Eckhardt, SG. Sunitinib: From Rational Design to Clinical Efficacy. J Clin Oncol 2007; 25: 884-896.

(64) Duensing, A, Heinrich, MC, Fletcher, CD et al. Biology of gastrointestinal stromal tumors: KIT mutations and beyond. Cancer Invest 2004; 22: 106-116.

(65) Rini, BI, Small, EJ. Biology and clinical development of vascular endothelial growth factor-targeted therapy in renal cell carcinoma. J Clin Oncol 2005; 23: 1028-1043.

(66) Hicklin, DJ, Ellis, LM. Role of the vascular endothelial growth factor pathway in tumor growth and angiogenesis. J Clin Oncol 2005; 23: 1011-1027.

(67) Takahashi, H, Shibuya, M. The vascular endothelial growth factor (VEGF)/VEGF receptor system and its role under physiological and pathological conditions. Clin Sci 2005; 109: 227-241.

(68) Strumberg, D, Schultheis, B, Adamietz, IA et al. Phase I dose escalation study of telatinib (BAY 57-9352) in patients with advanced solid tumours. Br J Cancer 2008; 99: 1579-1585.

(69) Teicher, BA, Ellis, LM (eds.). Antiangiogenic agents in cancer therapy. 2nd ed. Totowa, NJ, Humana Press, 2008.

(70) Kelly, RJ, Rixe, O. Axitinib-a selective inhibitor of the vascular endothelial growth factor (VEGF) receptor. Target Oncol 2009; 4: 207-305.

(71) Jain, RK, Duda, DG, Willett, CG et al. Biomarkers of response and resistance to antiangiogenic therapy. Nat Rev Clin Oncol 2009; 6: 327-338.

(72) Jubb, AM, Oates, AJ, Holden, S et al. Predicting benefit from anti-angiogenic agents in malignancy. Nat Rev Cancer 2006; 6: 626-635.

(73) Ebos, JM, Lee, CR, Christensen, JG et al. Multiple circulating proangiogenic factors induced by sunitinib malate are tumor-independent and correlate with antitumor efficacy. Proc Natl Acad Sci 2007; 104: 17069-17074.

(74) Azizi, M, Chedid, A, Oudard, S. Home blood-pressure monitoring in patients receiving sunitinib. N Engl J Med 2008; 358: 95-97.

(75) Burstein, HJ, Elias, AD, Rugo, HS et al. Phase II study of sunitinib malate, an oral multitargeted tyrosine kinase inhibitor, in patients with metastatic breast cancer previously treated with an anthracycline and a taxane. J Clin Oncol 2008; 26: 1810-1816.

(76) DePrimo, SE, Bello, C, Smeraglia, J et al. Circulating protein biomarkers of pharmacodynamic activity of sunitinib in patients with metastatic renal cell carcinoma: modulation of VEGF and VEGF-related proteins. J Transl Med 2007; 5: 32.

(77) Kontovinis, L, Papazisis, K, Touplikioti, P et al. Sunitinib treatment for patients with clear-cell metastatic renal cell carcinoma: clinical outcomes and plasma angiogenesis markers. BMC Cancer 2009; 9: 82.

(78) Norden-Zfoni, A, Desai, J, Manola, J et al. Blood-based biomarkers of SU11248 activity and clinical outcome in patients with metastatic imatinib-resistant gastrointestinal stromal tumor. Clin Cancer Res 2007; 13: 2643-2650.

(79) Rixe, O, Billemont, B, Izzedine, H. Hypertension as a predictive factor of Sunitinib activity. Ann Oncol 2007; 18: 1117.

(80) Motzer, RJ, Michaelson, MD, Redman, BG et al. Activity of SU11248, a multitargeted inhibitor of vascular endothelial growth factor receptor and platelet-derived growth factor receptor, in patients with metastatic renal cell carcinoma. J Clin Oncol 2006; 24: 16-24.

(81) George, S, Blay, JY, Casali, PG et al. Clinical evaluation of continuous daily dosing of sunitinib malate in patients with advanced gastrointestinal stromal tumour after imatinib failure. Eur J Cancer 2009; 45: 1959-1968.

(82) Ebos, JML, Lee, CR, Bogdanovic, E et al. Vascular endothelial growth factor-mediated decrease in plasma soluble vascular endothelial growth, factor receptor-2 levels as a surrogate biomarker for tumor growth. Cancer Res 2008; 68: 521-529.

(83) Sica, DA. Angiogenesis inhibitors and hypertension: An emerging issue. J Clin Oncol 2006; 24: 1329-1331.

(84) Sane, DC, Anton, L, Brosnihan, KB. Angiogenic growth factors and hypertension. Angiogenesis 2004; 7: 193-201.

(85) Mourad, JJ, des Guetz, G, Debbabi, H et al. Blood pressure rise following angiogenesis inhibition by bevacizumab. A crucial role for microcirculation. Ann Oncol 2008; 19: 927-934.

(86) Launay-Vacher, V, Deray, G. Hypertension and proteinuria: a class-effect of antiangiogenic therapies. Anticancer Drugs 2009; 20: 81-82.

(87) Izzedine, H, Ederhy, S, Goldwasser, F et al. Management of hypertension in angiogenesis inhibitor-treated patients. Ann Oncol 2009; 20: 807-815.

(88) Roodhart, JM, Langenberg, MH, Witteveen, E et al. The molecular basis of class side effects due to treatment with inhibitors of the VEGF/VEGFR pathway. Curr Clin Pharmacol 2008; 3: 132-143.

(89) Keizer, RJ, Gupta, A, Mac Gillavry, MR et al. A model of hypertension and proteinuria in cancer patients treated with the anti-angiogenic drug E7080. J Pharmacokinet Pharmacodyn 2010; 37: 347-363.

(90) Beal, SL, Sheiner, LB, Boeckmann, AJ. NONMEM Users Guide (1989 - 2006). Ellicott City, MD, Icon Development Solutions, 2006.

(91) Holford, N. Wings for NONMEM. 2007. URL: http://wfn.sourceforge.net

(92) Karlsson, MO, Savic, RM. Diagnosing model diagnostics. Clin Pharmacol Ther 2007; 82: 17-20.

(93) Efron, B. Bootstrap methods - another look at the Jackknife. Ann Stat 1979; 7: 1-26.

(94) Lindbom, L, Pihlgren, P, Jonsson, EN. PsN-Toolkit--a collection of computer intensive statistical methods for non-linear mixed effect modeling using NONMEM. Comput Methods Programs Biomed 2005; 79: 241-257.

(95) Hooker, A, Karlsson, MO. Conditional weighted residuals: a diagnostic to improve population PK/PD model building and evaluation. AAPS PharmSci 2005; 7: W5321.

(96) Jonsson, EN, Karlsson, MO. Xpose - an S-PLUS based population pharmacokinetic/pharmacodynamic model building aid for NONMEM. Comput Methods Programs Biomed 1999; 58: 51-64.

(97) Holford, NH and Karlsson, M. A Tutorial on Visual Predictive Checks [abstract 1434]. 17th Annual Meeting of the Population Approach Group in Europe; 2007 Jun 18-20, Marseille, France.

(98) Holford, NH. VPC, the visual predictve check - superiority to standard diagnostic (Rorschach) plots [abstract 738]. 14th Annual Meeting of the Population Approach Group in Europe; 2005 Jun 16-17, Pamplona, Spain.

(99) R Development Core Team. R: A language and environment for statistical computing. R Foundation for Statistical Computing, Vienna, Austria, 2008. URL: http://www.R-project.org

(100) Hicks, DR, Wolaniuk, D, Russell, A et al. A high-performance liquid chromatographic method for the simultaneous determination of venlafaxine and O-desmethylvenlafaxine in biological fluids. Ther Drug Monit 1994; 16: 100-107.

(101) Matoga, M, Pehourcq, F, Titier, K et al. Rapid high-performance liquid chromatographic measurement of venlafaxine and O-desmethylvenlafaxine in human plasma. Application to management of acute intoxications. J Chromatogr B Biomed Sci Appl 2001; 760: 213-218.

(102) Juan, H, Zhiling, Z, Huande, L. Simultaneous determination of fluoxetine, citalopram, paroxetine, venlafaxine in plasma by high performance liquid chromatography-electrospray ionization mass spectrometry (HPLC-MS/ESI). J Chromatogr B Analyt Technol Biomed Life Sci 2005; 820: 33-39.

(103) Siepmann, T, Ziemssen, T, Mueck-Weymann, M et al. The effects of venlafaxine on autonomic functions in healthy volunteers. J Clin Psychopharmacol 2007; 27: 687-691.

(104) Taft, DR, Iyer, GR, Behar, L et al. Application of a First-Pass Effect Model to Characterize the Pharmacokinetic Disposition of Venlafaxine after Oral Administration to Human Subjects. Drug Metab Dispos 1997; 25: 1215-1218.

(105) Gordi, T, Xie, R, Huong, NV et al. A semiphysiological pharmacokinetic model for artemisinin in healthy subjects incorporating autoinduction of metabolism

and saturable first-pass hepatic extraction. Br J Clin Pharmacol 2005; 59: 189-198.

(106) Rousseau, A, Leger, F, Le, MY et al. Population pharmacokinetic modeling of oral cyclosporin using NONMEM: comparison of absorption pharmacokinetic models and design of a Bayesian estimator. Ther Drug Monit 2004; 26: 23-30.

(107) Parker, VD, Richards, LS, Nichols, AI et al. The absolute bioavailability of an oral sustained-release formulation of desvenlafaxine succinate in healthy subjects. Clin Pharmacol Ther 2005; 77: P47.

(108) Central European Society for Anticancer Drug Research - EWIV. SOP14: Population Pharmacokinetic Analysis (version 02). 2007. URL: http://www.cesar.or.at

(109) Muth, EA, Moyer, JA, Haskins, JT et al. Biochemical, Neurophysiological, and Behavioral-Effects of Wy-45,233 and Other Identified Metabolites of the Antidepressant Venlafaxine. Drug Dev Res 1991; 23: 191-199.

(110) Dayneka, NL, Garg, V, Jusko, WJ. Comparison of four basic models of indirect pharmacodynamic responses. J Pharmacokinet Pharmacodyn 1993; 21: 457-478.

(111) Kenakin, T. Pharmacologic analysis of drug-receptor interaction. Philadelphia, Lippincott-Raven, 1997.

(112) Movin-Osswald, G, Hammarlund-Udenaes, M. Prolactin release after remoxipride by an integrated pharmacokinetic-pharmacodynamic model with intra- and interindividual aspects. J Pharmacol Exp Ther 1995; 274: 921-927.

(113) Mandema, JW, Wada, DR. Pharmacodynamic model for acute tolerance development to the electroencephalographic effects of alfentanil in the rat. J Pharmacol Exp Ther 1995; 275: 1185-1194.

(114) Bauer, JA, Fung, HL. Pharmacodynamic Models of Nitroglycerin-Induced Hemodynamic Tolerance in Experimental Heart-Failure. Pharm Res 1994; 11: 816-823.

(115) Ekblom, M, Hammarlund-Udenaes, M, Paalzow, L. Modeling of tolerance development and rebound effect during different intravenous administrations of morphine to rats. J Pharmacol Exp Ther 1993; 266: 244-252.

(116) Porchet, HC, Benowitz, NL, Sheiner, LB. Pharmacodynamic model of tolerance: application to nicotine. J Pharmacol Exp Ther 1988; 244: 231-236.

(117) Shi, J, Benowitz, NL, Denaro, CP et al. Pharmacokinetic-pharmacodynamic modeling of caffeine: tolerance to pressor effects. Clin Pharmacol Ther 1993; 53: 6-14.

(118) Duffull, S et al. WinPOPT Users Guide version 1.2. 2008. URL: http://www.winpopt.com

(119) Elsinghorst, PW, Gutschow, M. Synthesis of H-2- and C-13-labelled sunitinib and its primary metabolite. J Labelled Comp Rad 2009; 52: 360-365.

(120) Krambeer, C. Bestimmung der Biomarker VEGF-A, VEGF-C und sVEGFR-2 im Plasma nach Applikation von Sunitinib. Diplomarbeit, Universität Bonn, 2009.

(121) Houk, BE, Bello, CL, Kang, D et al. A population pharmacokinetic meta-analysis of sunitinib malate (SU11248) and its primary metabolite (SU12662) in healthy volunteers and oncology patients. Clin Cancer Res 2009; 15: 2497-2506.

(122) Savic, R, Jonker, Dl, Kerbusch, T et al. Implementation of a transit compartment model for describing drug absorption in pharmacokinetic studies. J Pharmacokinet Pharmacodyn 2007; 34: 711-726.

(123) Danhof, M, de Jongh, J, De Lange, ECM et al. Mechanism-based pharmacokinetic-pharmacodynamic modeling: Biophase distribution, receptor theory, and dynamical systems analysis. Annu Rev Pharmacol Toxicol 2007; 47: 357-400.

(124) Mendel, DB, Laird, AD, Xin, X et al. In vivo antitumor activity of SU11248, a novel tyrosine kinase inhibitor targeting vascular endothelial growth factor and platelet-derived growth factor receptors: determination of a pharmacokinetic/pharmacodynamic relationship. Clin Cancer Res 2003; 9: 327-337.

(125) Mager, DE, Jusko, WJ. Pharmacodynamic modeling of time-dependent transduction systems. Clin Pharmacol Ther 2001; 70: 210-216.

(126) Houk, BE, Bello, CL, Poland, B et al. Relationship between exposure to sunitinib and efficacy and tolerability endpoints in patients with cancer: results of a pharmacokinetic/pharmacodynamic meta-analysis. Cancer Chemother Pharmacol 2009; 66: 357-371.

(127) Crawley, M. The R book. Chichester, England, John Wiley & Sons, 2007.

(128) US Department of Health and Human Services, Food and Drug Administration. Sutent - Clinical pharmacology and biopharmaceutics review. 2006. URL: http://www.accessdata.fda.gov/drugsatfda_docs/nda/2006/021938_S000_Sutent _BioPharmR.pdf

(129) Pfizer Inc. Sutent Prescribing Information. 2010. URL: http://media.pfizer.com/files/products/uspi_sutent.pdf

(130) Troy, SM, Schultz, RW, Parker, VD et al. The effect of renal disease on the disposition of venlafaxine. Clin Pharmacol Ther 1994; 56: 14-21.

(131) Sheiner, LB, Stanski, DR, Vozeh, S et al. Simultaneous modeling of pharmacokinetics and pharmacodynamics: application to d-tubocurarine. Clin Pharmacol Ther 1979; 25: 358-371.

(132) Hempel, G, Karlsson, MO, de Alwis, DP et al. Population pharmacokinetic-pharmacodynamic modeling of moxonidine using 24-hour ambulatory blood pressure measurements. Clin Pharmacol Ther 1998; 64: 622-635.

(133) Shams, ME, Arneth, B, Hiemke, C et al. CYP2D6 polymorphism and clinical effect of the antidepressant venlafaxine. J Clin Pharm Ther 2006; 31: 493-502.

(134) Amchin, J, Ereshefsky, L, Zarycranski, W et al. Effect of venlafaxine versus fluoxetine on metabolism of dextromethorphan, a CYP2D6 probe. J Clin Pharmacol 2001; 41: 443-451.

(135) Fukuda, T, Nishida, Y, Zhou, Q et al. The impact of the CYP2D6 and CYP2C19 genotypes on venlafaxine pharmacokinetics in a Japanese population. Eur J Clin Pharmacol 2000; 56: 175-180.

(136) Fukuda, T, Yamamoto, I, Nishida, Y et al. Effect of the CYP2D6*10 genotype on venlafaxine pharmacokinetics in healthy adult volunteers. Br J Clin Pharmacol 1999; 47: 450-453.

(137) Grozinger, M, Dragicevic, A, Hiemke, C et al. Melperone is an inhibitor of the CYP2D6 catalyzed O-demethylation of venlafaxine. Pharmacopsychiatry 2003; 36: 3-6.

(138) Otton, SV, Ball, SE, Cheung, SW et al. Venlafaxine oxidation in vitro is catalysed by CYP2D6. Br J Clin Pharmacol 1996; 41: 149-156.

(139) Veefkind, AH, Haffmans, PM, Hoencamp, E. Venlafaxine serum levels and CYP2D6 genotype. Ther Drug Monit 2000; 22: 202-208.

(140) Yang, J, Jamei, M, Yeo, KR et al. Misuse of the well-stirred model of hepatic drug clearance. Drug Metab Dispos 2007; 35: 501-502.

(141) Moyer, JA, Muth, EA, Haskins, J et al. In vivo antidepressant profiles of the novel bicyclic compounds Wy-45.030 and Wy-45.881. Soc Neurosci 1984; Abstr 10: 261.

(142) Franklin, M, Clement, EM, Campling, G et al. Effect of venlafaxine on pineal melatonin and noradrenaline in the male rat. J Psychopharmacol 1998; 12: 371-374.

(143) Evans, ND, Godfrey, KR, Chapman, MJ et al. An identifiability analysis of a parent-metabolite pharmacokinetic model for ivabradine. J Pharmacokinet Pharmacodyn 2001; 28: 93-105.

(144) Webb, JA, Rostami-Hodjegan, A, Abdul-Manap, R et al. Contribution of dihydrocodeine and dihydromorphine to analgesia following dihydrocodeine administration in man: a PK-PD modelling analysis. Br J Clin Pharmacol 2001; 52: 35-43.

(145)   Johnson, TN, Rostami-Hodjegan, A, Goddard, JM et al. Contribution of midazolam and its 1-hydroxy metabolite to preoperative sedation in children: a pharmacokinetic-pharmacodynamic analysis. Br J Anaesth 2002; 89: 428-437.

(146)   Bello, CL, Sherman, L, Zhou, J et al. Effect of food on the pharmacokinetics of sunitinib malate (SU11248), a multi-targeted receptor tyrosine kinase inhibitor: results from a phase I study in healthy subjects. Anticancer Drugs 2006; 17: 353-358.

(147)   Horowitz, JR, Rivard, A, vanderZee, R et al. Vascular endothelial growth factor vascular permeability factor produces nitric oxide-dependent hypotension - Evidence for a maintenance role in quiescent adult endothelium. Arterioscler Thromb Vasc Biol 1997; 17: 2793-2800.

(148)   Coca, A. Circadian rhythm and blood pressure control: physiological and pathophysiological factors. J Hypertens Suppl 1994; 12: S13-S21.

(149)   Eppler, SM, Combs, DL, Henry, TD et al. A target-mediated model to describe the pharmacokinetics and hemodynamic effects of recombinant human vascular endothelial growth factor in humans. Clin Pharmacol Ther 2002; 72: 20-32.

(150)   Hormbrey, E, Gillespie, P, Turner, K et al. A critical review of vascular endothelial growth factor (VEGF) analysis in peripheral blood: is the current literature meaningful? Clin Exp Metastasis 2002; 19: 651-663.

(151)   Banks, RE, Forbes, MA, Kinsey, SE et al. Release of the angiogenic cytokine vascular endothelial growth factor (VEGF) from platelets: significance for VEGF measurements and cancer biology. Br J Cancer 1998; 77: 956-964.

(152)   Jelkmann, W. Pitfalls in the Measurement of Circulating Vascular Endothelial Growth Factor. Clin Chem 2001; 47: 617-623.

(153)   Rini, BI, Michaelson, MD, Rosenberg, JE et al. Antitumor activity and biomarker analysis of sunitinib in patients with bevacizumab-refractory metastatic renal cell carcinoma. J Clin Oncol 2008; 26: 3743-3748.

(154)   Kranz, A, Mattfeldt, T, Waltenberger, J. Molecular mediators of tumor angiogenesis: enhanced expression and activation of vascular endothelial growth factor receptor KDR in primary breast cancer. Int J Cancer 1999; 84: 293-298.

(155)   Motzer, RJ, Hutson, TE, Tomczak, P et al. Overall survival and updated results for sunitinib compared with interferon alfa in patients with metastatic renal cell carcinoma. J Clin Oncol 2009; 27: 3584-3590.

(156)   Ravaud, A, Sire, M. Arterial hypertension and clinical benefit of sunitinib, sorafenib and bevacizumab in first and second-line treatment of metastatic renal cell cancer. Ann Oncol 2009; 20: 966-967.

(157)   Rini, BI, Schiller, JH, Fruehauf, JP et al. Association of diastolic blood pressure (dBP) > 90 mmHg with overall survival (OS) in patients treated with axitinib (AG- 013736). J Clin Oncol (Meeting Abstracts) 2008; Abstr 3543.

(158)   Rixe, O, Dutcher, J, Motzer, R et al. Diastolic blood pressure (dBP) and pharmacokinetics (PK) as predictors of axitinib efficacy in metastatic renal cell cancer (mRCC). J Clin Oncol 2009; 27: 5045.

(159)   Kola, I. The state of innovation in drug development. Clin Pharmacol Ther 2008; 83: 227-230.

(160)   Murukesh, N, Dive, C, Jayson, GC. Biomarkers of angiogenesis and their role in the development of VEGF inhibitors. Br J Cancer 2009; 102: 8-18.

(161)   Duda, DG, Ancukiewicz, M, Jain, RK. Biomarkers of antiangiogenic therapy: how do we move from candidate biomarkers to valid biomarkers? J Clin Oncol 2010; 28: 183-185.

(162)   Levy, BI. Blood pressure as a potential biomarker of the efficacy angiogenesis inhibitor. Ann Oncol 2009; 20: 200-203.

(163)   van Heeckeren, WJ, Ortiz, J, Cooney, MM et al. Hypertension, proteinuria, and antagonism of vascular endothelial growth factor signaling: Clinical toxicity, therapeutic target, or novel biomarker? J Clin Oncol 2007; 25: 2993-2995.

9 Appendix

9.1 Venlafaxine Study

9.1.1 Tables

Table 9-1 Model building summary - Important steps of the **venlafaxine PK** model development

Model number	Model description	Random effects	Number of parameters (fixed/random)	OFV
1	1 compartment VEN, 1 compartment ODV, first-order absorption	$IIV(CL_{int,VEN})$ $IIV(CL_{ODV})$ $IIV(k_a)$	6/7	2990.1
2	2 compartment VEN, 1 compartment ODV, first-order absorption	Like model #1	8/7	2984.1
3	Structural model #1 + lag time	Like model #2	7/7	2973.8
4	1 compartment VEN, 1 compartment ODV, zero-order absorption	$IIV(CL_{int,VEN})$ $IIV(CL_{ODV})$ $IIV(k_0)$	6/7	2961.4
5	Structural model #4 + lag time	Like model #3	7/7	2953.5
6	Structural model #1 2 transit compartments of absorption	$IIV(CL_{int,VEN})$ $IIV(CL_{ODV})$ $IIV(MAT)$	6/7	2965.8
7	Structural model #1 3 transit compartments of absorption	Like model #6	6/7	2957.8
8	Structural model #1 4 transit compartments of absorption	Like model #6	6/7	2957.5
9	Structural model #7	Like model #6 + $IIV(f_m)$	6/8	2913.0
10	Structural model #7	Like model #6 + $IIV(f_m)IIV(V_{VEN})$	6/9	2912.8
11	Structural model #7 (**Final model**)	Like model #9	6/7	2916.5
12	Structural model #7 + nonhepatic clearance	Like model #9	7/7	2916.6
13	Structural model #5	$IIV(CL_{int,VEN})$ $IIV(CL_{ODV})$ $IIV(f_m),IIV(k_0)$	7/7	2914.1

OFV: objective function value; IIV: interindividual variability; VEN: venlafaxine; ODV: O-desmethylvenlafaxine; $CL_{int,VEN}$: intrinsic clearance of venlafaxine; CL_{ODV}: clearance of O-desmethylvenlafaxine; k_a: first-order absorption rate constant; k_0: zero-order absorption rate; V_{VEN}: volume of distribution of venlafaxine's central compartment; f_m: fraction of venlafaxine metabolized to O-desmethylvenlafaxine.

Table 9-2   Model building summary - Important steps of the **amplitude** model development

Model number	Model description	Random effects	Number of parameters (fixed/random)	OFV
1	Null model (only BL is estimated)	IIV(BL) proportional residual error	1/2	-76.8
2	Structural model #1	IIV(BL) additive residual error	1/2	-76.7
3	Structural model #1	IIV(BL) additive + proportional residual error	1/3	-76.9
4	$C_A \sim E$ linear relationship	Like model #1	2/2	-86.7
5	$C_A \sim E$ log-linear relationship	Like model #1	2/2	-85.7
6	E_{max} model	Like model #1	3/2	-87.5
7	Sigmoid E_{max} model	Like model #1	4/2	-87.5
8	Indirect response model (inhibition of k_{in})	Like model #1	3/2	-87.5
9	Indirect response model (stimulation of k_{out})	Like model #1	3/2	-87.5
10	Tolerance compartment model (Porchet et al. [116]) $$\frac{dC_M}{dt} = k_{tol} \cdot (C_A - C_M)$$ $$E = BL - \frac{S_E \cdot C_A}{1 + \frac{C_M}{TC_{50}}}$$	Like model #1	4/2	-94.1
11	Indirect counter-regulation (Bauer et al. [114]) $$\frac{dM}{dt} = k_1 \cdot S_E \cdot C_A - k_2 \cdot M$$ $$\frac{dT}{dt} = k_2 \cdot M - k_{out,T} \cdot T$$ $$E = BL - S_E \cdot C_A + T$$	Like model #1	5/2	-101.6
12*	Negative feedback model (Mandema et al. [113]) $$\frac{dT}{dt} = G \cdot k_{tol} \cdot (E - T)$$ $$\frac{dE}{dt} = S_E \cdot C_A - BL + T$$	Like model #1	4/2	-105.8

Table 9-2 continued

Model number	Model description	Random effects	Number of parameters (fixed/random)	OFV
13	Precursor pool model (Movin-Osswald et al. [112]) $\dfrac{dP}{dt} = k_0 - k_{in} \cdot P \cdot \dfrac{1}{1 + S_E \cdot C_A}$ $\dfrac{dE}{dt} = k_{in} \cdot P \cdot \dfrac{1}{1 + S_E \cdot C_A} - k_{out} \cdot E$	Like model #1	4/2	-86.5
14**	Receptor inactivation model (Kenakin[111]) $\dfrac{dAR}{dt} = k_{on} \cdot FR \cdot C_A + (k_{off} + k_3) \cdot AR$ $\dfrac{dIR}{dt} = k_3 \cdot AR - k_4 \cdot IR$ $\dfrac{dFR}{dt} = -k_{on} \cdot FR \cdot C_A + k_{off} \cdot AR + k_4 \cdot IR$ $E = BL - E_{max} \cdot \dfrac{AR}{AR + FR + IR}$	Like model #1	6/2	-
15	Modified Porchet model $\dfrac{dC_M}{dt} = k_{tol} \cdot (C_A - C_M)$ $E = BL - S_E \cdot C_A + S_T \cdot C_M$ (**Final model**)	Like model #1	4/2	-101.7
16	Structural model #15	Like model #1 + IIV(S_E)	4/3	-102.8
17	Structural model #15	Like model #1 + IIV(S_T)	4/3	-102.4
18	Structural model #15	Like model #1 + IIV(k_{tol})	4/3	-101.7

OFV: objective function value; IIV: interindividual variability; BL: baseline value; k_{in}: zero-order rate of production of response; k_{out}: first-order rate constant of loss of response; C_M: concentration of the mediator in the tolerance compartment; C_A: concentration of the active moiety ($R \cdot C_{ODV} + C_{VEN}$); k_{tol}: rate constant of development and disappearance of tolerance (i.e., tolerance delay); E: effect (i.e., amplitude); S_E: slope of the effect model; TC_{50}: concentration at half the maximal tolerance; M: mediator; $k_{1,2}$: first-order rate constants describing the kinetics of the mediator; T: tolerance; $k_{out,T}$: first-order rate constant of loss of tolerance; G: extent of tolerance development; k_0: production rate of the pool; AR: activated receptors; FR: free receptors; IR; inactive receptors; k_{on}: second-order receptor association rate constant; k_{off}: first-order receptor dissociation constant; $k_{3,4}$: first-order rate constants of production and loss of inactive receptors; E_{max}: maximal effect.

* Estimate of G close to 0, k_{tol} unrealistically high.
** Not converged.

Table 9-3 Model building summary - Important steps of the **33% recovery time** model development

Model number	Model description	Random effects	Number of parameters (fixed/random)	OFV
1	Null model (only BL is estimated)	IIV(BL) proportional residual error	1/2	-76.8
2	Structural model #1	IIV(BL) additive residual error	1/2	-76.7
3	Structural model #1	IIV(BL) additive + proportional residual error	1/3	-206.5
4	$C_A \sim E$ linear relationship	Like model #1	2/2	-207.6
5	$C_A \sim E$ log-linear relationship	Like model #1	2/2	-207.6
6	E_{max} model	Like model #1	3/2	-224.4
7	Sigmoid E_{max} model	Like model #1	4/2	-220.1
8	Indirect response model (inhibition of k_{in})	Like model #1	3/2	-225.0
9	Indirect response model (stimulation of k_{out})	Like model #1	3/2	-225.1
10	Tolerance compartment model (Porchet et al. [116]) $$\frac{dC_M}{dt} = k_{tol} \cdot (C_A - C_M)$$ $$E = BL - \frac{S_E \cdot C_A}{1 + \frac{C_M}{TC_{50}}}$$	Like model #1	4/2	-225.0
11	Indirect counter-regulation (Bauer et al. [114]) $$\frac{dM}{dt} = k_1 \cdot S_E \cdot C_A - k_2 \cdot M$$ $$\frac{dT}{dt} = k_2 \cdot M - k_{out,T} \cdot T$$ $$E = BL - S_E \cdot C_A + T$$	Like model #1	5/2	-225.0
12*	Negative feedback model (Mandema et al. [113]) $$\frac{dT}{dt} = G \cdot k_{tol} \cdot (E - T)$$ $$\frac{dE}{dt} = S_E \cdot C_A - BL + T$$	Like model #1	4/2	-228.5

Table 9-3 continued

Model number	Model description	Random effects	Number of parameters (fixed/random)	OFV
13	Precursor pool model (Movin-Osswald et al. [112]) $$\frac{dP}{dt} = k_0 - k_{in} \cdot P \cdot \frac{1}{1 + S_E \cdot C_A}$$ $$\frac{dE}{dt} = k_{in} \cdot P \cdot \frac{1}{1 + S_E \cdot C_A} - k_{out} \cdot E$$	Like model #1	4/2	-221.8
14**	Receptor inactivation model (Kenakin[111]) $$\frac{dAR}{dt} = k_{on} \cdot FR \cdot C_A + (k_{off} + k_3) \cdot AR$$ $$\frac{dIR}{dt} = k_3 \cdot AR - k_4 \cdot IR$$ $$\frac{dFR}{dt} = -k_{on} \cdot FR \cdot C_A + k_{off} \cdot AR + k_4 \cdot IR$$ $$E = BL - E_{max} \cdot \frac{AR}{AR + FR + IR}$$	Like model #1		-
15	Modified Porchet model $$\frac{dC_M}{dt} = k_{tol} \cdot (C_A - C_M)$$ $$E = BL - S_E \cdot C_A + S_T \cdot C_M$$ (**Final model**)	Like model #1	4/2	-235.9
16	Structural model #15	Like model #1 + IIV(S_E)	4/3	-236.0
17	Structural model #15	Like model #1 + IIV(S_T)	4/3	-236.2
18	Structural model #15	Like model #1 + IIV(k_{tol})	4/3	-233.9

OFV: objective function value; IIV: interindividual variability; BL: baseline value; k_{in}: zero-order rate of production of response; k_{out}: first-order rate constant of loss of response; C_M: concentration of the mediator in the tolerance compartment; C_A: concentration of the active moiety ($R \cdot C_{ODV} + C_{VEN}$); k_{tol}: rate constant of development and disappearance of tolerance (i.e., tolerance delay); E: effect (i.e., 33% recovery time); S_E: slope of the effect model; TC_{50}: concentration at half the maximal tolerance; M: mediator; $k_{1,2}$: first-order rate constants describing the kinetics of the mediator; T: tolerance; $k_{out,T}$: first-order rate constant of loss of tolerance; G: extent of tolerance development; k_0: production rate of the pool; AR: activated receptors; FR: free receptors; IR; inactive receptors; k_{on}: second-order receptor association rate constant; k_{off}: first-order receptor dissociation constant; $k_{3,4}$: first-order rate constants of production and loss of inactive receptors; E_{max}: maximal effect.

* Very high relative standard errors for k_{tol} and G (>180%).
** Not converged.

9.1.2 Figures

9.1.2.1 Goodness-of-fit Plots

Observations vs. Population Predictions

Observations vs. Individual Predictions

Conditional Weighted Residuals vs. Time After Dose

Conditional Weighted Residuals vs. Population Predictions
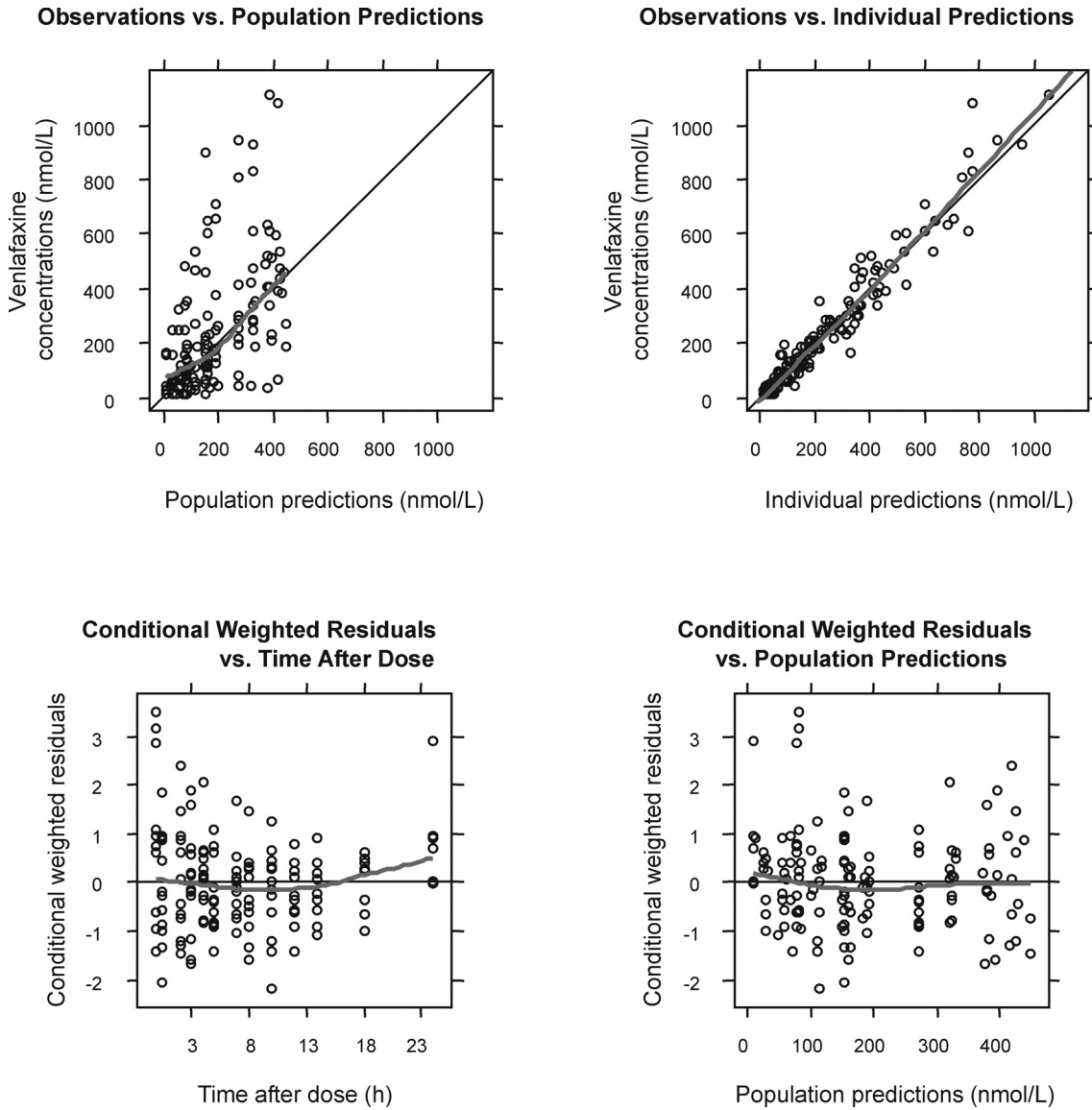
Figure 9-1 Standard goodness-of-fit plots for the prediction of **venlafaxine** plasma concentrations. ε-shrinkage was 6.2%. The grey line is a lowess smoother.

Observations vs. Population Predictions

Observations vs. Individual Predictions

**Conditional Weighted Residuals
vs. Time After Dose**

**Conditional Weighted Residuals
vs. Population Predictions**
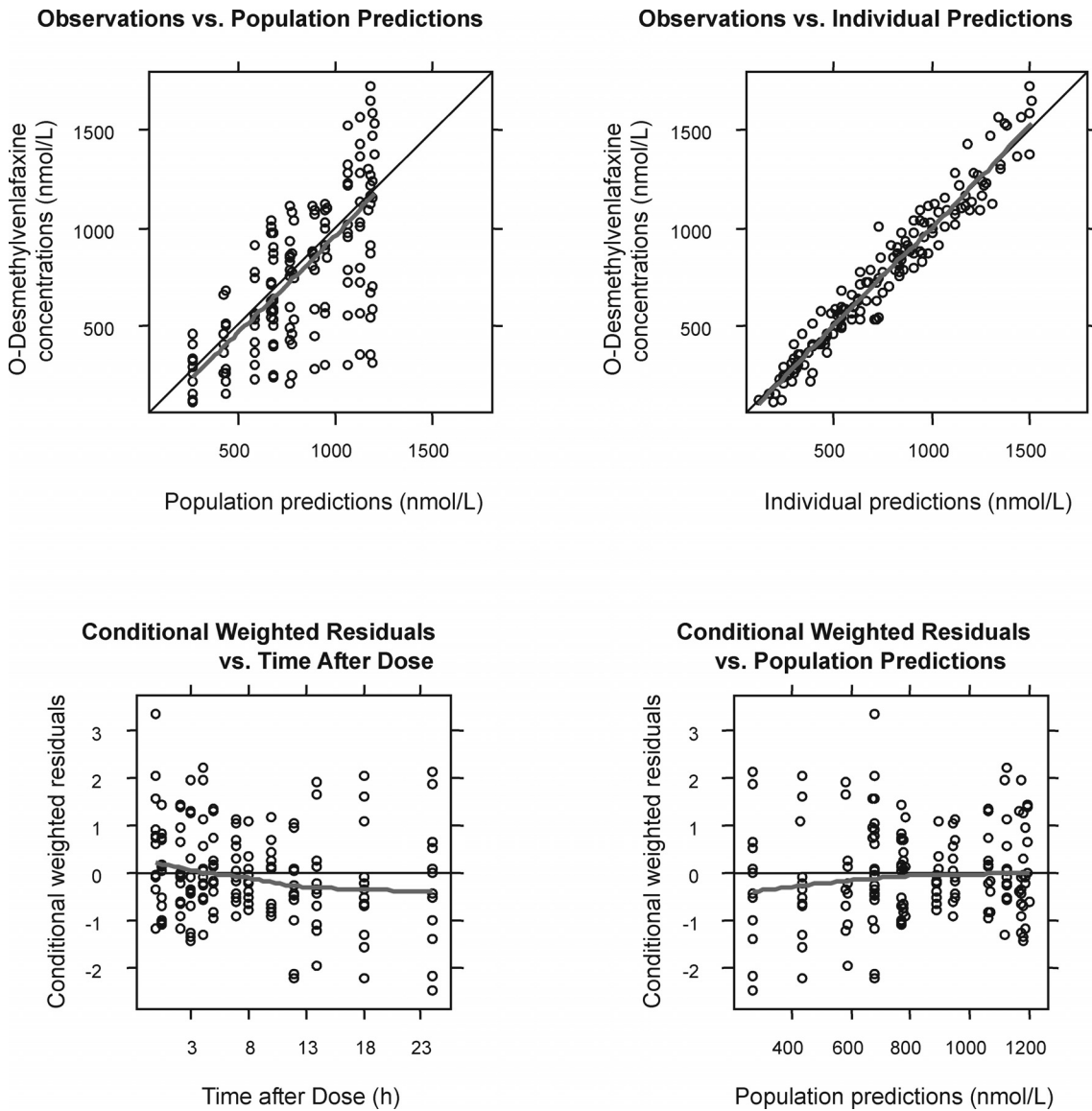
Figure 9-2 Standard goodness-of-fit plots for the prediction of **O-desmethylvenlafaxine** plasma concentrations. ε-shrinkage was 4.2%. The grey line is a lowess smoother.
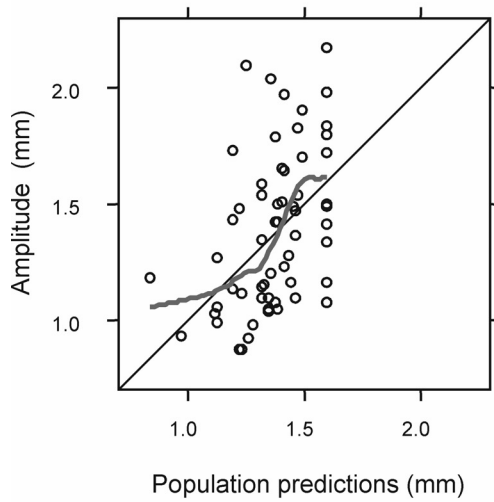
Observations vs. Population Predictions

Observations vs. Individual Predictions
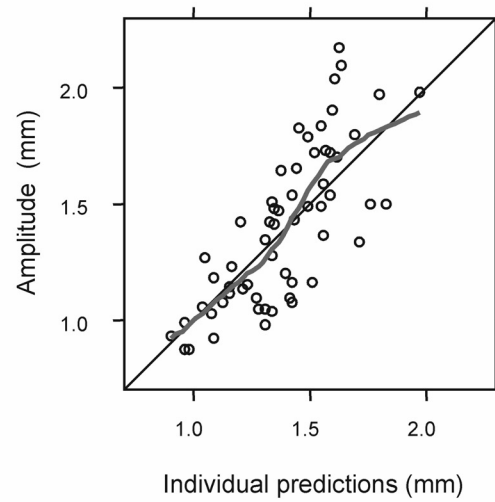
Conditional Weighted Residuals vs. Time After Dose
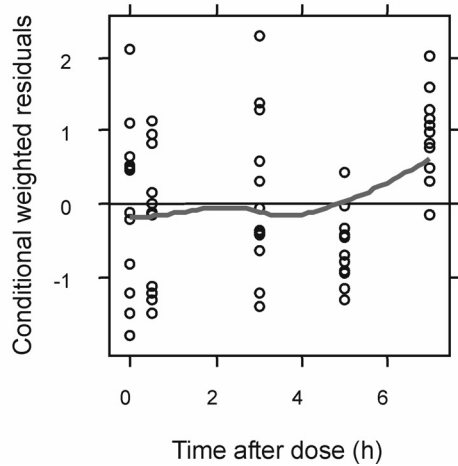
Conditional Weighted Residuals vs. Population Predictions
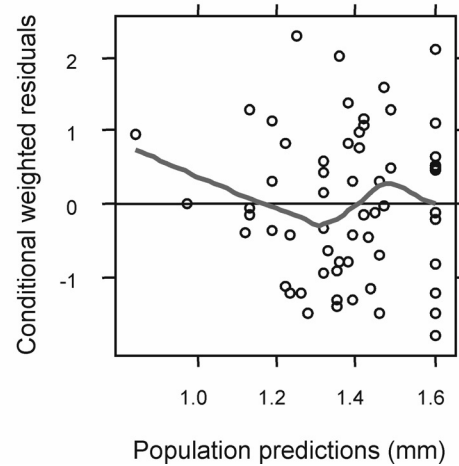
Figure 9-3   Standard goodness-of-fit plots for the prediction of the **amplitude.** ε-shrinkage was 7.1%. The grey line is a lowess smoother.
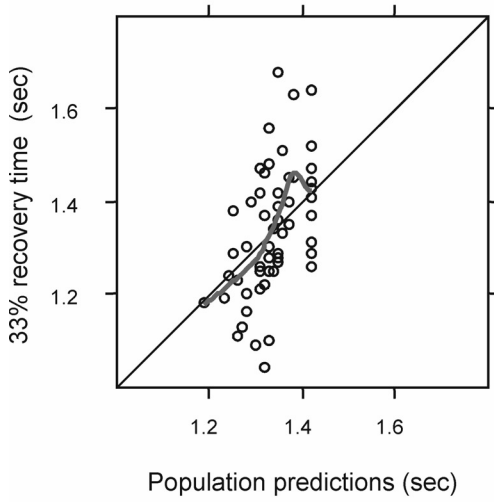
Observations vs. Population Predictions

Observations vs. Individual Predictions
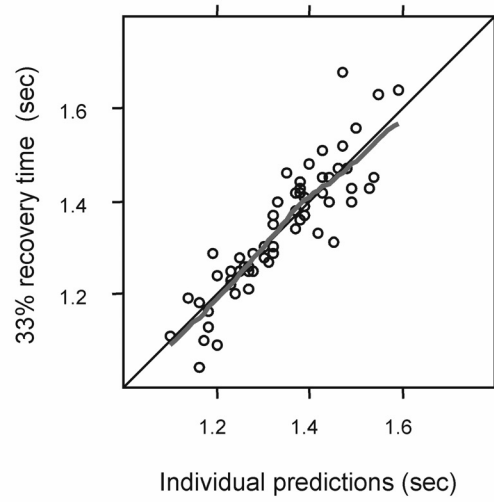
Conditional Weighted Residuals vs. Time After Dose
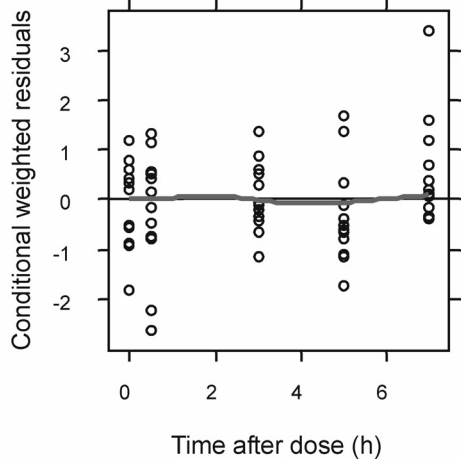
Conditional Weighted Residuals vs. Population Predictions
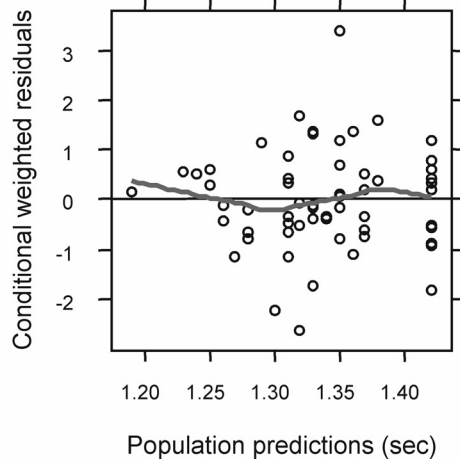
Figure 9-4 Standard goodness-of-fit plots for the prediction of the **33% recovery time**. ε-shrinkage was 8.8%. The grey line is a lowess smoother.

9.1.2.2   Sensitivity Analysis
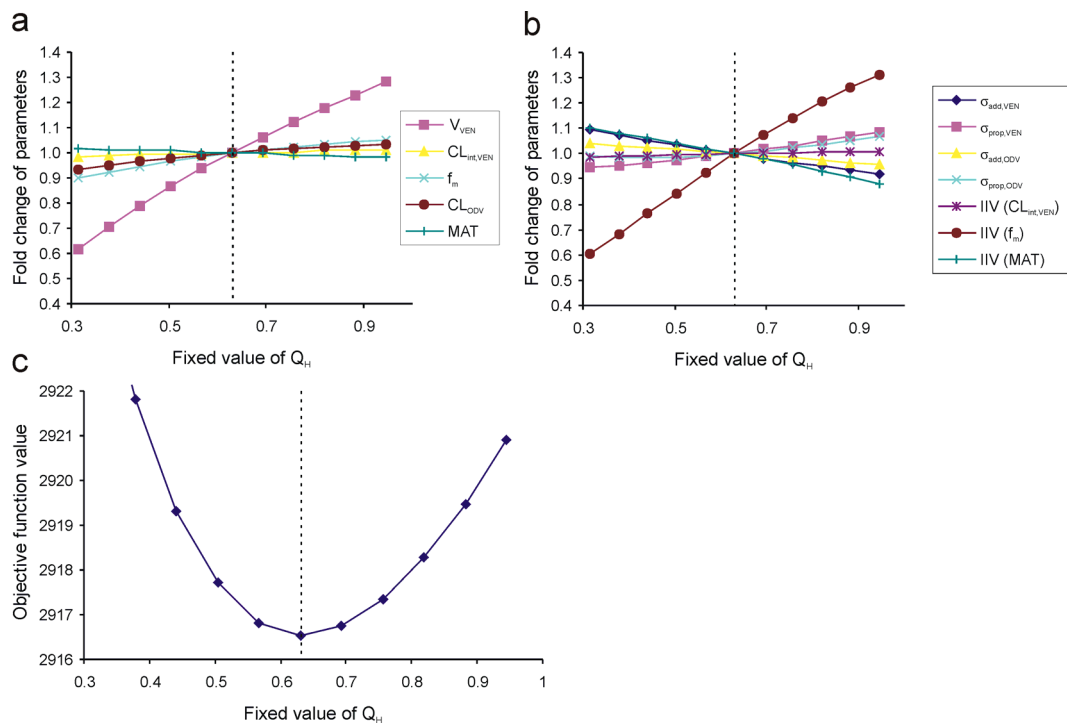
Figure 9-5   Sensitivity analysis of the liver plasma flow (Q_H). The graphs illustrate how different values of Q_H (0.32 to 0.95 L/h/kg) influence fixed-effect parameters (**a**), random-effects parameters (**b**) and the objective function (**c**) of the **venlafaxine PK** model. The vertical dotted line marks the fixed value of Q_H used in the final model.

IIV: interindividual variability; V_{VEN}: venlafaxine's volume of distribution; $CL_{int,VEN}$: intrinsic clearance of venlafaxine; f_m: fraction of venlafaxine metabolized to O-desmethylvenlafaxine; CL_{ODV}: clearance of O-desmethylvenlafaxine; MAT: mean absorption time; σ_{prop}: proportional residual variability; σ_{add}: additive residual variability.
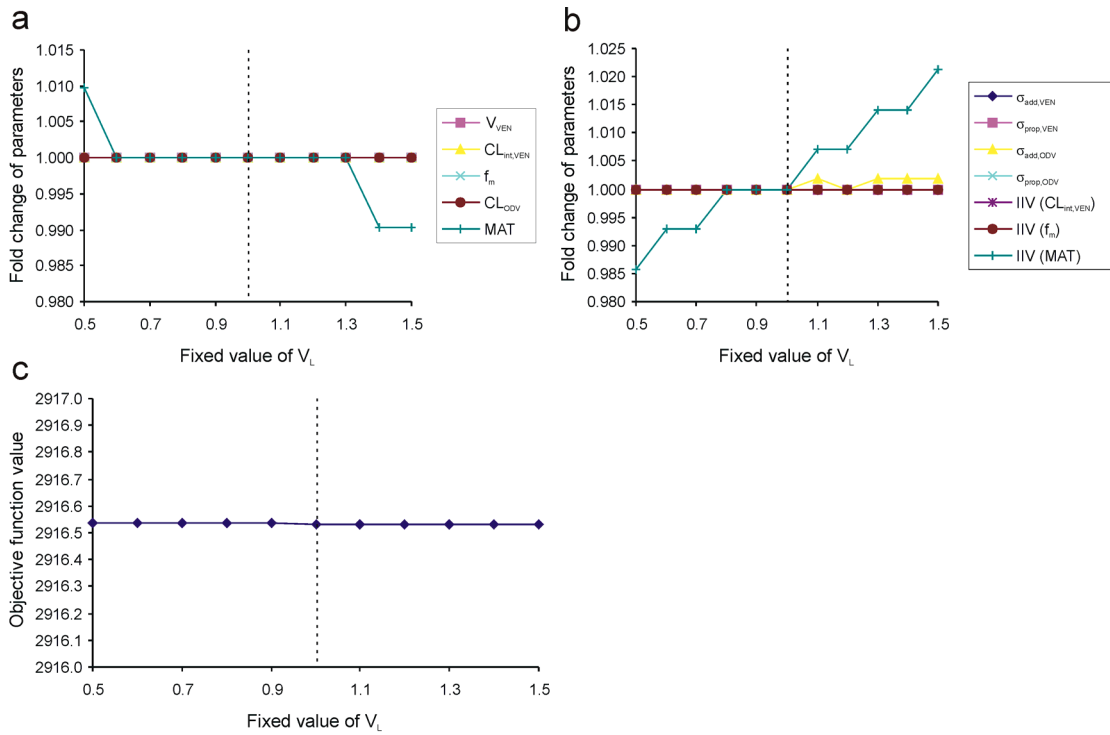
Figure 9-6 Sensitivity analysis of the volume of the liver compartment (V_L). The graphs illustrate how different values of V_L (0.5 to 1.5 L) influence fixed-effect parameters (**a**), random-effects parameters (**b**) and the objective function (**c**) of the **venlafaxine PK** model. The vertical dotted line marks the fixed value of V_L used in the final model. Symbols see Figure 9-5.
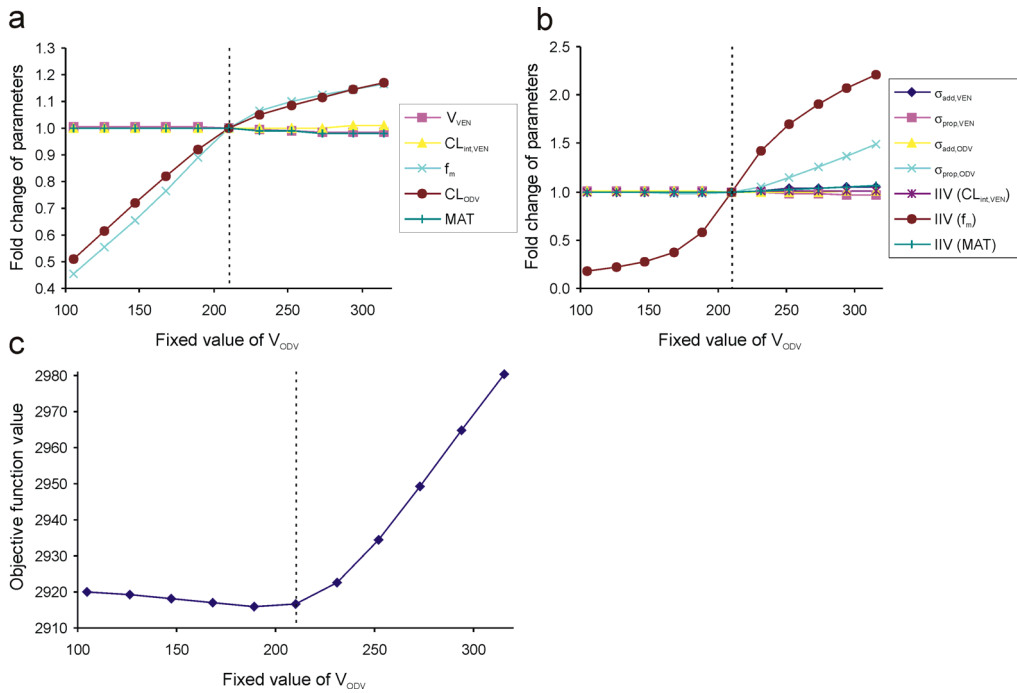
Figure 9-7   Sensitivity analysis of the volume of distribution of O-desmethylvenlafaxine (V_{ODV}). The graphs illustrate how different values of V_{ODV} (105 to 315 L) influence fixed-effect parameters (**a**), random-effects parameters (**b**) and the objective function (**c**) of the **venlafaxine PK** model. The vertical dotted line marks the fixed value of V_{ODV} used in the final model. Symbols see Figure 9-5.
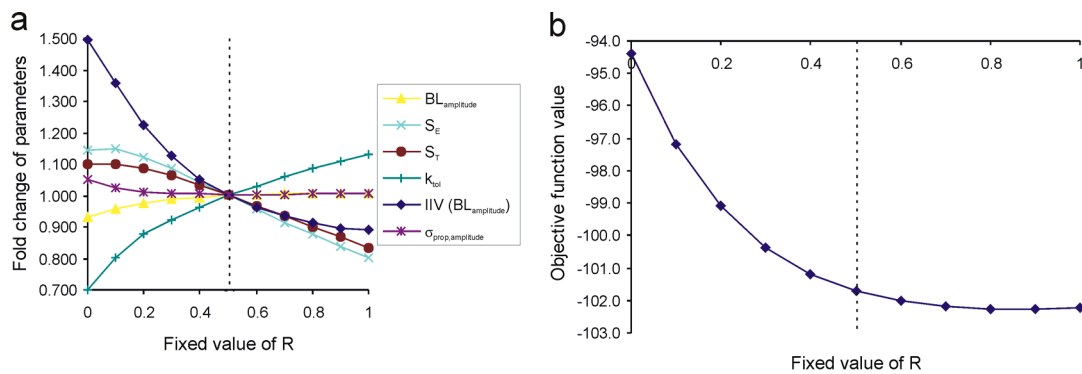
Figure 9-8   Sensitivity analysis of the relative potency (R) of O-desmethylvenlafaxine. The graphs illustrate how different values of R (0 to 1) influence fixed-effect and random-effects parameters (**a**) and the objective function (**b**) of the **amplitude** model. The vertical dotted line marks the fixed value of R used in the final model.

IIV: interindividual variability; CV: coefficient of variation; BL: baseline value; S_E: slope of the effect model; S_T: slope of the tolerance model; k_{tol}: rate constant of development and disappearance of tolerance (i.e., tolerance delay); σ_{prop}: proportional residual variability.
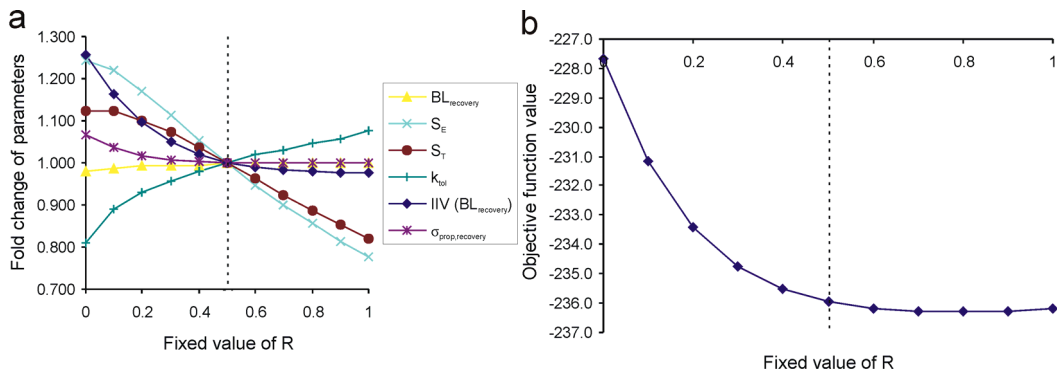
Figure 9-9 Sensitivity analysis of the relative potency (R) of O-desmethylvenlafaxine. The graphs illustrate how different values of R (0 to 1) influence fixed-effect and random-effects parameters (**a**) and the objective function (**b**) of the **33% recovery time** model. The vertical dotted line marks the fixed value of R used in the final model. Symbols see Figure 9-8.

9.1.3 NONMEM Codes

Code 9-1 NONMEM control stream for the **venlafaxine** pharmacokinetic model

```
$PROBLEM Venlafaxine - PK model

;------------------------
;  UNITS              |
;  TIME - HOURS       |
;  DOSE - NMOL        |
;  CP  - NMOL/L       |
;  CLEARANCES - L/HOUR   |
;  VOLUMES - L        |
;  LOQ - 28 NMOL/L    |
;------------------------

$INPUT ID TIME AMT ADDL II DV CMT EVID AGE HGT KG
       ;ADDL=Additional doses, II=dosing interval (see NONMEM Users Guide)

$DATA Data_input_file_PKven.csv

$SUBROUTINE ADVAN5
$MODEL
NCOMP=6
COMP(DEPOT1)   ;Transit compartment 1
COMP(DEPOT2)   ;Transit compartment 2
COMP(DEPOT3)   ;Transit compartment 3
COMP(LIVER)    ;Liver compartment
COMP(VEN)      ;Venlafaxine (VEN) compartment
COMP(ODV)      ;O-desmethylvenlafaxine (ODV) compartment

;INITIAL VALUES
$THETA
(0,200)      ; THVVEN   - Volume of distribution (Vd) of VEN
(0,100)      ; THCLVEN  - Intrinsic clearance of VEN
(0,0.7)      ; THFM     - Fraction metabolized to ODV
(210 FIX)    ; THVODV   - Vd of ODV
(0,18)       ; THCLODV  - Clearance of ODV
(0,1)        ; THMAT    - Mean absorption time
(0,30)       ; SD_VEN   - Additive residual error VEN
(0,0.2)      ; CV_VEN   - Proportional residual error VEN
(0,50)       ; SD_ODV   - Additive residual error ODV
(0,0.1)      ; CV_ODV   - Proportional residual error ODV

$OMEGA 0.1  ; ETACLVEN - Interindividual variability (IIV) of CLVEN
$OMEGA 0.1  ; ETAFM    - IIV of FM
$OMEGA 0.1  ; ETAMAT   - IIV of MAT

$SIGMA 1 FIX

$PK

;ERLANG ABSORPTION
 MAT  = THETA(6)*EXP(ETA(6))
 N    = 3                          ;Number of transit compartment
 KTR  = N/MAT                      ;Transit rate constant

;DISPOSITION AND METABOLISM
 VL   = 1                          ;Liver volume
 QL   = 0.63*KG                    ;Liver plasma flow

 VVEN = THVVEN
```

Code 9-1 continued

```
 CLVE  = THCLVEN * EXP(ETACLVEN)
TERM  = EXP(LOG(THFM/(1-THFM))+ETAFM) ;Logit transformation
 FM   =   TERM/(1+TERM)

 CLFM  = FM*CLVE                    ;Clearance of formation of ODV
 CLO   = CLVE-CLM                   ;Clearance of formation of other metabolites
 VODV  = THVODV
 CLOD  = THCLODV*EXP(ETA(5))

;Definition of volumes and rate constants of the ADVAN5 compartment system
 K12   = KTR
 K23   = KTR
 K34   = KTR
 K40   = CLO/VL
 K46   = CLFM/VL
 K60   = CLOD/VODV
 K45   = QL/VL
 K54   = QL/VVEN

 S4    = VL
 S5    = VVEN
 S6    = VODV

$ERROR
;PREDICTIONS AND RESIDUAL ERROR
IF (CMT.EQ.5) THEN
 IPRE = A(5)/VVEN                   ;Individual predicted VEN concentration
 IRES = DV - IPRE                   ;Individual residuals
 W    = SQRT(SD_VEN**2+CV_VEN**2*IPRE**2)  ;Combined residual error VEN
 Y    = IPRE+ERR(1)*W
ELSE
 IPRE = A(6)/VODV                   ;Individual predicted ODV concentration
 IRES = DV - IPRE                   ;Individual residuals
 W    = SQRT(SD_VEN**2+CV_VEN**2*IPRE**2)  ;Combined residual error ODV
 Y    = IPRE+ERR(1)*W
ENDIF
 DEL          = 0
 IF(W.EQ.0) DEL = 1                 ;To prevent division by 0
 IWRE         = IRES/(W+DEL)        ;Individual weighted residuals

$ESTIMATION SIG=3 PRINT=1 METHOD=1 MAXEVAL=9999 NOABORT INTER MSFO=msfo.msf
$COVARIANCE PRINT=E
```

Code 9-2   NONMEM control stream for the venlafaxine **amplitude** model

```
$PROBLEM  Venlafaxine - Amplitude model

;------------------------
;  UNITS              |
;  TIME - HOURS       |
;  DOSE - NMOL        |
;  CP  - NMOL/L       |
;  CLEARANCES - L/HOUR   |
;  VOLUMES - L        |
;  AMP - MM           |
;------------------------

$INPUT ID TIME AMT ADDL II DV AGE HGT KG
      MATx VVENx CLVEx VODVx CLODVx FMx ;Individual parameters from the previous PK
step
      ;DV=Amplitude

$DATA Data_input_file_AMP.csv

$SUBROUTINE ADVAN5
$MODEL
NCOMP=6
COMP(DEPOT1)   ;Transit compartment 1
COMP(DEPOT2)   ;Transit compartment 2
COMP(DEPOT3)   ;Transit compartment 3
COMP(LIVER)    ;Liver compartment
COMP(VEN)      ;Venlafaxine (VEN) compartment
COMP(ODV)      ;O-desmethylvenlafaxine (ODV) compartment
COMP(T1)       ;Tolerance compartment for VEN
COMP(T2)       ;Tolerance compartment for ODV

;INITIAL VALUES
$THETA
(0,1600)       ; THBL    - Baseline amplitude
(0,1.86)       ; THSE    - Slope of effect model
(0,1.52)       ; THST    - Slope of tolerance model
(0,1.38)       ; THKT0L  - Tolerance delay
(0.5 FIX)      ; THR     - Relative potency of ODV
(0,0.1)        ; CV_AMP  - Proportional residual error

$OMEGA 0.02    ; ETABL   - Interindividual variability in BL

$SIGMA 1 FIX

$PK
;PD-PART
 BL   = THBL/1000*EXP(ETABL)  ;Division by 1000 converts mm to µm in the results
 SE   = THSE/1000
 ST   = THST/1000
 KT0L = THKTOL
 R    = THR

;PK-PART
 MAT  = MATx       ;Description see PK model
 N    = 3
 KTR  = N/MAT
 VL   = 1
 QL   = 0.63*KG
 VVEN = VVENx
 CLVE = CLVEx
 FM   = FMx
 CLFM = FM*CLVE
```

Code 9-2 continued

```
 CLO   = CLVE-CLM
 VODV  = VODVx
 CLOD  = CLODVx

;Definition of volumes and rate constants of the ADVAN5 compartment system
 K12  = KTR
 K23  = KTR
 K34  = KTR
 K40  = CLO/VL
 K46  = CLFM/VL
 K60  = CLOD/VODV
 K45  = QL/VL
 K54  = QL/VVEN


 S4    = VL
 S5    = VVEN
 S6    = VODV
 S7    = V7
 S8    = V8


;TOLERANCE COMPARTMENTS
 ;For technical reasons in ADVAN5 two tolerance compartments had to be used, one for
each compound.
 ;This is however equivalent to the differential equation shown in equation 3-2.

 V7 = 0.0001 ;Negligible volume of the tolerance compartments
 V8 = 0.0001

 K67 = V7*KT0/VVEN
 K76 = KT0L
 K58 = V8*KT0/VODV
 K85 = KT0L

$ERROR
;Plasma concentrations of VEN and ODV
 CVEN = A(5)/VVEN        ; VEN concentration
 CODV = A(6)/VODV        ; ODV concentration
 CA   = CVEN+R*CODV      ; Active concentration

;Concentration of the hypothetical tolerance mediator(CM)
 CM1 = A(8)/V7
 CM2 = A(7)/V8
 CM  = CM1+R*CM2

;Individual response and residual error
 IPRE   = BL-SE*CA+ST*CM         ;Individual predicted amplitude

 IRES   = DV - IPRED             ;Individual residuals
 W      = CV_AMP*IPRED           ;Proportional residual error
 Y      = IPRED+ERR(1)*W

 DEL            = 0
 IF(W.EQ.0) DEL = 1              ;To prevent division by 0
 IWRE           = IRES/(W+DEL)   ;Individual weighted residuals

$ESTIMATION SIG=3 PRINT=1 METHOD=1 MAXEVAL=9999 NOABORT INTER
$COVARIANCE
```

Code 9-3   NONMEM control stream for the venlafaxine **33% recovery time** model

```
$PROBLEM  Venlafaxine - 33% Recovery time model

;------------------------
;  UNITS                |
;  TIME - HOURS         |
;  DOSE - NMOL          |
;  CP  - NMOL/L         |
;  CLEARANCES - L/HOUR  |
;  VOLUMES - L          |
;  REC - SEC            |
;------------------------

$INPUT ID TIME AMT ADDL II DV AGE HGT KG
       MATx VVENx CLVEx VODVx CLODVx FMx ;Individual parameters from the previous PK
step
       ;DV=33% Recovery time

$DATA Data_input_file_REC.csv

$SUBROUTINE ADVAN5
$MODEL
NCOMP=6
COMP(DEPOT1)   ;Transit compartment 1
COMP(DEPOT2)   ;Transit compartment 2
COMP(DEPOT3)   ;Transit compartment 3
COMP(LIVER)    ;Liver compartment
COMP(VEN)      ;Venlafaxine (VEN) compartment
COMP(ODV)      ;O-desmethylvenlafaxine (ODV) compartment
COMP(T1)       ;Tolerance compartment for VEN
COMP(T2)       ;Tolerance compartment for ODV

;INITIAL VALUES
$THETA
(0,1400)       ; THBL   - Baseline 33% recovery time
(0,1.86)       ; THSE   - Slope of effect model
(0,1.52)       ; THST   - Slope of tolerance model
(0,1.38)       ; THKT0L - Tolerance delay
(0.5 FIX)      ; THR    - Relative potency of ODV
(0,0.1)        ; CV_REC - Proportional residual error

$OMEGA 0.02    ; ETABL  - Interindividual variability in BL

$SIGMA 1 FIX

$PK
;PD-PART
 BL   = THBL/1000*EXP(ETABL)  ;Division by 1000 converts sec to msec in the results
 SE   = THSE/1000
 ST   = THST/1000
 KT0L = THKTOL
 R    = THR

;PK-PART
 MAT  = MATx      ;Description see PK model
 N    = 3
 KTR  = N/MAT
 VL   = 1
 QL   = 0.63*KG
 VVEN = VVENx
 CLVE = CLVEx
 FM   = FMx
```

Code 9-3 continued

```
 CLFM    = FM*CLVE
 CLO     = CLVE-CLM
 VODV    = VODVx
 CLOD    = CLODVx


;Definition of volumes and rate constants of the ADVAN5 compartment system
 K12     = KTR
 K23     = KTR
 K34     = KTR
 K40     = CLO/VL
 K46     = CLFM/VL
 K60     = CLOD/VODV
 K45     = QL/VL
 K54     = QL/VVEN


 S4      = VL
 S5      = VVEN
 S6      = VODV
 S7      = V7
 S8      = V8


;TOLERANCE COMPARTMENTS
 ;For technical reasons in ADVAN5 two tolerance compartments had to be used, one for
each compound.
 ;This is however equivalent to the differential equation shown in equation 3-2.

 V7 = 0.0001 ;Negligible volume of the tolerance compartments
 V8 = 0.0001

 K67 = V7*KT0/VVEN
 K76 = KT0L
 K58 = V8*KT0/VODV
 K85 = KT0L

$ERROR
;Plasma concentrations of VEN and ODV
 CVEN = A(5)/VVEN        ; VEN concentration
 CODV = A(6)/VODV        ; ODV concentration
 CA   = CVEN+R*CODV      ; Active concentration

;Concentration of the hypothetical tolerance mediator(CM)
 CM1 = A(8)/V7
 CM2 = A(7)/V8
 CM  = CM1+R*CM2

;Individual response and residual error
 IPRE   = BL-SE*CA+ST*CM         ;Individual predicted 33% recovery time

 IRES   = DV - IPRED             ;Individual residuals
 W      = CV_REC*IPRED           ;Proportional residual error
 Y      = IPRED+ERR(1)*W

 DEL            = 0
 IF(W.EQ.0) DEL = 1              ;To prevent division by 0
 IWRE           = IRES/(W+DEL)   ;Individual weighted residuals

$ESTIMATION SIG=3 PRINT=1 METHOD=1 MAXEVAL=9999 NOABORT INTER
$COVARIANCE
```

9.2   **Sunitinib Study**

9.2.1   **Tables**

Table 9-4   Model building summary - Important steps of the **sunitinib PK** model development

Model number	Model description	Random effects	Number of parameters (fixed/random)	OFV
1	1 compartment Sunitinib 1 compartment SU12662 Transit absorption	IIV(k_a) IIV(CL/F$_{sunitinib}$) IIV(CL/f$_{a,SU12662}$) additive+ prop. residual error	8/7	2948.4
2	2 compartments Sunitinib 1 compartment SU12662 Transit absorption	Like model #1	10/7	2478.5
3	2 compartments Sunitinib 2 compartments SU12662 Transit absorption	Like model #1	12/7	2686.6
4	Structural model #2	Like model #1 + IIV(V$_1$/F$_{sunitinib}$)	10/8	2439.8
5	Structural model #2	Like model #4 + IIV(V$_1$/f$_{a,SU12662}$)	10/9	1821.0
6	Structural model #2	Like model #5 + IIV(V$_2$/F$_{sunitinib}$)	10/10	1820.9
7	Structural model #2	Like model #5 + IIV(Q/F$_{sunitinib}$)	10/10	1821.0
8	Structural model #2	Like model #5 + IIV(N)	10/10	1764.7
9	Structural model #2	Like model #5 + IIV(MTT)	10/11	1721.9
10	Structural model #2	Like model #9 + IOV(MTT)	10/12	1635.5
11	Structural model #2	Like model #10 + OMEGA BLOCK[a]	10/18	1545.2
12	Structural model #2	Like model #11 without IOV(MTT)	10/17	1618.7
13	Structural model #2 (**Final Model**)	Like model #11 without IIV(MTT)	10/17	1545.2
14	Structural model #2	Like model #13 + IIV(RPS)	10/18	1541.2
15	1 compartment Sunitinib 1 compartment SU12662 Transit absorption	Like model #13	8/17	1659.6
16	2 compartments Sunitinib 1 compartment SU12662 First-order absorption	Like model #7 + OMEGA BLOCK[a]	8/15	2109.3

a   Covariance of volume and clearance parameters was estimated.

OFV: objective function value; IIV: interindividual variability; IOV: Interoccasion variability; RPS: ratio of presystemic to systemic metabolite formation; MTT: mean transit time; N: number of transit compartments; k_a: absorption rate constant; CL: clearance; V$_1$: volume of distribution of the central compartment; Q: intercompartmental clearance; V$_2$: volume of distribution of the peripheral compartment; F: bioavailability (f$_a$•[1-f$_{m,pre}$]); f$_a$: fraction of absorbed dose.

Table 9-5 Model building summary - Important steps of the sunitinib **blood pressure** model development

Model number	Model description	Random effects	Number of parameters (fixed/random)	OFV
Day 0 dataset				
1	Null model (only BL is estimated	IIV(BL$_{systolic}$) IIV(BL$_{diastolic}$)	2/4	877.3
2	Structural model #1	Like model #1 COV(BL$_{systolic}$,BL$_{diastolic}$)	2/5	867.9
3	1 cosine term (AMP$_1$, PS$_1$)	Like model #2	4/5	863.0
4	2 cosine terms, (AMP$_1$, AMP$_2$, PS$_1$)	Like model #2	5/5	860.7
5	2 cosine terms, (AMP$_1$, AMP$_2$, PS$_1$, PS$_2$)	Like model #2	6/5	854.7
6*	Structural model #5 with separate cosine terms for systolic and diastolic BP	Like model #2	8/5	-
7	Structural model #4 with separate cosine terms for systolic and diastolic BP	Like model #2	10/5	852.5
8	Structural model #5	Like model #2 + IIV(AMP1)	6/6	850.6
9	Structural model #5	Like model #2 + IIV(AMP1), IIV(AMP2)	6/7	846.2
Full dataset				
10	INH~BM linear relationship	IIV(BL$_{systolic}$) IIV(BL$_{diastolic}$) COV(BL$_{systolic}$,BL$_{diastolic}$) IIV($\alpha_{systolic}$), IIV($\alpha_{diastolic}$)	4/5	4623.9
11	Structural model #10 + baseline model #9	Like model #10 + IIV(AMP$_1$), IIV(AMP$_2$)	8/7	4576.1
12	Structural model #11	Like model #10 + COV($\alpha_{systolic}$,$\alpha_{diastolic}$)	8/8	4548.3
13	INH~BM power function	Like model #12	9/10	4546.7
14	INH~BM hyperbolic relationship	Like model #12	9/10	4552.9
15	Structural model #11 +slow signal transduction	Like model #12	9/10	4534.9
16*	Structural model #11	Like model #12 + IIV(τ)	9/11	-
17	Structural model #11 without PS$_1$, R$_{sl}$ fixed to 1 (**Final model**)	Like model #12	8/10	4535.9

OFV: objective function value; IIV: interindividual variability; BL: baseline value; BP: blood pressure; AMP$_{1,2}$: amplitude of the first or second cosine term; PS$_{1,2}$: phase shift of the first or second cosine term; α: intrinsic efficacy parameter; τ: transduction time; COV: covariance; R$_{sl}$: relative contribution of the slow signal transduction.

* Not converged.

Table 9-6 Model building summary - Important steps of the sunitinib **VEGF-A** model development

Model number	Model description	Random effects	Number of parameters (fixed/random)	OFV
Day 0 dataset				
1	Null model (only BL is estimated)	IIV(BL) proportional residual error	1/2	581.6
2	1 cosine term (AMP_1, PS_1)	Like model #1	3/2	576.8
3	2 cosine terms, (AMP_1, AMP_2, PS_1)	Like model #1	4/2	576.6
4	2 cosine terms, (AMP_1, AMP_2, PS_1, PS_2)	Like model #1	5/2	574.8
Full dataset				
5	INH~BM linear relationship	IIV (BL) IIV(α)	2/3	3120.7
6	INH~BM hyperbolic relationship	Like model #5	3/3	3148.6
7	INH~BM power function	Like model #5	3/3	3028.3
8	Structural model #7 + signal transduction	Like model #5	4/3	3016.7
9	Structural model #8	Like model #5 + IIV(τ)	4/4	2941.2
10	Structural model #8	Like model #9 + IIV(γ)	4/5	2941.2
11	Structural model #8 + study part as covariate (**Final model**)	Like model #9	5/4	2937.3
12	Structural model #11 γ fixed to 1	Like model #9	4/4	3022.9
13	Structural model #11	Like model #9 without IIV(τ)	5/3	3010.5
14	Structural model #11 without signal transduction	Like model #5	4/3	3022.5

OFV: objective function value; IIV: interindividual variability; BL: baseline value; $AMP_{1,2}$: amplitude of the first or second cosine term; $PS_{1,2}$: phase shift of the first or second cosine term; INH: fractional tyrosine kinase inhibition; BM: biomarker; α: intrinsic activity parameter; τ: transduction time; γ: shape parameter of the power function.

Table 9-7 Model building summary - Important steps of the sunitinib **sVEGFR-2** model development

Model number	Model description	Random effects	Number of parameters (fixed/random)	OFV
Day 0 dataset				
1	Null model (only BL is estimated)	IIV(BL) proportional residual error	1/2	1167.5
2	1 cosine term (AMP_1, PS_1)	Like model #1	3/2	1152.8
3	2 cosine terms, (AMP_1, AMP_2, PS_1)	Like model #1	4/2	1152.6
4	2 cosine terms, $(AMP_1, AMP_2, PS_1, PS_2)$	Like model #1	5/2	1152.1
5	Structural model #2	Like model #1 + IIV(AMP_1)	3/3	1151.9
Full dataset				
6	INH~BM inverse linear relationship	IIV(BL) IIV(α)	3/3	5691.8
7	Structural model #6 + baseline model #2	Like model #6	5/3	5688.7
8	INH~BM inverse hyperbolic relationship	Like model #6	4/3	5699.2
9*	INH~BM inverse power function	Like model #6	4/3	5662.2
10	Structural model #6 (**Final model**)	Like model #6 + IIV(k_{out})	3/4	5684.2
11	Structural model #6 + study part as covariate	Like model #10	4/4	5682.9

OFV: objective function value; IIV: interindividual variability; BL: baseline value; $AMP_{1,2}$: amplitude of the first or second cosine term; $PS_{1,2}$: phase shift of the first or second cosine term; INH: fractional tyrosine kinase inhibition; BM: biomarker; α: intrinsic activity parameter; k_{out}: rate of loss of VEGFR-2 response.

* Model overparameterized; large relative standard error of α (>400%); high correlation between fixed effect parameters.

9.2.2   Figures

9.2.2.1   Goodness-of-fit Plots
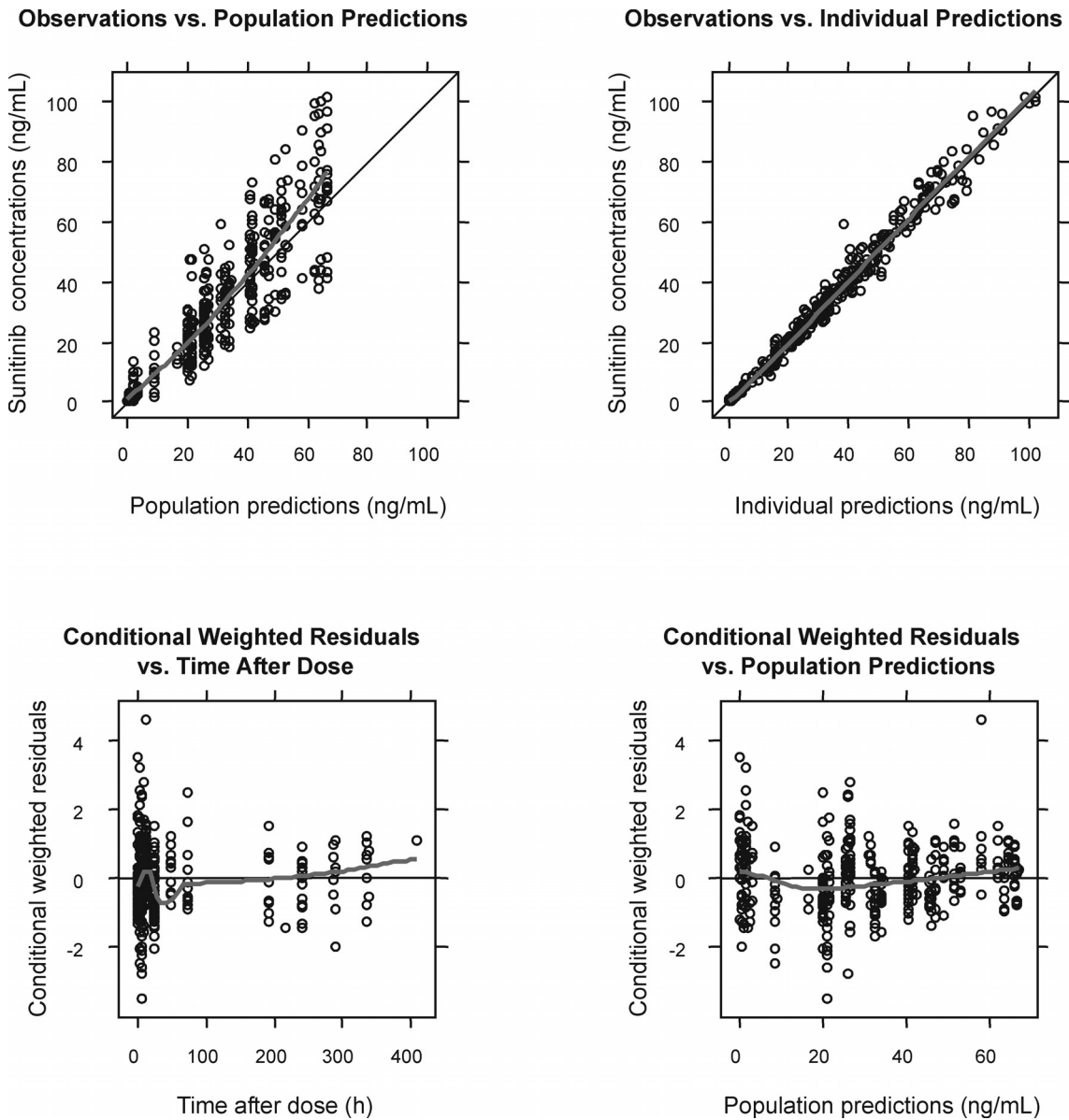
Figure 9-10   Standard goodness-of-fit plots for the prediction of **sunitinib** plasma concentrations. ε-shrinkage was 7.7%. The grey line is a lowess smoother.
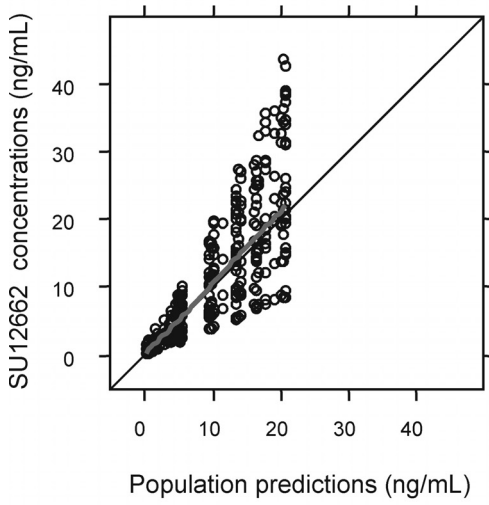
Observations vs. Population Predictions

Observations vs. Individual Predictions
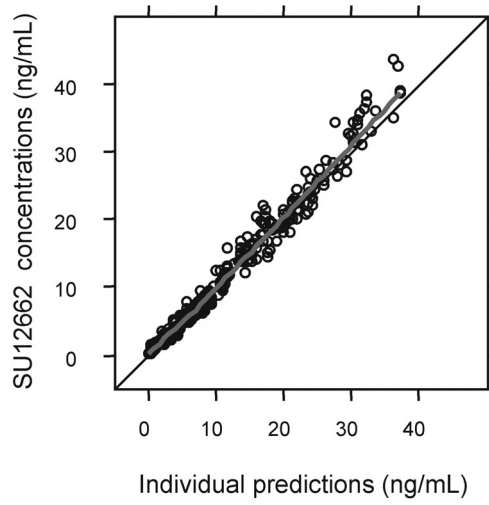
Conditional Weighted Residuals vs. Time After Dose
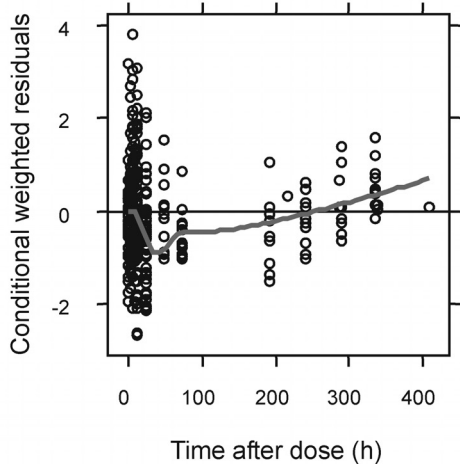
Conditional Weighted Residuals vs. Population Predictions
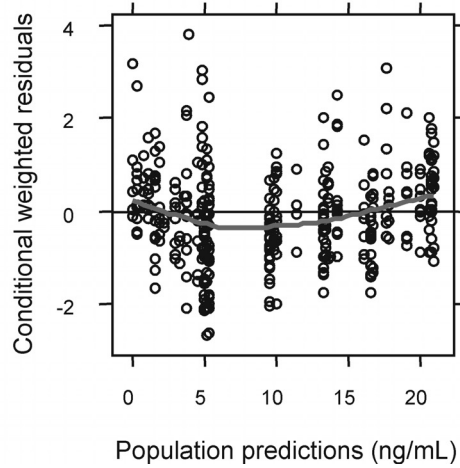
Figure 9-11   Standard goodness-of-fit plots for the prediction of **SU12662** plasma concentrations. ε-shrinkage was 3.0%. The grey line is a lowess smoother.

Observations vs. Population Predictions

Observations vs. Individual Predictions

Conditional Weighted Residuals vs. Time After Dose

Conditional Weighted Residuals vs. Population Predictions
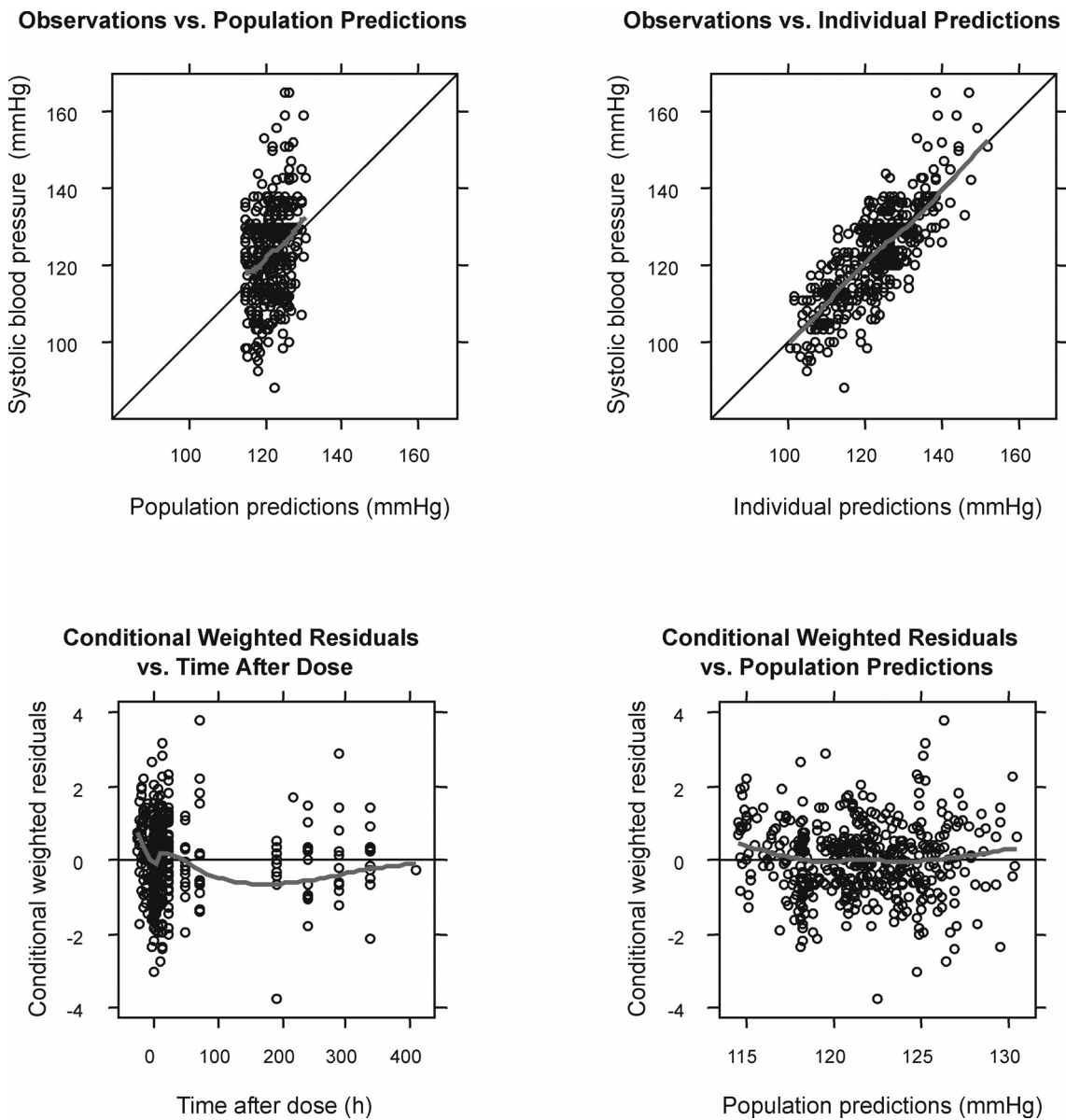
Figure 9-12   Standard goodness-of-fit plots for the prediction of **systolic blood pressure.** ε-shrinkage was 2.8%. The grey line is a lowess smoother.
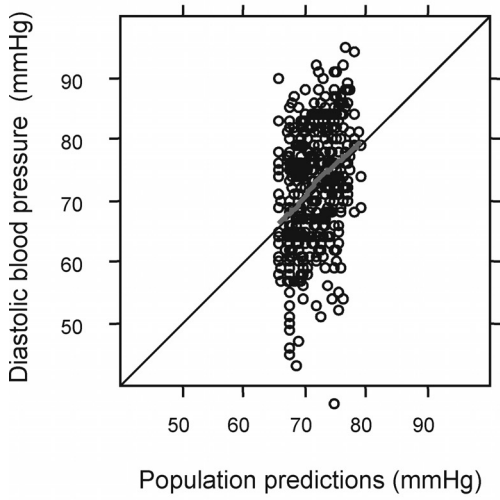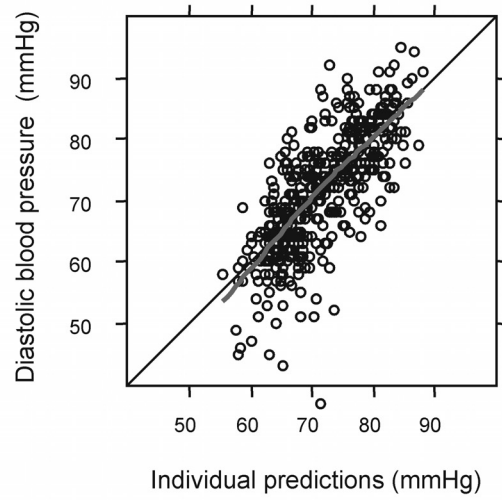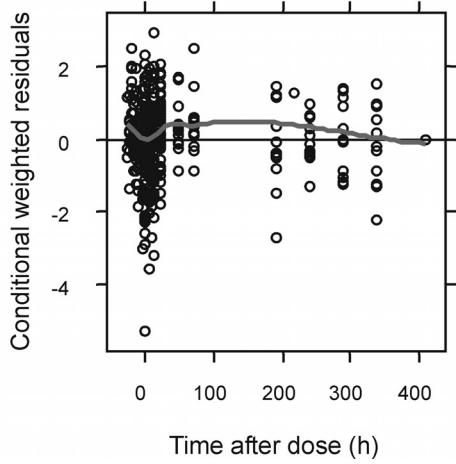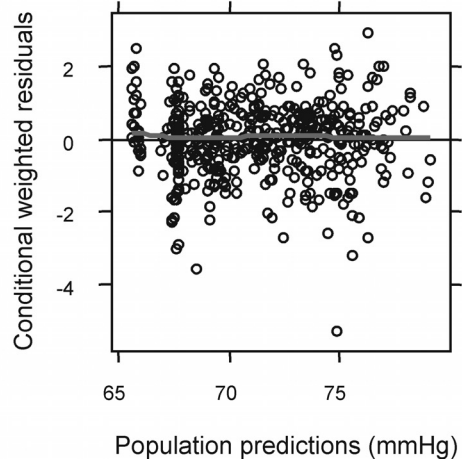
Figure 9-13 Standard goodness-of-fit plots for the prediction of **diastolic blood pressure.** ε-shrinkage was 2.0%. The grey line is a lowess smoother.

Observations vs. Population Predictions

Observations vs. Individual Predictions

Conditional Weighted Residuals vs. Time After Dose

Conditional Weighted Residuals vs. Population Predictions
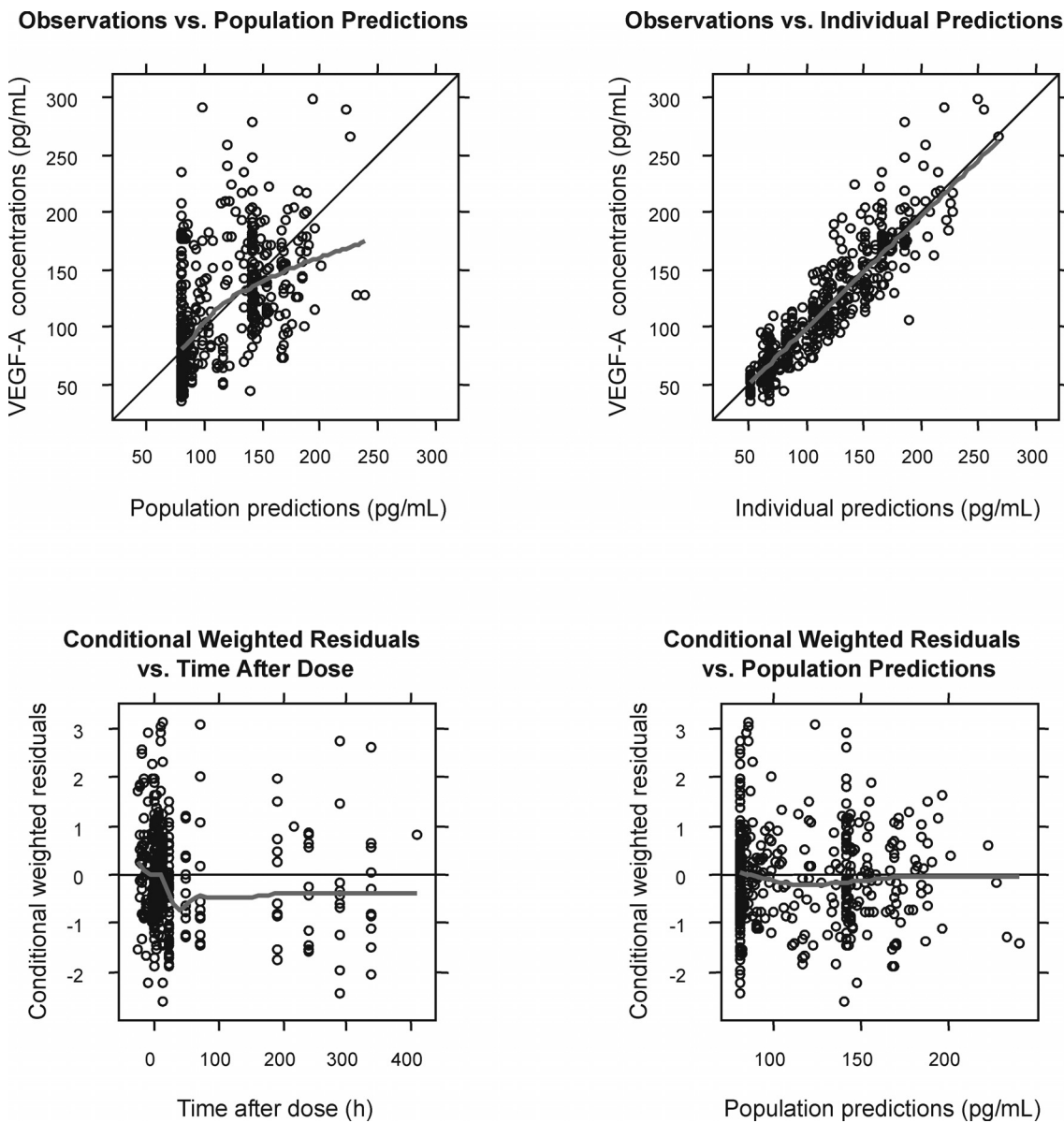
Figure 9-14 Standard goodness-of-fit plots for the prediction of **VEGF-A** plasma concentrations. ε-shrinkage was 3.1%. The grey line is a lowess smoother.

Observations vs. Population Predictions

Observations vs. Individual Predictions

Conditional Weighted Residuals vs. Time After Dose

Conditional Weighted Residuals vs. Population Predictions
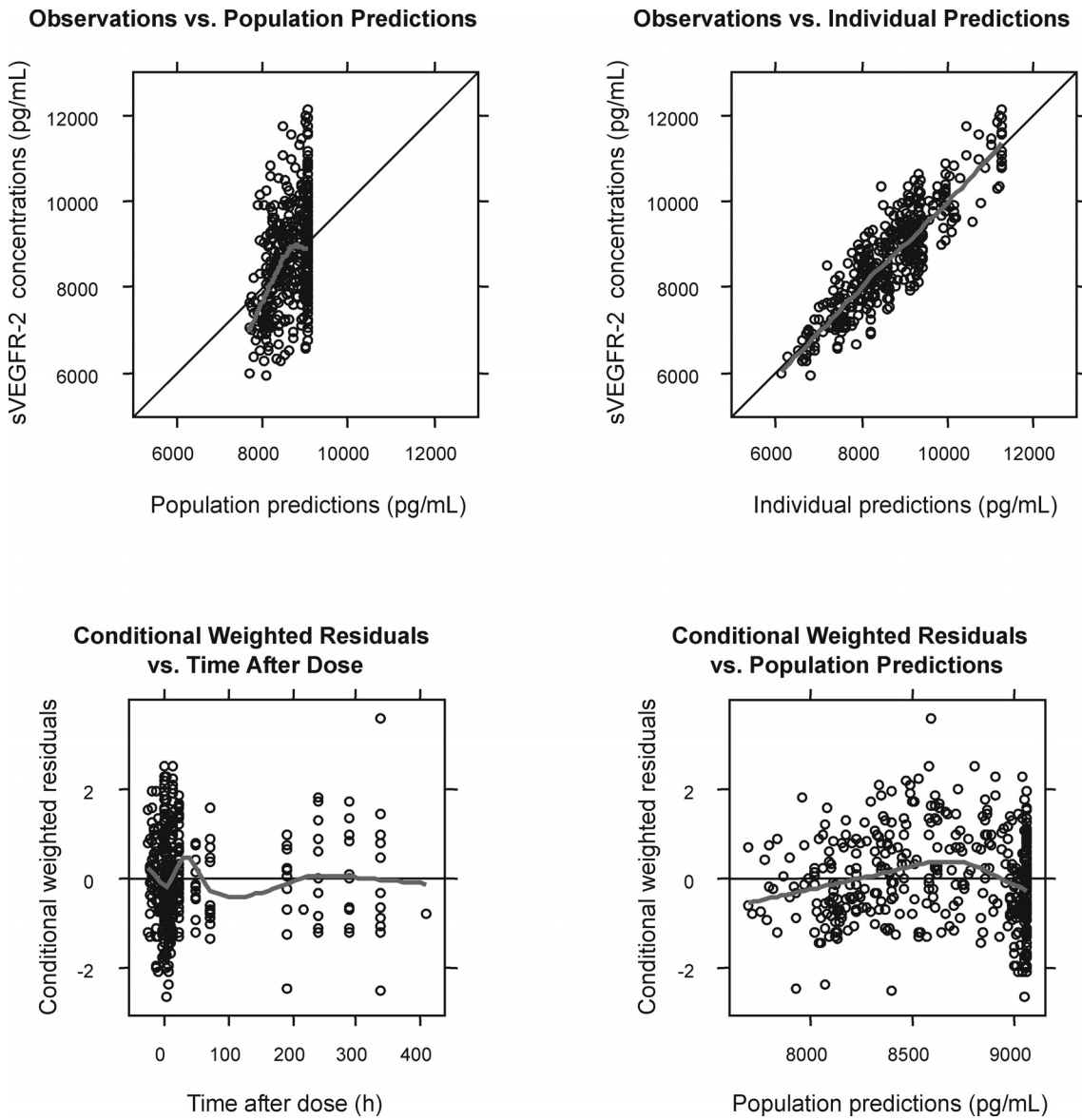
Figure 9-15 Standard goodness-of-fit plots for the prediction of **sVEGFR-2** plasma concentrations. ε-shrinkage was 3.2%. The grey line is a lowess smoother.

9.2.2.2   Sensitivity Analysis
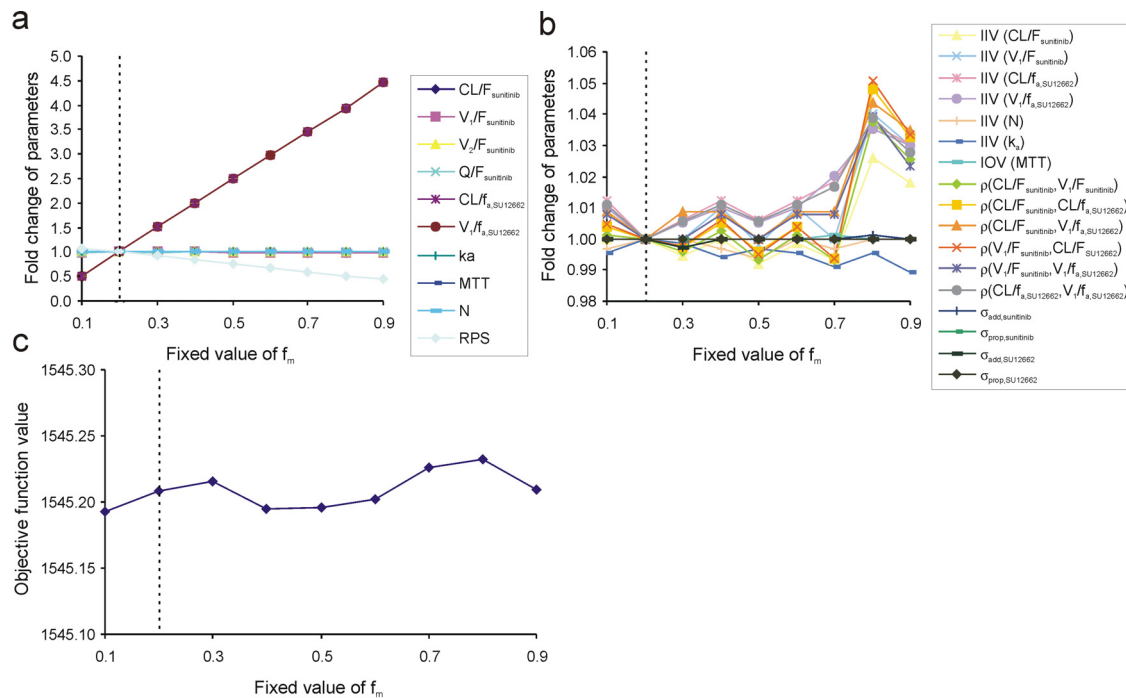
Figure 9-16   Sensitivity analysis of the fraction metabolized to SU12662 (f_m). The graphs illustrate how different values of f_m (0.1 to 0.9) influence fixed-effect (**a**), random-effects parameters (**b**) and the objective function (**c**) of the **sunitinib PK** model. The vertical dotted line marks the fixed value of f_m used in the final model.

IIV: interindividual variability; RPS: ratio of presystemic to systemic metabolite formation; MTT: mean transit time; N: number of transit compartments; k_a: absorption rate constant; CL: clearance; V_1: volume of distribution of the central compartment; Q: intercompartmental clearance; V_2: volume of distribution of the peripheral compartment; F: bioavailability ($f_a \cdot [1-f_{m,pre}]$); f_a: fraction of absorbed dose; ρ: correlation coefficient; σ_{add}: additive residual variability; σ_{prop}: proportional residual variability.
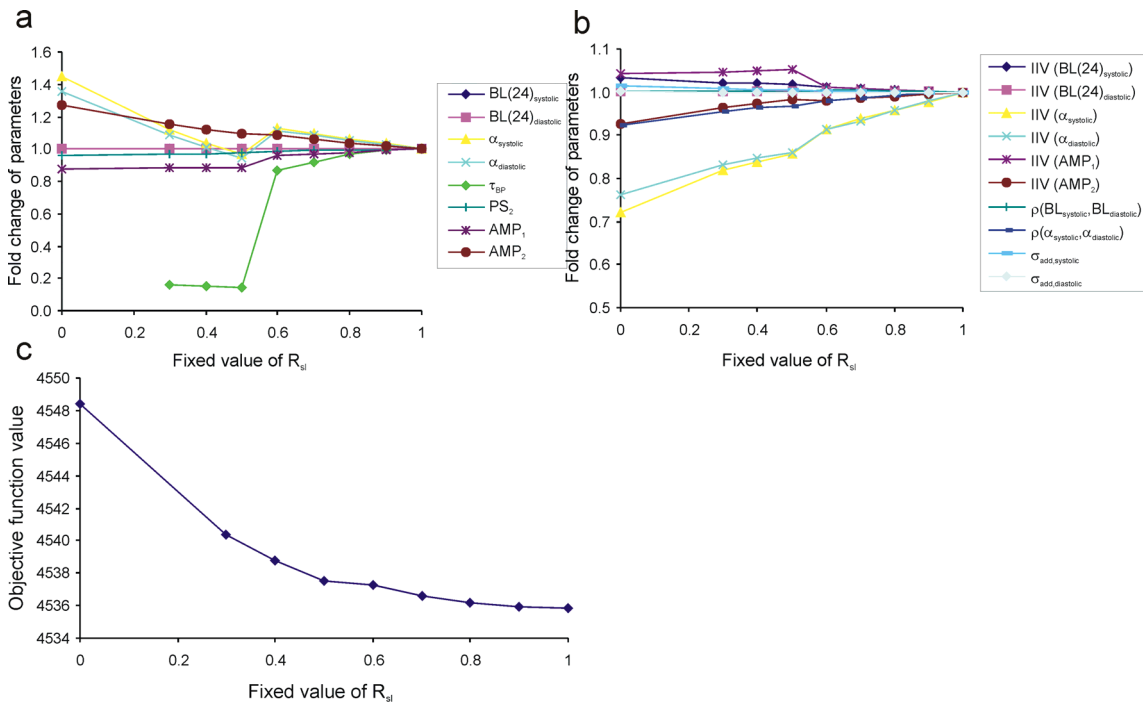
Figure 9-17   Sensitivity analysis of the relative contribution of the slow, transduced signal to the effect (R_{sl}). The graphs illustrate how different values of R_{sl} (0 to 1) influence fixed-effect (**a**), random-effects parameters (**b**) and the objective function (**c**) of the sunitinib **blood pressure** model. The vertical dotted line marks the fixed value of R_{sl} used in the final model. Note: Runs with R_{sl} set to 0.1 and 0.2 did not converge.

IIV: interindividual variability; $BL(24)_{systolic,diastolic}$: average systolic or diastolic blood pressure over 24 hours; BL: baseline value; $AMP_{1,2}$: amplitude of the first or second cosine term; PS_2: phase shift of the second cosine term; α: intrinsic activity parameter; τ: transduction time; ρ: correlation coefficient; σ_{add}: additive residual variability.
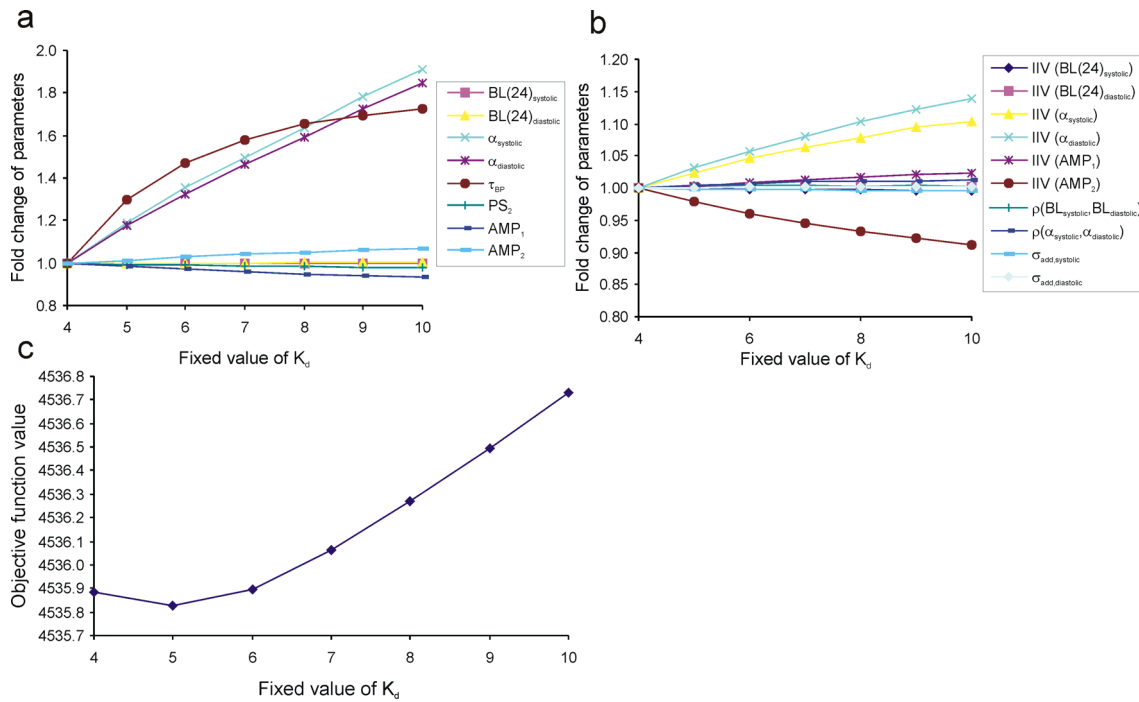
Figure 9-18   Sensitivity analysis of the dissociation constant (K_d). The graphs illustrate how different values of K_d (4 to 10) influence fixed-effect (**a**), random-effects parameters (**b**) and the objective function (**c**) of the sunitinib **blood pressure** model. Note: Runs with K_d fixed to values <4 did not converge. Symbols see Figure 9-17.
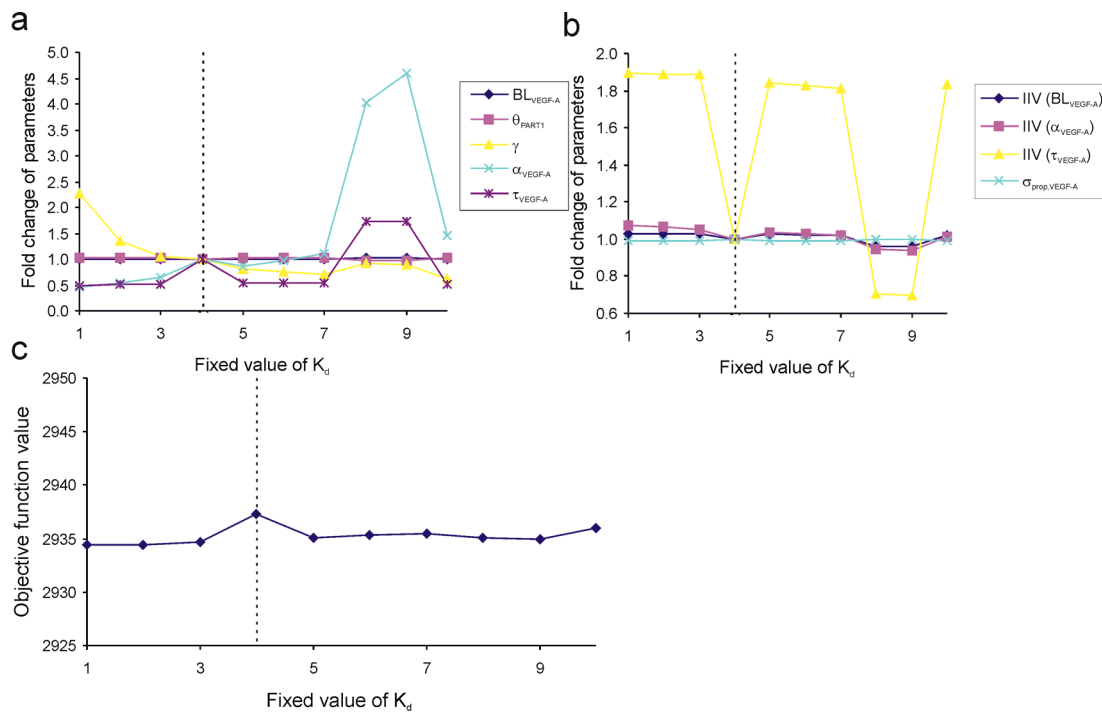
Figure 9-19   Sensitivity analysis of the dissociation constant (K_d). The graphs illustrate how different values of K_d (1 to 10) influence fixed-effect (**a**), random-effects parameters (**b**) and the objective function (**c**) of the sunitinib **VEGF-A** model. The vertical dotted line marks the fixed value of K_d used in the final model.

IIV: interindividual variability; BL: baseline value; θ_{PART1}: baseline adjustment for subjects from the first part of the study; γ: shape parameter; α: intrinsic activity parameter; τ: transduction time; σ_{prop}: proportional residual variability.
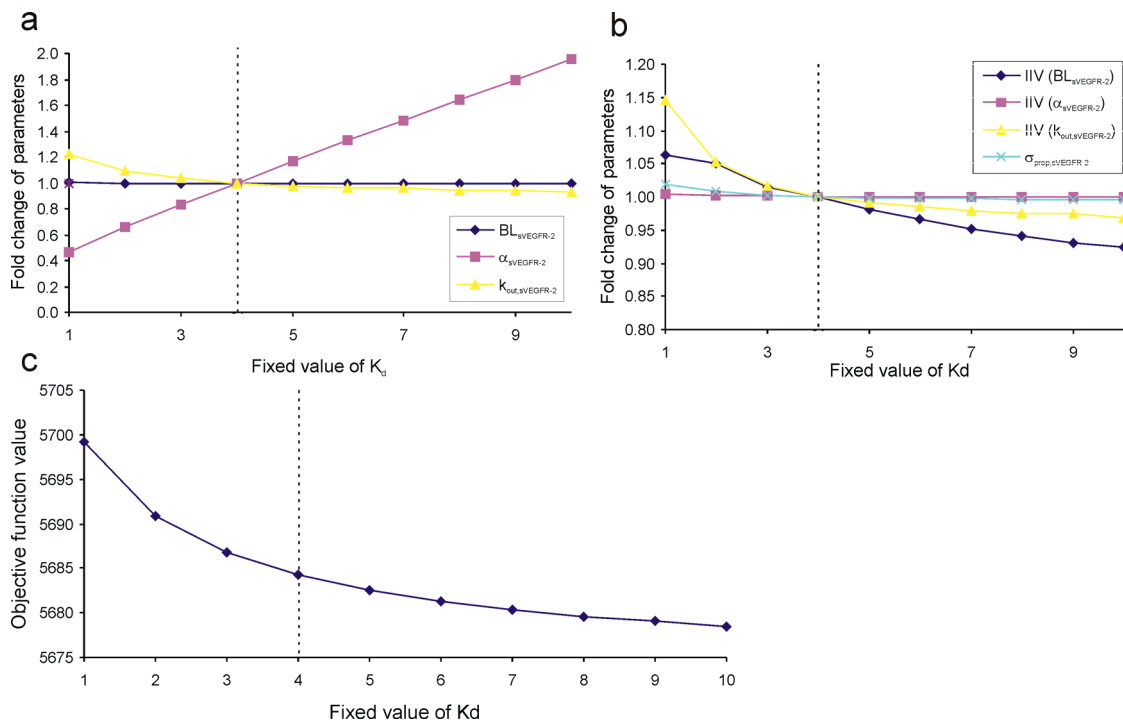
Figure 9-20   Sensitivity analysis of the dissociation constant (K_d). The graphs illustrate how different values of K_d (1 to 10) influence fixed-effect (**a**), random-effects parameters (**b**) and the objective function (**c**) of the sunitinib **sVEGFR-2** model. The vertical dotted line marks the fixed value of K_d used in the final model.

IIV: interindividual variability; BL: baseline value; α: intrinsic activity parameter; k_{out}: rate of loss of biomarker response; σ_{prop}: proportional residual variability.

9.2.3 NONMEM and R Codes

Code 9-4 NONMEM control stream for the **sunitinib** pharmacokinetic model

```
$PROBLEM Sunitinib - Pharmacokinetic model

;----------------------------------------
;  UNITS                                 |
;  TIME - HOURS                          |
;  DOSE - UG                             |
;  CP  - NG/ML  -> UG/L                  |
;  LLOQ - 0.06 NG/ML                     |
;  CL - L/HOUR                           |
;  VOLUMES - L                           |
;----------------------------------------

$INPUT ID TIME AMT DV EVID D1M2 BQL CMT OCC PART AGE BW HGT SEX
       ;DV = sunitinib or SU12662 plasma concentrations

$DATA Data_input_file_PKsun.csv

$SUBROUTINE ADVAN6 TOL=4

$MODEL
NCOMP=4
COMP=(DEPOTD,DEFDOSE)  ;Dosing compartment
COMP=(CENTRAL)         ;Sunitinib central compartment
COMP=(PERIPH)          ;Sunitinib peripheral compartment
COMP=(MET)             ;SU12662 central compartment

;INITIAL VALUES
$THETA
(0,30)          ; THCL   - Clearance/F of sunitinib
(0,1500)        ; THV1   - Central volume of distribution (Vd)/F of sunitinb
(0,200)         ; THV2   - Peripheral Vd/F
(0,2.5)         ; THQ    - Intercompartmental clearance/F of sunitinib
(0.1,0.5)       ; THKA   - Absorption rate constant
(0.001,1.3)     ; THMTT  - Mean transit time
(0,1.3,5)       ; THN    - Number of transit compartments
(0,2.0)         ; THRPS  - Ratio of presystemic to systemic metabolism
(0.21 FIX)      ; THFM   - Fraction metabolized to SU12662
(1 FIX)         ; THFABS - Fraction of dose absorbed
(0,14)          ; THCLM  - Clearance/FABS of SU12662
(0,1410)        ; THVM1  - Vd/FABS of SU12662
(0,0.06)        ; SD_PAR - Additive residual error sunitinib
(0,0.10)        ; CV_PAR - Proportional residual error sunitinib
(0,0.06)        ; SD_MET - Additive residual error SU12662
(0,0.10)        ; CV_MET - Proportional residual error SU12662

$OMEGA BLOCK(4)
0.074                     ; ETACL  - Interindividual variability (IIV) of CL
0.0793 0.109              ; ETAV1  - IIV of V1
0.02 0.02 0.168           ; ETACLM - IIV of CLM
0.02 0.02 0.0185 0.205    ; ETAVM1 - IIV of VM1 (Covariances are the off-diagonal elements)

$OMEGA 0.1            ; ETAN   - IIV of N
$OMEGA 0.05          ; ETAKA   - IIV of KA
$OMEGA  BLOCK(1) 0.95 ; KPMTT1  - Interoccasion variability in MTT
$OMEGA  BLOCK(1) SAME ; KPMTT2
$OMEGA  BLOCK(1) SAME ; KPMTT3
$OMEGA  BLOCK(1) SAME ; KPMTT4
$OMEGA  BLOCK(1) SAME ; KPMTT5
```

Code 9-4 continued

```
$SIGMA 1 FIX

$PK

;Increase maximum number of integrations of the differential equations
"FIRST
" COMMON /PRCOMG/ IDUM1,IDUM2,IMAX,IDUM4,IDUM5
" INTEGER IDUM1,IDUM2,IMAX,IDUM4,IDUM5
" IMAX=99000000

 FM   = THFM
 RPS  = THRPS

 ;The following function is needed for the calculation of FPRE and FSYSS
 ;under the condition that FM=FPRE+(1-FPRE)*FSYSS and RPS=FPRE/FSYSS and FM,FSYS,FPRE<1

 SQ   = SQRT(1+2*RPS+RPS**2-4*RPS*FM)
 FPRE = 0.5+0.5*RPS-0.5*SQ
 FSYS = FPRE/RPS

 FABS = THFABS
 FD   = (1-FPRE)*FABS      ;Bioavailability of sunitinib (FD=F)

 KA   = THKA*EXP(ETAKA)
 CL   = FD*THCL*EXP(ETACL)
 V1   = FD*THV1*EXP(ETAV1)
 V2   = FD*THV2
 Q    = FD*THQ
 CLM  = THCLM*EXP(ETACLM)
 VM1  = THVM1*EXP(ETAVM1)

;INTEROCASSION VARIABILITY IN MTT
OCC1=0
OCC2=0
OCC3=0
OCC4=0
OCC5=0
IF(OCC.EQ.1) OCC1=1
IF(OCC.EQ.2) OCC2=1
IF(OCC.EQ.3) OCC3=1
IF(OCC.EQ.4) OCC4=1
IF(OCC.EQ.5) OCC5=1

IOV=OCC1*KPMTT1+OCC2*KPMTT2+OCC3*KPMTT3+OCC4*KPMTT4+OCC5*KPMTT5
MTT=THMTT*EXP(IOV)

 N  = THN*EXP(ETAN)
 KTR=(N+1)/MTT              ;Transit rate constant

 S2=V1
 S3=V2
 S4=VM1

;SETTING UP THE DOSE
IF(NEWIND.NE.2) THEN
 TDOS=0                 ;For every new individual the time of the first dose is set to 0
 DOSE=0                 ;Reset dose
ENDIF

;TIME AFTER DOSE
IF(AMT.GT.0) THEN       ;If a dosing event is found in the data file
 TDOS=TIME              ;time of dosing and the dose are set accordingly
 DOSE=AMT*FABS
ENDIF
 TAD=TIME-TDOS          ;Time after dose
```

Code 9-4 continued

```
;DELETE NONMEMS DOSE RECORD
 F1=0                    ;This necessary for the transit model to work

;STERLING APPROXIMATION OF (LOG) FACULTY N (see Savic et al. 2007)
 L=LOG(2.5066)+(N+0.5)*LOG(N)-N

$DES
 X=0.00001  ;To avoid LOG(0) when DOSE=0

;TRANSIT COMPARTMENTS OF ABSORPTION (see Savic et al. 2007)
IF(T.GE.TDOS)THEN ; IF CURRENT TIME GREATER THAN TDOS
 DADT(1)=EXP(LOG(DOSE+X)+LOG(KTR+X)+N*LOG(KTR*(T-TDOS)+X)-KTR*(T-TDOS)-L)-(1-
FPRE)*KA*A(1)-(FPRE)*KA*A(1)
ELSE
 DADT(1)=EXP(LOG(DOSE+X)+LOG(KTR+X)+N*LOG(KTR*T +X)-KTR*T-L)-(1-FPRE)*KA*A(1)-
(FPRE)*KA*A(1)
ENDIF

;DISPOSITION
 DADT(2)= (1-FPRE)*KA*A(1)-Q/V1*A(2)+Q/V2*A(3)-CL/V1*A(2) ;Sunitinib central compartment
 DADT(3)=                  +Q/V1*A(2)-Q/V2*A(3)           ;Sunitinib peripheral compartment
 DADT(4)=    FPRE*KA*A(1)-CLM/VM1*A(4)     +CL/V1*A(2)*FSYS ;SU12662 central
compartment


$ERROR
;PREDICTIONS AND RESIDUAL ERROR
IF (CMT.EQ.2) THEN
 IPRE  = A(2)/V1                          ;Individual predicted sunitinib
concentration
 IRES  = DV - IPRE                        ;Individual residuals
 W     = SQRT(SD_PAR**2+CV_PAR**2*IPRE**2)  ;Combined residual error sunitinib
 Y     = IPRE+ERR(1)*W
ELSE
 IPRE  = A(4)/VM1                         ;Individual predicted SU12662 concentration
 IRES  = DV - IPRE                        ;Individual residuals
 W     = SQRT(SD_MET**2+CV_MET**2*IPRE**2)  ;Combined residual error sunitinib
 Y     = IPRE+ERR(1)*W
ENDIF
 DEL          = 0
 IF(W.EQ.0) DEL = 1                       ;To prevent division by 0
 IWRE         = IRES/(W+DEL)              ;Individual weighted residuals

$ESTIMATION SIG=2 PRINT=1 METHOD=1 INTER MAXEVAL=9999 NOABORT MSFO=msfo.msf
$COVARIANCE PRINT=E
```

Code 9-5   NONMEM control stream for the sunitinib **blood pressure** model

```
$PROBLEM Sunitinib - Blood pressure model

;---------------------------------------
;  UNITS                                |
;  TIME - HOURS                         |
;  DOSE - UG                            |
;  CP  - NG/ML  -> UG/L                 |
;  VOLUMES - L                          |
;  BP - mmHg                            |
;---------------------------------------

$INPUT ID TIME AMT DV EVID CMT PART AGE BW HGT SEX
       KAx MTTx Nx RPSx FM=DROP CLx V1x Qx V2x CLMx VM1x ;Individual parameters from the
previous PK step
          ;TIME relative to 6 AM on Day 0 - this is necessary in order to include
          ;the baseline measurements of day 0
          ;DV = systolic or diastolic blood pressure

$DATA Data_input_file_BP.csv

$SUBROUTINE ADVAN6 TOL=4

$MODEL
NCOMP=7
COMP=(DEPOTD,DEFDOSE)  ;Dosing compartment
COMP=(CENTRAL)         ;Sunitinib central compartment
COMP=(PERIPH)          ;Sunitinib peripheral compartment
COMP=(MET)             ;SU12662 central compartment
COMP=(SYS)             ;Systolic blood pressure (BP)
COMP=(DIA)             ;Diastolic BP
COMP=(SST)             ;Slow signal transduction

;INITIAL VALUES
$THETA
(0,118)         ; THBLS     - Average baseline systolic BP over 24 hours
(0,68)          ; THBLD     - Average baseline diastolic BP over 24 hours
(0.125)         ; THALSY    - Intrinsic activity (alpha) for systolic BP
(0.217)         ; THALDI    - Intrinsic activity (alpha) for diastolic BP
(4 FIX)         ; THKD      - Dissociation constant
(0,100)         ; THTAU     - Signal transduction time for slow signal
(0 FIX)         ; THPS1     - Phase shift 1
(1.31)          ; THPS2     - Phase shift 2
(0.0177)        ; THAMP1    - Amplitude of first cosine term
(-0.0209)       ; THAMP2    - Amplitude of second cosine term
(0,7.37)        ; ADD_SYS   - Additive residual error systolic BP
(0,6.63)        ; ADD_DIA   - Additive residual error diastolic BP

$OMEGA BLOCK(2)
0.00474              ; ETABLS  - Interindividual variability (IIV) of BLS
0.00420 0.00764      ; ETABLD  - IIV of BLD (covariance is the off-diagonal element)
$OMEGA BLOCK(2)
0.517                ; ETAALSY - IIV of ALSY
0.31 0.294           ; ETAALDI - IIV of ALSY (covariance is the off-diagonal element)
$OMEGA 0.63          ; ETAAMP1 - IIV of AMP1
$OMEGA 0.368         ; ETAAMP2 - IIV of AMP2

$SIGMA 1 FIX
```

Code 9-5 continued

```
$PK

;Increase maximum number of integrations of the differential equations
"FIRST
" COMMON /PRCOMG/ IDUM1,IDUM2,IMAX,IDUM4,IDUM5
" INTEGER IDUM1,IDUM2,IMAX,IDUM4,IDUM5
" IMAX=99000000

;DRUG SPECIFIC
 KD   = THKD

;SYSTEM SPECIFIC
 BLS  = THBLS*EXP(ETABLS)
 BLD  = THBLD*EXP(ETABLD)
 ALDI = THALDI*EXP(ETAALDI)
 ALSY = THALSY*EXP(ETAALSY)
 TAU  = THTAU

;CIRCADIAN VARIATION
 PS1  = THPS1
 AMP1 = THAMP1*EXP(ETAAMP1)

 PS2  = THPS2
 AMP2 = THAMP2*EXP(ETAAMP2)

;PK PART
 FABS = 1                  ;Fraction absorbed
 FM   = 0.21               ;Fraction metabolized
 RPS  = RPSx               ;Ratio FPRE/FSYS

 SQ   = SQRT(1+2*RPS+RPS**2-4*RPS*FM)
 FPRE = 0.5+0.5*RPS-0.5*SQ ;Fraction metabolized presystemically
 FSYS = FPRE/RPS           ;Fraction metabolized systemically

 KA  = KAx                 ;Description see PK model
 CL  = CLx
 V1  = V1x
 V2  = V2x
 Q   = Qx
 CLM = CLMx
 VM1 = VM1x
 MTT = MTTx
 N   = Nx
 KTR=(NN+1)/MTT            ;Transit rate constant

 S2=V1
 S3=V2
 S4=VM1

;SETTING UP THE DOSE
IF(NEWIND.NE.2) THEN
 TDOS=26                ;For every new individual the time of the first dose is set to
 ON=0                   ;to 26h after 6 AM on day 0
 DOSE=0                 ;Reset dose
ENDIF

;TIME AFTER DOSE
IF(AMT.GT.0) THEN       ;If a dosing event is found in the data file
 TDOS=TIME              ;time of dosing and the dose are set accordingly
 ON=1                   ;Switch on the transit compartments when a dose is given
 DOSE=AMT*FABS
ENDIF
TAD=TIME-TDOS          ;Time after dose
```

Code 9-5 continued

```
 ;DELETE NONMEMS DOSE RECORD
 F1=0                 ;This necessary for the transit model to work

;STERLING APPROXIMATION OF (LOG) FACULTY N (see Savic et al. 2007)
 L=LOG(2.5066)+(N+0.5)*LOG(N)-N

;INITIALIZATION OF SLOW TRANSDUCTION COMPARTMENT
 A_0(7)=0

$DES
 X=0.00001  ;To avoid LOG(0) when DOSE=0

;TRANSIT COMPARTMENTS OF ABSORPTION (see Savic et al. 2007)
IF(T.GE.TDOS)THEN
 DADT(1)=ON*EXP(LOG(DOSE+X)+LOG(KTR+X)+N*LOG(KTR*(T-TDOS)+X)-KTR*(T-TDOS)-L)-(1-
FPRE)*KA*A(1)-(FPRE)*KA*A(1)
ELSE
 DADT(1)=ON*EXP(LOG(DOSE+X)+LOG(KTR+X)+N*LOG(KTR*T +X)-KTR*T-L)-(1-FPRE)*KA*A(1)-
(FPRE)*KA*A(1)
ENDIF

;DISPOSITION
 DADT(2)= (1-FPRE)*KA*A(1)-Q/V1*A(2)+Q/V2*A(3)-CL/V1*A(2)        ;Sunitinib central
compartment
 DADT(3)=                 +Q/V1*A(2)-Q/V2*A(3)                   ;Sunitinib peripheral
compartment
 DADT(4)=     FPRE*KA*A(1)-CLM/VM1*A(4)      +CL/V1*A(2)*FSYS ;SU12662 central
compartment

;TYROSINE KINASE INHIBITION
 AC= A(4)/VM1*(1-0.90)+A(2)/V1*(1-0.95)       ;Unbound active concentration (outside of
$DES)
 IF(AC.LE.0) AC=0                             ; 95% PB sunitinib, 90% PB SU12662

 INH   = FC/(KD+FC)                           ;Fractional tyrosine kinase inhibition
 DADT(7)=1/TAU*INH-1/TAU*A(7)            ;Slow signal transduction

$ERROR
 ACx   = A(4)/VM1*(1-0.90)+A(2)/V1*(1-0.95) ;Unbound active concentration
 INHx  = ACx/(KD+ACx)                        ;Fractional tyrosine kinase inhibition

;CIRCADIAN VARIATION
 ;TIME+6 because clock time is 6 AM when TIME=0
 CBLS  =BLS*(1+(AMP1*COS((TIME+6)*6.283/24-PS1)+AMP2*COS((TIME+6)*6.283/12-PS2)))
 CBLD  =BLD*(1+(AMP1*COS((TIME+6)*6.283/24-PS1)+AMP2*COS((TIME+6)*6.283/12-PS2)))

;PREDICTIONS AND RESIDUAL ERROR
IF(CMT.EQ.5) THEN
 IPRE  = CBLS*(1+ALSY*(INHx+A(7)))  ;Individual predicted systolic blood pressure (BP)
 IRES  = DV - IPRE               ;Individual residuals
 W     = ADD_SYS                 ;Additive residual error systolic BP
 Y     = IPRE+ERR(1)*W
ELSE
 IPRE  = CBLD*(1+ALDI*(INHx+A(7)))  ;Individual predicted diastolic BP
 IRES  = DV - IPRE               ;Individual residuals
 W     = ADD_DIA                 ;Additive residual error diastolic BP
 Y     = IPRE+ERR(1)*W
ENDIF
 DEL         = 0
 IF(W.EQ.0) DEL = 1              ;To prevent division by 0
 IWRE        = IRES/(W+DEL)      ;Individual weighted residuals

$ESTIMATION SIG=3 PRINT=1 METHOD=1 INTER MAXEVAL=9999 NOABORT MSFO=msfo.msf
$COVARIANCE PRINT=E
```

Code 9-6 NONMEM control stream for the sunitinib **VEGF-A** model

```
$PROBLEM Sunitinib - VEGFA model

;----------------------------------------
;  UNITS                                 |
;  TIME - HOURS                          |
;  DOSE - UG                             |
;  CL - L/HOUR                           |
;  VOLUMES - L                           |
;  VEGFA - PG/ML                         |
;----------------------------------------

$INPUT ID TIME AMT DV EVID CMT PART AGE BW HGT SEX
       KAx MTTx Nx RPSx FM=DROP CLx V1x Qx V2x CLMx VM1x ;Individual parameters from the
previous PK step
          ;TIME relative to 6 AM on Day 0 - this is necessary in order to include
          ;the baseline measurements of day 0
          ;DV = VEGFA concentrations

$DATA Data_input_file_VEGF-A.csv

$SUBROUTINE ADVAN6 TOL=4

$MODEL
NCOMP=5
COMP=(DEPOTD,DEFDOSE)  ;Dosing compartment
COMP=(CENTRAL)         ;Sunitinib central compartment
COMP=(PERIPH)          ;Sunitinib peripheral compartment
COMP=(MET)             ;SU12662 central compartment
COMP=(TRANS)           ;VEGFA transduction compartment

$THETA
(0,100)        ; THBLVA       - Baseline VEGFA
(0,0.75)       ; THPART       - Fractional difference of BLVA in PART1
(4 FIX)        ; THKD         - Dissociation constant
(0,0.8)        ; THALVA       - Intrinsic activity (alpha)
(0,3)          ; THGAM        - Exponent of the power function
(0,10)         ; THTAU        - Signal transduction time
(0,0.2)        ; CV_VA        - Proportional residual error

$OMEGA 0.05    ; ETABLVA      - Interindividual variability in BLVA
$OMEGA 0.5     ; ETAALPHA     - IIV of ALPHA
$OMEGA 0.4     ; ETATAU       - IIV of TAU

$SIGMA 1 FIX

$PK

;Increase maximum number of integrations of the differential equations
"FIRST
" COMMON /PRCOMG/ IDUM1,IDUM2,IMAX,IDUM4,IDUM5
" INTEGER IDUM1,IDUM2,IMAX,IDUM4,IDUM5
" IMAX=99000000

;DRUG SPECIFIC
 KD   = THKD

;SYSTEM SPECIFIC
IF(PART.EQ.2) THE
 BLPART = THBLVA*THPART**0       ; PART2
ELSE
 BLPART = THBLVA*THPART**1       ; PART1
ENDIF
```

Code 9-6 continued

```
 BLVA  = BLPART*EXP(ETABLVA)

 ALVA  = THALPHA*EXP(ETAALPHA)
 TAU   = THTAU*EXP(ETATAU)
 GAM   = THGAM

;PK PART
 FABS  =  1                    ;Fraction absorbed
 FM    =  0.21                 ;Fraction metabolized
 RPS   =  RPSx                 ;Ratio FPRE/FSYS

 SQ   =  SQRT(1+2*RPS+RPS**2-4*RPS*FM)
 FPRE =  0.5+0.5*RPS-0.5*SQ   ;Fraction metabolized presystemically
 FSYS =  FPRE/RPS             ;Fraction metabolized systemically

 KA  = KAx                     ;Description see PK model
 CL  = CLx
 V1  = V1x
 V2  = V2x
 Q   = Qx
 CLM = CLMx
 VM1 = VM1x
 MTT = MTTx
 N   = Nx
 KTR=(NN+1)/MTT                ;Transit rate constant

 S2=V1
 S3=V2
 S4=VM1

;SETTING UP THE DOSE
IF(NEWIND.NE.2) THEN
 TDOS=26              ;For every new individual the time of the first dose is set to
 ON=0                 ;to 26h after 6 AM on day 0
 DOSE=0              ;Reset dose
ENDIF

;TIME AFTER DOSE
IF(AMT.GT.0) THEN       ;If a dosing event is found in the data file
 TDOS=TIME             ;time of dosing and the dose are set accordingly
 ON=1                  ;Switch on the transit compartments when a dose is given
 DOSE=AMT*FABS
ENDIF
 TAD=TIME-TDOS        ;Time after dose

;DELETE NONMEMS DOSE RECORD
 F1=0                  ;This necessary for the transit model to work

;STERLING APPROXIMATION OF (LOG) FACULTY N (see Savic et al. 2007)
 L=LOG(2.5066)+(N+0.5)*LOG(N)-N

;INITIALIZATION OF TRANSDUCTION COMPARTMENT
 A_0(5)=0

$DES
 X=0.00001  ;To avoid LOG(0) when DOSE=0

;TRANSIT COMPARTMENTS OF ABSORPTION (see Savic et al. 2007)
IF(T.GE.TDOS)THEN
 DADT(1)=ON*EXP(LOG(DOSE+X)+LOG(KTR+X)+N*LOG(KTR*(T-TDOS)+X)-KTR*(T-TDOS)-L)
        -(1-FPRE)*KA*A(1)-(FPRE)*KA*A(1)
ELSE
 DADT(1)=ON*EXP(LOG(DOSE+X)+LOG(KTR+X)+N*LOG(KTR*T +X)-KTR*T-L)-(1-FPRE)*KA*A(1)-
(FPRE)*KA*A(1)
ENDIF
```

Code 9-6 continued

```
;DISPOSITION
 DADT(2)= (1-FPRE)*KA*A(1)-Q/V1*A(2)+Q/V2*A(3)-CL/V1*A(2)      ;Sunitinib central
compartment
 DADT(3)=                  +Q/V1*A(2)-Q/V2*A(3)               ;Sunitinib peripheral
compartment
 DADT(4)=    FPRE*KA*A(1)-CLM/VM1*A(4)      +CL/V1*A(2)*FSYS ;SU12662 central
compartment

;TYROSINE KINASE INHIBITION
 AC= A(4)/VM1*(1-0.90)+A(2)/V1*(1-0.95)     ;Unbound active concentration (outside of
$DES)
 IF(AC.LE.0) AC=0                           ; 95% PB sunitinib, 90% PB SU12662

 INH   = FC/(KD+FC)                         ;Fractional tyrosine kinase inhibition
 DADT(5)=(INH**GAM-A(5))/TAU                ;Signal Transduction of INH

$ERROR
 IPRED  = BLVA*(1+ALVA*A(5))    ;Individual predicted VEGFA concentrations
 IRES   = DV - IPRED            ;Individual residuals
 W      = CV_VA*IPRED           ;Proportional residual error
 Y      = IPRED+ERR(1)*W

 DEL          = 0
 IF(W.EQ.0) DEL = 1             ;To prevent division by 0
 IWRE         = IRES/(W+DEL)  ;Individual weighted residuals

$ESTIMATION SIG=2 PRINT=1 METHOD=1 INTER MAXEVAL=9999 NOABORT MSFO=msfo.msf
$COVARIANCE PRINT=E
```

Code 9-7   NONMEM control stream for the sunitinib **sVEGFR-2** model

```
$PROBLEM Sunitinib - VEGFR2 model

;----------------------------------------
;  UNITS                                 |
;  TIME - HOURS                          |
;  DOSE - UG                             |
;  CL - L/HOUR                           |
;  VOLUMES - L                           |
;  VEGFR2 - PG/ML                        |
;----------------------------------------

$INPUT ID TIME AMT DV EVID CMT PART AGE BW HGT SEX
       KAx MTTx Nx RPSx FM=DROP CLx V1x Qx V2x CLMx VM1x ;Individual parameters from the
previous PK step
          ;TIME relative to 6 AM on Day 0 - this is necessary in order to include
          ;the baseline measurements of day 0
          ;DV = VEGFR2 concentrations

$DATA Data_input_file_sVEGFR-2.csv

$SUBROUTINE ADVAN6 TOL=4

$MODEL
NCOMP=5
COMP=(DEPOTD,DEFDOSE)  ;Dosing compartment
COMP=(CENTRAL)         ;Sunitinib central compartment
COMP=(PERIPH)          ;Sunitinib peripheral compartment
COMP=(MET)             ;SU12662 central compartment
COMP=(VEGFR2)          ;VEGFR2 compartment

$THETA
(0,9000)       ; THBLVR      - Baseline VEGFR2
(4 FIX)        ; THKD        - Dissociation constant
(0,1)          ; THALVR      - Intrinsic activity
(0,0.002)      ; THKOUT      - Rate of loss of VEGFR2 response
(0,0.05)       ; CV_VR2      - Proportional residual error
```

Code 9-7 continued

```
$OMEGA 0.0105  ; ETABLVR2    - Interindividual variability in BLVR2
$OMEGA 0.6    ; ETAALPHA    - IIV of ALPHA
$OMEGA 0.01   ; ETAKOUT     - IIV of KOUT


$SIGMA 1 FIX


$PK

;Increase maximum number of integrations of the differential equations
"FIRST
" COMMON /PRCOMG/ IDUM1,IDUM2,IMAX,IDUM4,IDUM5
" INTEGER IDUM1,IDUM2,IMAX,IDUM4,IDUM5
" IMAX=99000000

;DRUG SPECIFIC
 KD   = THKD

;SYSTEM SPECIFIC
 BLVR  = THBLVR2*EXP(ETABLVR2)
 ALVR  = THALPHA*EXP(ETAALPHA)
 KOUT  = THKOUT*EXP(ETAKOUT)

;PK PART
 FABS = 1                  ;Fraction absorbed
 FM   = 0.21               ;Fraction metabolized
 RPS  = RPSx               ;Ratio FPRE/FSYS

 SQ  = SQRT(1+2*RPS+RPS**2-4*RPS*FM)
 FPRE = 0.5+0.5*RPS-0.5*SQ  ;Fraction metabolized presystemically
 FSYS = FPRE/RPS           ;Fraction metabolized systemically

 KA  = KAx                 ;Description see PK model
 CL  = CLx
 V1  = V1x
 V2  = V2x
 Q   = Qx
 CLM = CLMx
 VM1 = VM1x
 MTT = MTTx
 N   = Nx
 KTR=(NN+1)/MTT            ;Transit rate constant

 S2=V1
 S3=V2
 S4=VM1

;SETTING UP THE DOSE
IF(NEWIND.NE.2) THEN
 TDOS=26                ;For every new individual the time of the first dose is set to
 ON=0                   ;to 26h after 6 AM on day 0
 DOSE=0                 ;Reset dose
ENDIF

;TIME AFTER DOSE
IF(AMT.GT.0) THEN       ;If a dosing event is found in the data file
 TDOS=TIME              ;time of dosing and the dose are set accordingly
 ON=1                   ;Switch on the transit compartments when a dose is given

DOSE=AMT*FABS
ENDIF
 TAD=TIME-TDOS          ;Time after dose

;DELETE NONMEMS DOSE RECORD
 F1=0                   ;This necessary for the transit model to work

;STERLING APPROXIMATION OF (LOG) FACULTY N (see Savic et al. 2007)
 L=LOG(2.5066)+(N+0.5)*LOG(N)-N
```

Code 9-7 continued

```
;INITIALIZATION OF THE VEGFR2 COMPARTMENT
 A_0(5)=BLVR

KIN=BLVR*KOUT ;Rate of production of the VEGFR2 response

$DES
 X=0.00001  ;To avoid LOG(0) when DOSE=0

;TRANSIT COMPARTMENTS OF ABSORPTION (see Savic et al. 2007)
IF(T.GE.TDOS)THEN
 DADT(1)=ON*EXP(LOG(DOSE+X)+LOG(KTR+X)+N*LOG(KTR*(T-TDOS)+X)-KTR*(T-TDOS)-L)-(1-
FPRE)*KA*A(1)-(FPRE)*KA*A(1)
ELSE
 DADT(1)=ON*EXP(LOG(DOSE+X)+LOG(KTR+X)+N*LOG(KTR*T +X)-KTR*T-L)-(1-FPRE)*KA*A(1)-
(FPRE)*KA*A(1)
ENDIF

;DISPOSITION
 DADT(2)= (1-FPRE)*KA*A(1)-Q/V1*A(2)+Q/V2*A(3)-CL/V1*A(2)        ;Sunitinib central
compartment
 DADT(3)=                   +Q/V1*A(2)-Q/V2*A(3)                 ;Sunitinib peripheral
compartment
 DADT(4)=     FPRE*KA*A(1)-CLM/VM1*A(4)        +CL/V1*A(2)*FSYS ;SU12662 central
compartment

;TYROSINE KINASE INHIBITION
 AC= A(4)/VM1*(1-0.90)+A(2)/V1*(1-0.95)        ;Unbound active concentration (outside of
$DES)
 IF(AC.LE.0) AC=0                              ; 95% PB sunitinib, 90% PB SU12662

 INH    = FC/(KD+FC)                           ;Fractional tyrosine kinase inhibition
 DADT(5)= KIN*(1/(1+ALVR*INH))-KOUT*A(5)    ;Indirect response model

$ERROR
 IPRED  = A(5)                ;Individual predicted VEGFR2 concentrations
 IRES   = DV - IPRED          ;Individual residuals
 W      = CV_VR2*IPRED        ;Proportional residual error
 Y      = IPRED+ERR(1)*W

 DEL          = 0
 IF(W.EQ.0) DEL = 1           ;To prevent division by 0
 IWRE         = IRES/(W+DEL)  ;Individual weighted residuals

$ESTIMATION SIG=2 PRINT=1 METHOD=1 INTER MAXEVAL=9999 NOABORT MSFO=msfo.msf
$COVARIANCE PRINT=E
```

Code 9-8   R code for the clinical trial simulation

```
################################################################################
#                                                                              #
#      Clinical trial simulation of blood-pressure-based dose individualization      #
#                                                                              #
################################################################################

#Loading additional packages
require(splus2R)
require(hapsim)
require(survival)

#Fixed effects parameters
#-----------------------------------------------------------------------------
thCL_F_sunitinib<-32.4
thCL_fa_SU12662 <-14.6
fm              <-0.21
fub_sunitinib   <-0.05
fub_SU12662     <-0.1
thBL_dia        <-67.6
thAlpha_dia     <-0.145
Kd              <-4

#Concatenate parameters that will be subject to Monte Carlo simulation
theta <- c(thCL_F_sunitinib,thCL_fa_SU12662,thBL_dia,thAlpha_dia)
npar  <- length(theta) #number of fixed effect parameters

#Variance-covariance matrix for the random effects:
#-----------------------------------------------------------------------------
omCL_F_sunitinib <- 0.073
omCL_fa_SU12662  <- 0.167
covCL            <- 0.0776
omBL_dia         <- 0.0075
omalpha_dia      <- 0.411

#Combine in 4x4 matrix
omega <- matrix(c(omCL_F_sunitinib,covCL,           0,        0,
                  covCL,           omCL_fa_SU12662,0,        0,
                  0,               0,              omBL_dia,0,
                  0,               0,              0,        omalpha_dia)
                  ,nrow=4,ncol=4,byrow=TRUE)

#Residual error of diastolic blood pressure
#-----------------------------------------------------------------------------
sigma <- 6.6

# Treatment schedule
#-----------------------------------------------------------------------------
dose    <- 50      # Initial dose (mg)
tau     <- 24      # Dosing interval (h)
dayson  <- 28      # Days on treatment per cycle
cymax   <- 20      # Maximum number of cycles to be simulated (study duration)
cylength<- 42      # Cycle length in days
cydays  <- cylength*(c(1:cymax)-1)+dayson  # Days of patient status
                                           # assessment (day 28 in every cycle)
nrep    <- 500     # Number of trial replicates
npat    <- 150     # Number of patients
ngroup <- 2        # Number of treatment groups

BP_target <- 1.16 # Blood pressure target increase (relative to baseline)

# Initialize arrays where (intermediate) results are stored
#-----------------------------------------------------------------------------
MCarray     <- rep(NA,(npat*npar*nrep))  # Here Monte Carlo simulated individual
dim(MCarray)<- c(npat,npar,nrep)     # paramters will be stored
```

Code 9-8 continued

```
# Final results arrays
FinTAB      <- rep(NA,(14*nrep))
dim(FinTAB)<- c(14,nrep)
sumTAB      <- rep(NA,(length(cydays)*(nrep+4)*2))
dim(sumTAB)<- c(length(cydays),(nrep+4),2)

# Intermediate results arrays
IntTAB      <- rep(NA,(npat*8*nrep))
dim(IntTAB)<- c(npat,8,nrep)
dBPBL       <- data.frame(matrix(data=NA,nrow=npat,ncol=nrep))
KM          <- as.list(1:nrep)
COX         <- as.list(1:nrep)

for (repli in 1:nrep){  # Replicate loop begins here
    ## Monte Carlo simulation ##
    #--------------------------------------------------------------------------------
    #For every trial replicate a new set of patients is simulated

    # Random sampling from the variance-covariance matrix
    etas   <- rmvnorm(npat, mean=rep(0,ncol(omega)), cov=omega)
    # Intermediate matrix of individual parameters
    par.ind <- matrix(rep(theta,npat),nrow=npat,byrow=T)

    for (n in 1:npat){
            par.ind[n,1]<-par.ind[n,1]*exp(etas[n,1]) # CL_F_sunitinib
            par.ind[n,2]<-par.ind[n,2]*exp(etas[n,2]) # CL_fa_SU12662
            par.ind[n,3]<-par.ind[n,3]*exp(etas[n,3]) # BL_diastolic
            par.ind[n,4]<-par.ind[n,4]*exp(etas[n,4]) # Alpha_dia
    }
    MCarray[,,repli]<-par.ind  # Store in the Monte Carlo array
    #--------------------------------------------------------------------------------

    gr.size1<-npat/ngroup    # Size of group1 (standard dose group, SDG)
    gr.size2<-npat-gr.size1  # Size of group2 (individualized dose group, IDG)
    start<-1                  # Start patient-counter counter for group1
    end<-gr.size1             # Last patient of group1

    for (gr in 1:ngroup){    # First "treat" group1 then group2
      if (gr==2){
      start<-gr.size1+1
      end<-npat
      }
      for (pat in start:end){ # Treat every individual sequentially
         ### Initialize patient specific variables
         doseI            <- dose # Individual dose
         F_EVENTS         <- 0    # Counts if patient experienced fatigue
         STAT             <- 0    # Status: 0 = alive , 1 = dead
         AHT              <- 0    # Antihypertensive therapy; 0 = NO , 1 = YES
         etime            <- 0    # Elapsed time
         prev.time        <- 0    # Previous time
         cyc              <- 1    # Cycle number

         ## Individual parameters for the current
          # patient in the current replicate
         iCL_F_sunitinib  <- MCarray[pat,1,repli]
         iCL_fa_SU12662   <- MCarray[pat,2,repli]
         iBL_dia          <- MCarray[pat,3,repli]
         iAlpha_dia       <- MCarray[pat,4,repli]
         # baseline blood pressure (with random error)
         dBPBL[pat,repli]  <- iBL_dia+rnorm(1,0,sigma)

         #----------------------------------------------------------------------------
             while (STAT==0 && cyc<=cymax){
               # Continue treatment as long as patient
               # is alive and maximum number of
               # cycles has not been reached
               IntTAB[pat,7,repli] <- doseI # Save current dose
               IntTAB[pat,8,repli] <- AHT   # Save antihypertensive treatment status
```

Code 9-8 continued

```
          ## Calculate AUCs and concentrations
          #----------------------------------------------------------------------
          AUC_sunitinib <-     doseI/iCL_F_sunitinib
          AUC_SU12662   <- fm*doseI/iCL_fa_SU12662
          AUCsum        <- AUC_sunitinib+AUC_SU12662
          AUCdaily      <- AUC_sunitinib*28/42     # Average daily AUC
                                                   #  as used by Houk et al. 2009

          sunitinib_Css <- 1000*AUC_sunitinib/tau  # Steady-state (SS)
                                                   #  concentration of
                                                   #  sunitinib (ng/mL)
          SU12662_Css   <- 1000*AUC_SU12662/tau    #  SS concentration of SU12662
          ACss          <- (SU12662_Css*fub_SU12662       # Sum of unbound
                            +sunitinib_Css*fub_sunitinib) #  concentrations at SS
                                                          #(=active concentration)


          ## Calculate diastolic blood pressure (dBP) at SS (with residual error)
          #----------------------------------------------------------------------
          INH           <- ACss/(Kd+ACss)          # at steady-state INH=ISIG=TSIG
          dBP           <- iBL_dia*(1+iAlpha_dia*(INH+INH))+rnorm(1,0,sigma)
          dBPrel        <- dBP/dBPBL[pat,repli]    # dBP relative to pretreatment
                                                   #  value
          # Start antihypertensive treatment if dBP >= 100 mmHg
          # (hypertension according to CTCv4.0 grade 3 )
          if (dBP>=100) AHT<-1

          ## Calculate survival
          #----------------------------------------------------------------------
          # Parameters of the Weibull survival function from Houk et al. 2009
          bl <-  110      # baseline
          sl <-  485      # slope
          gam <- 1.78     # gamma

          phi   <- (bl+sl*AUCdaily)
          ctime <- cylength*(cyc-1)+dayson # current time in days
          etime <- ctime-prev.time        # elapsed time since previous assessment

          # Survival function
          St <- exp(-(log(2)*(ctime/phi)**gam))
          # Probability density function
          PDF<- (log(2)*(gam/ctime)*(ctime/phi)**(gam)*
                (exp(-(log(2)*(ctime/phi)**gam))))
          # Hazard rate
          Ht <- PDF/St
          # Probability of death since last assessment (in the interval etime)
          Pd <- Ht*etime
          # Draw random sample from a binomial distribution with probability pE
          STAT  <- rbinom(1,1,Pd) # 0 = alive, 1 = dead
          ## Dose individualization
          #----------------------------------------------------------------------
          # Assess if patient has fatigue
          #----------------------------------------------------------------------
          FATIGUE <- 0   # Reset fatigue indicator in every cycle
          # Calculate probability of grade 3/4 Fatigue
          # according to FDA Pharmacometrics Review of sunitinib
          pF    <- exp(0.5144*AUCsum-3.2164)/
                (1+exp(0.5144*AUCsum-3.2164))   # Total probability in 17 cycles
          pFcyc <- 1-(1-pF)**(1/17)             # Probability per cycle
          # Random sample from a binomial distribution with probability pF
          FATIGUE<-rbinom(1,1,pFcyc)     # 0 = no fatigue, 1 = fatigue event
            if (FATIGUE==1 && doseI>25){ # If patient has fatigue and current
             doseI<-doseI-12.5           #  dose is >25 mg then reduce dose
             F_EVENTS<-1                 # Save if patient experienced fatigue
             }
```

Code 9-8 continued

```
                   #-------------------------------------------------------------------
                   # Blood-pressure-based dose individualization
                   #-------------------------------------------------------------------
                   if (gr==2) { # if current patient belongs to IDG
                      if (FATIGUE==0 && doseI<87.5 && AHT==0){
                         # only increase dose if patient has currently no fatigue
                         # and is not on antihypertensive treatment
                         # and the upper dose limit of 87.5 mg has not been reached

                         if (dBPrel<BP_target) { # If dBP increase is below the target
                             doseI<-doseI+12.5   # then increase dose by 12.5 mg
                         }
                      }
                   }

               IntTAB[pat,1,repli]<-pat      # current ID
               IntTAB[pat,2,repli]<-gr       # current group
               IntTAB[pat,3,repli]<-ctime    # Save current time
               IntTAB[pat,4,repli]<-STAT     # status
               IntTAB[pat,5,repli]<-F_EVENTS # number of fatigue events
               IntTAB[pat,6,repli]<-cyc      # save current cycle number
               prev.time<-ctime              # set previous time to current time
               cyc<-cyc+1                    # count up the cycle number
          }# End of cycle loop
       }# End of patient loop
    }# End of group loop


  ### Analysis of trial results
  #---------------------------------------------------------------------------------
    # Apply cox-proportional model for the comparison between the two groups
    COX[[repli]] <- coxph(Surv(IntTAB[,3,repli],IntTAB[,4,repli])~IntTAB[,2,repli])

    # Number of patients with severe fatigue events
    FES  <- sum(IntTAB[IntTAB[,2,repli]==1,5,repli]) # in the SDG
    FEI  <- sum(IntTAB[IntTAB[,2,repli]==2,5,repli]) # in the IDG
    FESp <- 100*FES/(gr.size1)                       # as percentage
    FEIp <- 100*FEI/(gr.size2)
    pFE  <- prop.test(c(FES,FEI),c((gr.size1),(gr.size2))) #P-value for the difference
                                                     # in fatigue incidence

    # Number of patients receiving AHT
    AHTs  <-sum(IntTAB[IntTAB[,2,repli]==1,8,repli]) # in the SDG
    AHTi  <-sum(IntTAB[IntTAB[,2,repli]==2,8,repli]) # in the IDG
    AHTsp <- 100*AHTs/(gr.size1)                     # as a percentage
    AHTip <- 100*AHTi/(gr.size2)

    # Median time to death
    TTDS <- median(IntTAB[IntTAB[,2,repli]==1,3,repli]) # in the SDG
    TTDI <- median(IntTAB[IntTAB[,2,repli]==2,3,repli]) # in the IDG
    p    <- summary(COX[[repli]])[[9]][3]               # P-value (log-rank test)
    HR   <- summary(COX[[repli]])[[7]][1]               # Hazard ratio IDG/SDG

    FinTAB[1,repli] <- repli
    FinTAB[2,repli] <- TTDS
    FinTAB[3,repli] <- TTDI
    FinTAB[4,repli] <- TTDI-TTDS
    FinTAB[5,repli] <- p
    FinTAB[6,repli] <- FESp
    FinTAB[7,repli] <- FEIp
    FinTAB[8,repli] <- FEIp-FESp
    FinTAB[9,repli] <- pFE[[3]]
    FinTAB[10,repli]<- HR
    FinTAB[11,repli]<- LdoseS
    FinTAB[12,repli]<- LdoseI
    FinTAB[13,repli]<- AHTsp
    FinTAB[14,repli]<- AHTip
}# End of replicate loop
```

Code 9-8 continued

```
### FINAL RESULTS
-------------------------------------------------------------------------------
-
# Overall survival (i.e., median time to death) (95% CI):
quantile(FinTAB[2,],  c(0.5,0.025,0.975), na.rm=T) # in the SDG
quantile(FinTAB[3,],  c(0.5,0.025,0.975), na.rm=T) # in the IDG
# Hazard ratio (95% CI)
quantile(FinTAB[10,], c(0.5,0.025,0.975), na.rm=T)
# log-rank p-value (95% CI)
quantile(FinTAB[5,],  c(0.5,0.025,0.975), na.rm=T)
# Incidence(%) of severe fatigue (95% CI)
quantile(FinTAB[6,],  c(0.5,0.025,0.975), na.rm=T) # in SDG
quantile(FinTAB[7,],  c(0.5,0.025,0.975), na.rm=T) # in the IDG
#Percentage of patients requiring AHT
quantile(FinTAB[13,], c(0.5,0.025,0.975), na.rm=T) # in SDG
quantile(FinTAB[14,], c(0.5,0.025,0.975), na.rm=T) # in IDG
```

Publications

Original Publications

Lindauer, A, Di Gion, P, Kanefendt, F, et al. Pharmacokinetic/pharmacodynamic modeling of biomarker response to sunitinib in healthy volunteers. Clin Pharmacol Ther 2010; 87:601-8

Lindauer, A, Eickhoff, C, Kloft, C, et al. Population pharmacokinetics of high-dose carboplatin in children and adults. Ther Drug Monit 2010; 32:159-68

Lentz, F, Drescher, A, **Lindauer, A**, et al. Pharmacokinetics of a novel anticancer ruthenium complex (KP1019, FFC14A) in a phase I dose-escalation study. Anticancer drugs 2009; 20:97-103

Lindauer, A, Siepmann, T, Oertel, R, et al. Pharmacokinetic/Pharmacodynamic modelling of venlafaxine: pupillary light reflex as a test system for noradrenergic effects. Clin Pharmacokinet 2008; 47:721-731

Conference Contributions

Oral communications

PK/PD Modeling of Sunitinib. Annual meeting of the Central European Society for Anticancer Drug research (CESAR), October 29-31, 2009, Heidelberg, Germany

Dose individualisation based on population pharmacokinetic models. Meeting of the Central European Society for Anticancer Drug research (CESAR), February 6, 2009, Frankfurt, Germany

Poster presentations

Santos, B, **Lindauer, A**, Coll, R, et al. Pharmacokinetics of a novel non-benzodiazepine hypnotic drug, GF-015535-00 in healthy volunteers. 20th Congress of the European Sleep Research Society, September 14-18, 2010, Lisbon, Portugal

Kanefendt, F, **Lindauer, A**, Kinzig, M, et al. Pharmacokinetics and pharmacodynamics of sunitinib and its primary metabolite (SU12662) in metastatic colorectal cancer patients. Annual meeting of the Central European Society for Anticancer Drug research (CESAR), July 1-3, 2010, St. Gallen, Switzerland

Drescher, A, **Lindauer, A**, Pieck, AC, et al. Pharmacokinetic/Pharmacodynamic Modeling of Platinum-DNA-Adduct Formation in Leukocytes after Oxaliplatin Infusion. Annual meeting of the population approach group in Europe (PAGE), June 8-11, 2010, Berlin, Germany

Nock, V, **Lindauer, A**, Jaehde, U, et al. Leukopenia following high-dose chemotherapy with autologous stem cell retransfusion in patients with testicular cell cancer. Annual meeting of the population approach group in Europe (PAGE), June 8-11, 2010, Berlin, Germany

DiGion, P, **Lindauer, A**, Kanefendt, F, et al. Pharmacokinetic/pharmacodynamic modeling of sunitinib after oral administration in healthy subjects. Annual meeting of the American Society for Clinical Pharmacology and Therapeutics (ASCPT), March 17-20, 2010, Atlanta, USA

Rühs, H, Höckel, M, **Lindauer, A**, et al. Population pharmacokinetic analysis of etoposide based on high and low dose concentration-time profiles. Annual meeting of the Central European Society for Anticancer Drug research (CESAR), October 29-31, 2009, Heidelberg, Germany

Rühs, H, Höckel, M, **Lindauer, A**, et al. Population pharmacokinetics of etoposide based on a wide range of administered doses. Annual meeting of the German Pharmaceutical Society (DPhG), September 28 - October 1, 2009, Jena, Germany

Lindauer, A, Kanefendt, F, Krambeer, C, et al. Pharmacokinetic / Pharmacodynamic Modeling of Sunitinib in Healthy Volunteers. Annual meeting of the population approach group in Europe (PAGE), June 23-26, 2009, St. Petersburg, Russia

Lindauer, A, Eickhoff, C, Kloft, C, et al. Population pharmacokinetics of high-dose carboplatin. Annual meeting of the population approach group in Europe (PAGE), June 18-20, 2008, Marseille, France

Lindauer, A, Eickhoff, C, Kloft, C, et al. Factors affecting the pharmacokinetics of high-dose carboplatin: a population approach. Annual meeting of the Central European Society for Anticancer Drug research (CESAR), June 12-14, 2008, Goettingen, Germany

Lindauer, A, Siepmann, T, Oertel, R, et al. Pharmacokinetic / pharmacodynamic modeling of venlafaxine. Annual meeting of the German Pharmaceutical Society (DPhG), October 10-13, 2007, Erlangen, Germany